VŠB – TECHNICAL UNIVERSITY OF OSTRAVA
Nanotechnology Centre

DOCTORAL DISSERTATION

Surface activation of ordered mesoporous silica materials by cobalt and rhodium

Ing. Lenka Kuboňová

Supervisor: Prof. Ing. Lucie Obalová, Ph.D.

Study program: Nanotechnology

Ostrava, 2015

VŠB – TECHNICKÁ UNIVERZITA OSTRAVA
Centrum nanotechnologií

DISERTAČNÍ PRÁCE

Povrchová aktivace uspořádaných mezoporézních křemičitých materiálů kobaltem a rhodiem

Ing. Lenka Kuboňová

Školitel: Prof. Ing. Lucie Obalová, Ph.D.

Studijní program: Nanotechnologie

Ostrava, 2015

Declaration

I declare that I elaborated this doctoral dissertation independently and I used only those references summarized in List of references.

In Ostrava 20/07/2015 …….....

Ing. Lenka Kuboňová

Acknowledgements

I would like to thank to people who have helped me with my dissertation thesis:

Prof. Ing. Lucie Obalová, Ph.D. from Institute of Environmental Technology, VŠB-TU Ostrava, for her professional suggestions, personal and friendly approach as the supervisor of my dissertation,

Prof. Pegie Cool and Prof. Vera Meynen from Laboratory of Adsorption and Catalysis, Department of Chemistry, University of Antwerp, Belgium, for the possibility to use any laboratory equipment in Laboratory of adsorption and catalysis, for their advices and welcoming approach,

Team of Laboratory of Adsorption and Catalysis, Department of Chemistry, University of Antwerp, Belgium, for EPMA, N_2 sorption, FTIR-PAS and TGA analyses and for memorable experiences,

Team of Nanotechnology Centre, VŠB-TU Ostrava: Ing. Světlana Kozubová for SEM-EDX measurements, Ing. Kateřina Mamulová Kutláková, Ph.D. for XRD analysis, and Ing. Pavlína Peikertová, Ph.D. for IR and Raman spectroscopy analyses,

Ing. Dagmar Fridrichová from Institute of Environmental Technology, VŠB-TU, Ostrava for TPD-NH_3, TPR-H_2 and pulse chemisorption measurements,

Doc. Ing. Libor Čapek, Ph.D. from Department of Physical Chemistry, University of Pardubice, for the discussion of results from DR UV-Vis spectroscopy analysis,

Ing. Květuše Jirátová, Ph.D. from Institute of Chemical Process Fundamentals of the ASCR, v.v.i., Prague, for AAS and TPR-H_2 measurements,

Prof. Ing. František Kovanda, CSc. from Department of Solid State Chemistry, University of Chemistry and Technology, Prague, for AAS analysis,

Prof. Dr. Hab. Piotr Kuśtrowski and Mgr. Anna Wach from Organic Technology Research Group, Department of Chemical Technology, Faculty of Chemistry, Jagiellonian University, Krakow, Poland, for XPS analysis,

Ing. Petr Maršolek from Institute of Environmental Technology, VŠB-TU Ostrava, for professional support with GC-TCD analysis,

Team of Laboratory of air protection, Institute of Environmental Technology, VŠB-TU Ostrava, for technical support and for memorable experiences,

And finally my family members for their trust and support.

The presented work was financially supported by Czech Science Foundation (project no. GA14-13750S), by Ministry of Education, Youth and Sports of the Czech Republic in the "National Feasibility Program I" (project no. LO1208 "Theoretical Aspects of Energetic Treatment of Waste

and Environment Protection against Negative Impacts") and by the projects of specific research of VSB – TU Ostrava (nos. SP2012/25, SP2012/196, SP2013/110, SP2014/88 and SP2015/125).

Abstract

Three different types of ordered mesoporous silica materials, MCM-41, aluminum incorporated into the silica framework MCM-41 (Al-MCM-41) and SBA-15, were prepared. Apart from elemental composition, they differed in textural and structural properties. Furthermore, aluminum was grafted on the silica surfaces by Molecular Designed Dispersion (MDD) method. Finally, the transition metal (cobalt or rhodium) was applied for the surface activation of the silica supports by MDD technique. Much higher initial concentration of cobalt acetylacetonate complex (3.2 $mmol_{Co(acac)2}.g_{support}^{-1}$) was applied than the concentrations of rhodium acetylacetonate complex (0.2–0.01 $mmol_{Rh(acac)3}.\ g_{support}^{-1}$). The prepared catalysts were characterized by different techniques such as AAS, EPMA, EDX, TGA, N_2 physisorption, SEM, XRD, IR and Raman spectroscopy, DR UV-Vis spectroscopy, XPS, TPD-NH_3, TPR-H_2 and pulse chemisorption of H_2 and their catalytic activities were tested for two reactions of environmental application: N_2O decomposition (in inert and real conditions and in the presence of the reducing agent) and CO oxidation at low temperatures (below 450 °C).

The Co-grafted catalysts showed poor activity (14 %) in catalytic N_2O decomposition in the inert condition at 450°C and at GHSV 15648 h^{-1}. This was in agreement with TPR-H_2 study as Co-grafted catalysts showed very low hydrogen consumption within the temperature range of catalytic tests of N_2O decomposition. The carbon monoxide as the reducing agent can facilitate the reduction of cobalt which was confirmed as the N_2O conversion increased up to 26 % at 450°C (at GHSV 15648 h^{-1}). The non-specified oxide Co_xO_y was detected by DR UV-vis and Raman spectroscopy as well as cobalt spinel phase by XRD analysis in the sample Al-MCM+Co. This catalyst contained both cobalt ions (Co^{2+} as well as Co^{3+}) as determined by TPR-H_2 experiments which seems to be beneficial for the catalytic activity of CO oxidation. On the other hand, a specific ration between Co^{2+} and Co^{3+} ions is not definitely required as the most active catalyst in the reaction of CO oxidation was SBA+Co containing tetrahedral Co^{2+} ions interacting with the support as determined by DR UV-vis analysis. More active sites were distributed on SBA+Co per unit surface area than on other Co-grafted catalysts by expressing the catalytic activity as converted CO molecules per unit BET surface area. Therefore, it is expected that the most important for the catalytic activity is better and higher distribution of cobalt species on the silica support.

In the case of Rh-grafted catalysts, the activity of the catalysts with the same initial rhodium loading (0.2 $mmol_{Rh(acac)3}.g_{support}^{-1}$) in the reaction of N_2O decomposition under the inert and real conditions (the presence of O_2, water vapor and NO) was found in the order: Al-MCM+Rh > MCM+Al+Rh > SBA+Rh ≈ MCM+Rh. It was proven experimentally (by TPR-H_2 and pulse chemisorption of H_2) that aluminum incorporated into the structure of MCM-41 enhanced rhodium dispersion on the support which was beneficial for its catalytic activity in the reaction of N_2O

decomposition. Nearly the same catalytic activities of MCM+Rh(2.7 %) and SBA+Rh(2.7 %) supports the fact that differences in mesoporous structures of MCM-41 and SBA-15 did not play the key role in the reaction of N_2O decomposition within the applied amount of rhodium and experimental conditions of N_2O decomposition.

Keywords: Ordered mesoporous silica; Aluminum; Cobalt; Rhodium; Molecular designed dispersion; Incorporation; Catalysis, N_2O decomposition; CO oxidation.

Abstrakt

Tři různé typy uspořádaných mesoporézních křemičitých materiálů, MCM-41, hliník začleněný do křemičité struktury MCM-41 (Al-MCM-41) a SBA-15, byly připraveny. Kromě elementárního složení se lišily v texturních a strukturních vlastnostech. Kromě toho byl hliník nanesen na povrchu křemičité struktury tzv. metodou Molecular Designed Dispersion (MDD). Nakonec byl použit přechodný kov (kobalt nebo rhodium) pro aktivaci křemičitých nosičů pomocí MDD techniky. Byla použita mnohem vyšší počáteční koncentrace acetylacetonátových komplexů kobaltu (3,2 $mmol_{Co(acac)2}.g_{nosič}^{-1}$) než byla koncentrace acetylacetonátových komplexů rhodia (0,2–0,01 $mmol_{Rh(acac)3}.g_{nosič}^{-1}$). Připravené katalyzátory byly charakterizovány různými instrumentálními metodami AAS, EPMA, EDX, TGA, N_2 fyzisorpce, SEM, RTG difrakce, IČ a Ramanova spektroskopie, DR UV-Vis spektroskopie, XPS, TPD-NH_3, TPR-H_2 a pulzní chemisorpce vodíku a jejich katalytické aktivity byly testovány na dvou reakcích týkajících se problematiky ochrany životního prostředí: rozklad N_2O (v inertních a reálných podmínkách a v přítomnosti redukčního činidla) a oxidaci CO při nízkých teplotách (pod 450 °C).

Kobaltové katalyzátory vykazovaly slabou aktivitu (14 %) v reakci katalytického rozkladu N_2O v inertních podmínkách. Tento výsledek souhlasí s měřením TPR-H_2, kdy kobaltové katalyzátory vykazovaly velmi nízkou spotřebu H_2 v rozmezí teplot katalytických testů rozkladu N_2O. Bylo potvrzeno, že oxid uhelnatý jako redukční činidlo usnadňuje redukci kobaltu, jelikož konverze N_2O se zvýšila na 26 % při 450 °C (při prostorové rychlosti GHSV 15648 h^{-1}). Nespecifikovaný oxid Co_xO_y byl detekován pomocí DR UV-vis a Ramanovy spektroskopie stejně jako spinel kobaltu pomocí RTG difrakce ve vzorku Al-MCM+Co. Tento katalyzátor obsahoval oba ionty kobaltu (Co^{2+} a Co^{3+}), což bylo určeno pomocí TPR-H_2, a jejich přítomnost se jeví jako prospěšná pro katalytickou aktivitu oxidace CO. Na druhé straně, specifický poměr mezi Co^{2+} a Co^{3+} ionty není definitivně nezbytný vzhledem k tomu, že nejaktivnějším katalyzátorem v reakci oxidace CO byl SBA+Co obsahující tetraedrické Co^{2+} ionty vázané na nosiči podle DR UV-vis analýzy. Více aktivních míst na jednotku plochy bylo rozmístěno na SBA+Co ve srovnání s ostatními kobaltovými katalyzátory vyjádřením katalytické aktivity jako počet zreagovaných molekul CO na jednotku BET plochy. Z tohoto důvodu se předpokládá, že nejdůležitější pro katalytickou aktivitu je lepší a vyšší rozmístění iontů kobaltu na křemičitých nosičích.

V případě rhodiových katalyzátorů, aktivita katalyzátorů se stejnou počáteční koncentrací rhodia (0,2 $mmol_{Rh(acac)3}.g_{nosič}^{-1}$) v reakci rozkladu N_2O v inertních a reálných podmínkách (přítomnost O_2, vodní páry a NO) byla v pořadí: Al-MCM+Rh > MCM+Al+Rh > SBA+Rh ≈ MCM+Rh. Experimentálně bylo prokázáno (pomocí TPR-H_2 a pulzní chemisorpce vodíku), že hliník začleněný do struktury MCM-41 zvyšuje disperzi rhodia na nosiči, což zvýšilo aktivitu katalyzátoru v reakci rozkladu N_2O. Téměř stejná katalytická aktivita MCM+Rh (2,7 %) a

SBA+Rh (2,7 %) podporuje skutečnost, že rozdíly v mezoporézní struktuře MCM-41 a SBA-15 nehrály klíčovou úlohu v reakci rozkladu N_2O v rámci použitého množství rhodia a experimentálních podmínek rozkladu N_2O.

Klíčová slova: Uspořádané mezoporézní křemičité materiály; Hliník; Kobalt; Rhodium; Nanášení molekul; Inkorporace; Katalýza, Rozklad N_2O; Oxidace CO.

CONTENT

1 INTRODUCTION

Catalysis is one of the most important technologies in the industry, controlling more than 90 % of chemical processes. Catalysis is also important for the environmental protection and the abatement of gaseous and liquid pollutants. This work is focused on the catalytic decomposition of gas pollutants, nitrous oxide and carbon monoxide.

Nitrous oxide (N_2O) contributes to the destruction of stratospheric ozone layer and the global warming. The global warming potential of N_2O is 310 greater than carbon dioxide and 21 times than methane. The primary natural sources of N_2O are the biological processes that proceed in soils and oceans. The main industrial sources of N_2O emissions are nitric and adipic acid plants. The ambient level of N_2O is 327 ppb in 2014 and has been increasing in recent years, (0.2–0.3 % per year), (http://www.epa.gov/climatechange/science/indicators/ghg/ghg-concentrations.html, http://www.enn.com/ecosystems/article/42147). The catalytic decomposition of N_2O is so far considered as the most effective and cost-efficient option for N_2O abatement and has been widely studied by many research teams. Despite of this fact, it is still problematic to find a catalyst with sufficient activity and stability in real off-gas conditions such as the presence of water, oxygen and NO_x from nitric acid production plants (Pérez-Ramírez, 2003).

High amounts of carbon monoxide (CO) are emitted to the air (1.09 billion tons in 2000), (Royer, 2011). Its main sources are from transportation, power plants and industrial processes, and domestic activities. Carbon monoxide is a precursor of ground-level ozone which can cause serious respiratory problems due to its high affinity with hemoglobin. It is a highly flammable gas, however, homogeneous CO combustion in polluted air (50–50 000 ppm) is impossible. It is also not very soluble in water. The catalytic oxidation of CO into CO_2 is necessary for CO abatement. The catalytic converters in 1970s in the Unites States of America and in 1990s in Europe showed the great activity of noble metals for CO oxidation (Royer, 2011). However, the application of other transition metals has been interesting due to the increasing price of noble metals.

So far, a lot of solid catalysts have been studied including i) monocrystals and unsupported metals, ii) pure metal oxides, iii) mixed metal oxides and iv) supported metals (silica, alumina, titania, zirconia, zeolites and others). The required properties of catalyst performance are high reactivity, selectivity and stability. For the practical application, supported metal oxide catalysts are better than unsupported metal oxides due to higher dispersion of metals with the combination of larger specific surface area of catalyst supports. The ordered mesoporous silica materials belong to the group of supports with large surface area and narrow pore size distribution. First ordered mesoporous silica materials were reported in 1990s (Meynen, 2009). Three different support materials of such kind were used in this work: MCM-41, Al-MCM-41 (aluminum incorporated

within MCM-41 structure) and SBA-15. They have different compositional, textural and structural properties.

In the case of Al-MCM-41, aluminum was presented in literature (Hussain, 2013) as the element generating acid sites, enhancing dispersion and stability of metals. Its incorporation into the structure also strengthens hydrothermal stability of MCM-41.

For the activation of support surfaces by catalytically active metals, the method called Molecular Designed Dispersion (MDD) was applied in this work assuming high concentration and dispersion of metals on silica supports.

The most active metals for the N_2O catalytic decomposition are cobalt and copper from transition metals, rhodium and ruthenium from noble metals (Kapteijn, 1996). Very active catalysts are based on calcined hydrotalcites, zeolites and alumina supports. For the catalytic CO oxidation, noble metals are more active than the other ones, however, some oxides such as cobalt and copper showed a good activity. Therefore, cobalt and rhodium were selected to this work.

It is essential to understand and characterized the morphology and the texture of prepared catalysts, their elemental composition, the coordination and oxidation state of catalytically active metals, their reducibility, the acidity of catalyst surfaces and the distribution of metal sites for better understanding of the catalytic activities and catalyst applications. In this work, prepared catalysts were tested for the catalytic decomposition and reduction of N_2O and CO oxidation at low temperatures (below 450 °C).

2 OBJECTIVES

The aim of this doctoral dissertation was to contribute to surface activation of ordered mesoporous silica materials and their application as catalysts to deal with the environmental and health issues of nitrous oxide and carbon monoxide.

The following tasks have been solved:

- Preparation of three different ordered mesoporous silica materials (MCM-41, Al-MCM-41 with different Si/Al ratios, SBA-15) with different pore size distribution, with or without the presence of aluminum.
- Grafting of aluminum by Molecular Designed Dispersion in comparison with aluminum incorporated in MCM-41 structure (Al-MCM-41) presuming good dispersion and stability of metals and increase of the acidity of silica supports.
- Use of Molecular Designed Dispersion method for the grafting of two different metals (cobalt and rhodium) known as the active ones for the redox reactions.
- Characterization of prepared catalysts by different analytical methods: atomic absorption spectroscopy, electron probe microanalysis, scanning electron microscopy with energy dispersive X-ray analysis, nitrogen sorption, thermogravimetric analysis, X-ray powder diffraction, diffuse reflectance UV-Vis spectroscopy, infrared spectroscopy, Raman spectroscopy, X-ray photoelectron spectroscopy, temperature programmed desorption of ammonia, temperature programmed reduction by hydrogen and pulse chemisorption.
- Testing of activity of catalysts grafted by cobalt for the reaction of N_2O decomposition, N_2O reduction by CO and CO oxidation and their comparison.
- Testing of activity of catalysts grafted by rhodium for the N_2O decomposition in inert and real conditions of waste gases from the production of nitric acid (the influence of O_2, H_2O and NO) followed by stability tests.
- Correlation of the properties of catalysts with their catalytic activities.

3 THEORETICAL PART

3.1 Supports of catalysts

Supported catalysts play a significant role in many industrial processes. The support provides high surface area desirable for high dispersion of metal active sites on the catalyst surface resulting in high number of reactive sites and high catalytic activity. Ordered mesoporous materials are such materials with high surface area, high pore volume and narrow pore size distribution (with mesopore diameters between 2 and 50 nm defined by IUPAC).

3.1.1 Ordered mesoporous silica materials

To overcome the pore size limitation of zeolites, the research has been focused on the enlargement of the pore size into the mesoporous range of silica and non-silica materials. In zeolites, each atom has a well-defined position in the structure, however, in mesoporous materials the atoms have no specific position. Therefore the pore walls are amorphous. The ordering of the final structure is due to the pore arrangements, not due to the atom ordering.

The first ordered mesoporous materials were reported in 1992 by Mobil and are known as M41S with various types of MCM (Mobil Composition of Matter) materials in the mesoporous range. A new group of highly ordered mesoporous silicas was synthesized in 1998 and is denoted as SBA (Santa Barbara Acids) materials. The structure of 2D hexagonal is typical for SBA-15 material and its analogue is called PHTS (Plugged hexagonal templated silica). In addition to SBA-15, PHTS has microporous amorphous nanoparticles (so called plugs) in the uniform mesoporous structure resulting in higher mechanical and hydrothermal stability of PHTS. The result of the addition of swelling agent to the synthesis of SBA-15 is mesostructured cellular foam (MCF). In contrast to SBA-15, PHTS and MCF which are made in acidic media, MSU (Michigan State University) materials are made in neutral media. The various types of MSU materials are called MSU-X where X is a number or a letter. A similar approach of ordered mesoporous silicas preparation can be applied for synthesis of templated mesoporous transition metal oxides as described by Meynen and co-authors (2009).

The advantage of ordered mesoporous materials are: (i) 2–3 times higher surface area than traditional mesoporous supports (silica gels, activated alumina) leading to higher concentration of active sites, (ii) narrow pore size distribution, (iii) bigger pore diameter suitable to process bulky molecules which are problematic in microporous zeolites (with micropore diameters less than 2 nm defined by IUPAC). Their disadvantage can be poor hydrothermal and mechanical stability with further weakening of the silica framework.

Ordered mesoporous silicas have been used as supports for catalyst synthesis by incorporation of active sites in silica walls or by deposition of active species on the surface of materials. The modification mainly focuses on tuning of redox and acid-basic properties of supports in order to improve the catalytic performance and mass transfer of reacting molecules.

Mesoporous samples are synthetized by polymerization of silica source around organic surfactant molecules in a solvent, mainly aqueous one. During the stirring period, silicate ions undergo hydrolysis and pre-condensation followed by the condensation at increased temperatures. The products are recovered, washed and dried. Finally, organic templates are removed upon the calcination or the extraction in order to form pore structure (Fig. 1). The ordering of pores and the stability of pore walls can be influenced by synthesis conditions such as surfactants, silica sources, solvents, pH, time, temperatures, additives etc. (Collart, 2001, 2003, Meynen, 2009, Urraca, 2006).

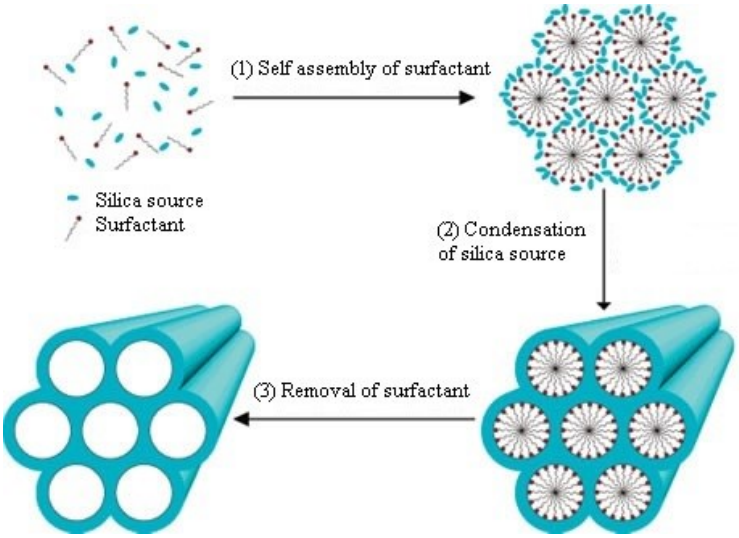

Fig. 1. The liquid crystal templating (LCT) mechanism proposed by Beck (1992), (1) formation of micellar rod around the surfactant micelle producing hexagonal array of rods, (2) incorporation of inorganic precursor (silica, silica-alumina) around the rod-like structure (3) calcination to remove surfactant micelle and formation of mesoporous molecular sieve (http://info.chem.strath.ac.uk/people/academic/lorraine_gibson/research/sorbents).

- **MCM-41 (mesostructured silica SiO_2)**

MCM-41 has the ordered mesoporous hexagonal structure with mesopore diameters between 1.5–10 nm depending on the template, additives and synthesis parameters. MCM-41 has very high surface area (up to 1200 $m^2.g^{-1}$), high pore volume (up to 1.0 $ml.g^{-1}$), and narrow pore size distribution in parallel positioning. The pore walls are quite thin (between 1.0–1.5 nm) which leads to low hydrothermal and mechanical stability (Meynen, 2009).

- **SBA-15 (mesostructured silica SiO_2)**

The main difference between MCM-41 and SBA-15 are in the dimension of pores and pore walls and the presence of micropores (Fig. 2). SBA-15 has the ordered mesoporous hexagonal structure with mesopore diameters between 4–14 nm . SBA-15 is characterized by very high surface area (up to 800 $m^2.g^{-1}$) and pore volume and narrow pore size distribution. The pore walls are thicker (3–6 nm) than MCM-41 responsible for higher hydrothermal stability. The structure is the combination of micropores interconnecting the mesopore channels. The micropores are produced during the synthesis due to the penetration of polyethylene oxide chains in the silica walls, forming micropores after calcination (Urraca, 2006).

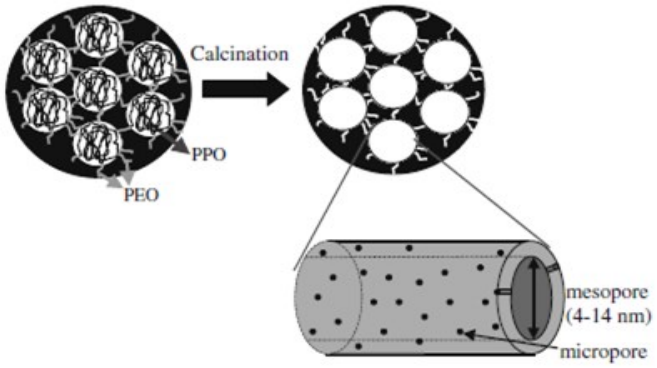

Fig. 2. SBA-15 structure before and after calcination (Meynen, 2009).
Note: PEO = poly (ethylene oxide), PPO = poly (propylene oxide).

- **Al-MCM-41 (mesostructured aluminosilicate $(SiO_2)_x(Al_2O_3)_y$)**

Different aluminum sources (such as aluminum sulphate and sodium aluminate) have been used to introduce the aluminum in its tetrahedral coordination in the silica framework (Collart, 2003). MCM-41 with aluminum incorporated into the silica structure preserves the ordered mesoporous hexagonal structure with mesopore diameters in narrow pore size distribution, very high surface area and high pore volume.

3.1.2 Silica versus alumina

- **Silica (SiO_2)**

The silica surface is almost inert in comparison with surfaces of metal oxides. Silica consists of particles that can be regarded as polymers of interlinked tetrahedral SiO_4 units. The structure terminates either in siloxane groups (≡Si-O-Si≡) with the oxygen on surface or silanol groups (≡Si-OH, isolated, vicinal or geminal silanols). The siloxane bridges create hydrophobic parts on the pore surface whereas the silanol groups are hydrophilic. Isolated OHs are far separated for the

hydrogen bond interaction (> 3 A), vicinal OHs can form H-bond (< 3A), while geminal OHs are too close to form H-bond (Baltes, 2001).

Silanol number describes the amount of surface hydroxyls varying as it is the function of temperature. The determination of quantity of hydroxyl groups is important in order to rationalize the grafting method. The density of silanols in the ordered mesoporous materials is lower than in pure silica. The silanol number for fully hydroxylated silica (pretreated by vacuum drying at 200 °C) is 4.6 $OH.nm^{-2}$, for MCM-48 is 0.9 $OH.nm^{-2}$, for SBA-15 is 0.9–1.0 $OH.nm^{-2}$ (Collart, 2003, Urraca, 2006). The defined amounts of silanol groups were determined experimentally by i) hexamethyldisilazane (HMDS) reacting with hydrophilic silanols evolving ammonia ii) which was captured in boric acid creating borate iii) which was titrated with HCl. This experimental method is described in detail in the literature (Vansant, 1995). The silanol number is generally higher in SBA-15 and MCM-48 than in MCM-41 expecting more stabilizing groups available for the interaction with reactive molecules. The exact values may differ, e.g. SBA-15 (2.8–5.3 $OH.nm^{-2}$), MCM-41 (1.4–3.0 $OH.nm^{-2}$) (Limnell, 2011); SBA-15 (5–6 $OH.nm^{-2}$), MCM-41 (3–4 $OH.nm^{-2}$) (Kozlova, 2010); SBA-15 and MCM-48 (13 mmol $SiOH.m^{-2}$), MCM-41 (2 mmol $SiOH.m^{-2}$) (Harris, 2008).

- **Alumina (Al_2O_3)**

Alumina is the general name for transition aluminas divided in: i) low temperature phase from 250 to 500 °C (η-, χ-, γ-Al_2O_3) containing the amount of water and other stabilizing compounds and ii) high temperature phase formed at 800–1000 °C (δ-, θ-, κ-) containing only small amount of stabilizing mixtures. The thermal transformation from low to high temperature phase is irreversible. The crystalline α-alumina is formed at temperatures above 1200 °C. The surface of alumina is heterogeneous containing hydroxyl groups and coordinatively unsaturated (c.u.s.) Al^{3+} species. The framework possesses negative charges that can be compensated by protons creating acidic (Brönsted) functional groups.

From the point of view of metal dispersion, the alumina surface is superior to the silica surface. For instance, loadings of vanadium were 5 times higher without the formation of crystalline V_2O_5 on the alumina surface (Baltes, 2001, Hlaváč, 1981, Van Der Voort, 1996).

3.2 Molecular designed dispersion

The surface hydroxyl groups of the silica structure or silanols could assume the role of anchoring point. The metal complexes, such as acetylacetonate complexes, interact with the silanol groups, releasing a ligand, which removes the proton of the hydroxyl group. Simultaneously, the covalent bond is formed between the remaining part of complex and the $Si\text{-}O^-$ anion group on the surface. Dry organic solvents should be preferred to water because water adsorbs onto silanol groups

blocking the access for any reacting complex. Also the complexes are in most cases moisture sensitive as well as the silica structure. Finally, the calcination is performed in order to remove the complex ligands and obtain desired metal oxides on the surface. The prolonged calcination at 773 K assumes that all organic ligands are removed. The described grafting method is known as Molecular Designed Dispersion (MDD) controlling the grafting of metals and their distribution on material surfaces (Collart, 2003).

3.2.1 Reaction mechanism of MDD

- **H-bonding versus ligand exchange**

There are two principles of interaction between the acetylacetonate (acac) complexes and the hydroxyl groups of support:

- H-bridges between the pseudo pi system of acetylacetonate ligand and the proton of silanol;
- Ligand exchange mechanism: the covalent metal-oxygen-support bond, the ligand is removed as Hacac (Fig. 3).

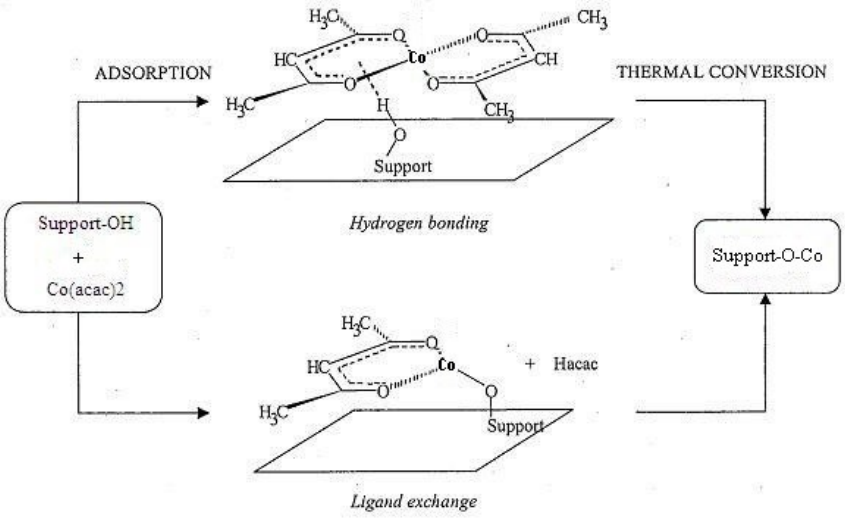

Fig. 3. The scheme of the interaction of e.g. cobalt acetylacetonate complexes with a silica surface described as MDD method.

Metal complexes should contain nucleophilic ligands to participate in **H-bonding** and in ion exchange interactions and having the required basicity to interact with surface protons, such as those found on silica. For **ligand exchange reactions**, the basic character of ligands is not sufficient to ensure the affinity of complexes for the surface. For a sufficiently basic nucleophile in a rather unstable metal complex, the acidic surface proton may initiate acid-catalyzed substitution reaction for which the ligand leaves the metal complex as a stable molecule to be replaced by a

group from the surface, such as (SiO^{-1}) (Van der Voort, 1997). The presence of aluminum should result in the ligand exchange reaction and consequently in the formation of covalent metal-O-Al bonds (Weckhuysen, 2000).

As an example, the adsorption of $VO(acac)_2$ complexes on silica enables the creation of supported VO_x catalysts with V loading of 0.5 $mmol.g^{-1}$ (2.5 wt%) with all species in strictly tetrahedral configuration and no formation of microcrystallites. The interaction of $VO(acac)_2$ with the alumina support yields more complicated surface configuration in comparison to silica (Fig. 4). The adsorption of $VO(acac)_2$ on the alumina surface proceeds by the ligand exchange mechanism (Eqs. 1–3). The evolved Hacac immediately reacts with alumina surface forming Al-acac surface species and H^+ ions associate with the support forming silanol groups. At loadings higher than 0.3 mmol V/g alumina, the neutral and acidic OH groups involve in H-bond interaction (Eq. 4). Vanadium loading of higher than 2.2 $mmol.g^{-1}$ (11 wt% of vanadium) can be prepared with no formation of crystalline V_2O_5 which is 5 times higher than on silica surface (Baltes, 2000, Van Der Voort, 1996).

$$Al^{3+}\ (c.u.s.) + VO(acac)_2 \rightarrow [Al(acac)_x]^{(3-x)+}\ (crystalline) + VO_x \quad (1)$$

$$2\ Al\text{-}OH + VO(acac)_2 \rightarrow (Al\text{-}O)_2\text{-}V{=}O + 2Hacac \quad (2)$$

$$Al\text{-}OH + VO(acac)_2 \rightarrow (Al\text{-}O)\text{-}V{=}O\text{-}(acac) + Hacac \quad (3)$$

$$Al\text{-}OH + VO(acac)_2 \rightarrow Al\text{-}OH \cdot (acac)\text{-}V{=}O\text{-}(acac) \quad (4)$$

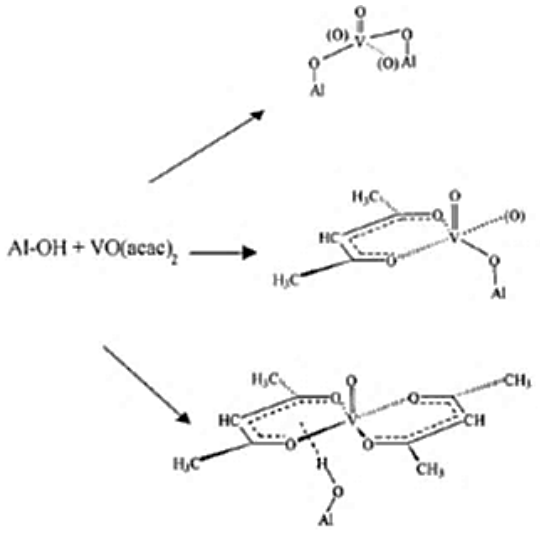

Fig. 4. The interaction of acetylacetonate complexes with the alumina surface, as a function of the surface loading (Baltes, 2000).

Opposite to this reaction pattern, the complexes $Cu(acac)_2$ in very close contact with the surface of the fumed silica Cab-O-Sil (Cu loadings < 3.5 wt%) showed the H-bonding interactions with the

quasi-pi electrons of complexes. Samples at higher loadings forming multilayers of complexes show that not all complexes were H-bonded (Kenvin, 1991).

The surfaces of supports are quite heterogeneous containing basic, acidic and neutral hydroxyl groups as well as coordinately unsaturated sites (c.u.s), such as Lewis acid Al^{3+} sites in the case of alumina support. The interaction of metal acetylacetonates with the reactive surface sites is influenced by their shape, stability and metal ions in the complexes as studied in detail by Van Veen (1989), Kenvin (1991) or Van der Voort (1997).

- **Controlling parameters of MDD**

The controlling parameters of MDD method are: (i) the pretreatment temperature of the support, (ii) the concentration of the complexes in solution and (iii) the washing procedure after reaction.

(i) The pretreatment temperature (200 °C) assures more silanols available for bonding of acac complexes and further better uniformity and dispersion of metals.

(ii) The selection of initial acac complex concentrations result in well dispersed acac complexes with controllable surface loadings. Multilayers occur before a complete monolayer is formed with an increasing initial concentration of acac complexes. They are deposited not in close interaction with the support and aggregates into crystalline clusters.

(iii) In order to avoid the formation of crystals, a washing procedure is performed after the reaction, which removes the excess of adsorbed acac complexes and reduces the metal loading. The solvent should not coordinate to the complex and should not form H-bond to the support. Methanol, toluene and acetonitrile were used for various acac complexes. For instance, vanadium loading on silica support increased in the order: methanol < acetonitrile < toluene (Baltes, 2001).

3.2.2 Acetylacetonate (acac) complexes

- **Characterization of complexes**

Beta-diketonate complexes are neutral transition metal beta-diketonates having a strong affinity to the support surface and developing monolayer films. Metal acetylacetonates (2, 4 – pentanedianato complexes) belong to this group. In the early 1990s, these complexes renewed the interest as precursors for the deposition of metal oxides in methods like MDD (Molecular Design Deposition), ALE (Atomic Layer Epitaxy) or ALD (Atomic Layer Deposition).

The ease of the MDD method mainly depends on geometry of complexes, their stability and metal ions in the complexes. The structure of beta-diketonate complexes depends on the oxidation state and the coordination of the central metal ion. Divalent metal ions have usually a square planar (e.g. Cu^{2+}, Pt^{2+}, Ni^{2+}) or tetrahedral (e.g. Co^{2+}) structures. Trivalent metal ions (e.g Al^{3+}, Cr^{3+}) form octahedral arrangements of the oxygen atoms. The planar complexes show a high adsorption

capacity whereas the octahedral complexes are sterically hindered to approach the surface. Oxygen-metal bonds create the pseudo π system in the ligands. Some metal complexes form polynuclear species as the result of sharing beta-diketonols between adjacent metal ions. Metals known to form such "polymer structures" include Mg^{2+}, Ni^{2+}, Co^{2+}, Mn^{2+}, Fe^{2+} and Ln^{3+}.

Acetylacetonate complexes were proven to be outstanding in dispersing metals onto a silicate surface as they react very easily with the silanol groups. Their bulky ligands are able to isolate the central metal ion on the support surface allowing their high dispersion. They reduce the probability of metal clustering as the metal atoms are kept further away from each other. They also present the advantage of being less moisture sensitive, making their handling more convenient. The stabilities of metal acac complexes vary widely. Cr(III) and Cu(II) acac complexes are stable at 191 °C whereas Co(II), Fe(III) and Mn(III) acac compounds decompose rapidly at this temperature. Their thermal stabilities influence their chemical reactivity to ligand substitution reactions. The stable complexes show symmetries as unsupported complexes, while the unstable complexes show structures that are different from parent complexes (Baltes, 2001, Collart, 2003, Kenvin, 1991, Urraca, 2006, Van der Voort, 1997, Weckhuysen, 2000).

- **Monolayer capacity and theoretical surface coverage**

The simple calculation of the loading capacity on the surface assuming that the theoretical surface coverage is equal to 1 can be performed. It is important to know the surface area of the support and the mean cross-sectional area of the acac complex (Eq. 5).

$$V_m = \frac{S_{BET}}{A_m \cdot 10^{-18} \cdot N_A} \tag{5}$$

where V_m – monolayer capacity (mol.g^{-1}), S_{BET} – BET surface area (m^2.g^{-1}), A_m – cross-sectional area of acac complex (nm^2), N_A – Avogadro´s number, 6.022.10^{23} mol^{-1}.

The mean cross-sectional area 0.6 nm^2 was reported for different acac complexes ($Cr(acac)_2$, Haukka (1994); $Al(acac)_3$, Ahenah (2000); $VO(acac)_2$, Baltes (2001)). In this work, mean cross-sectional areas were calculated: $Al(acac)_3$ = 0.89 nm^2, $Co(acac)_2$ = 0.56 nm^2, and $Rh(acac)_3$ = 1.0 nm^2 (Fig. 5). The molecules of acac complexes were modelled by the program NWChem 6.3 (Valiev, 2010).

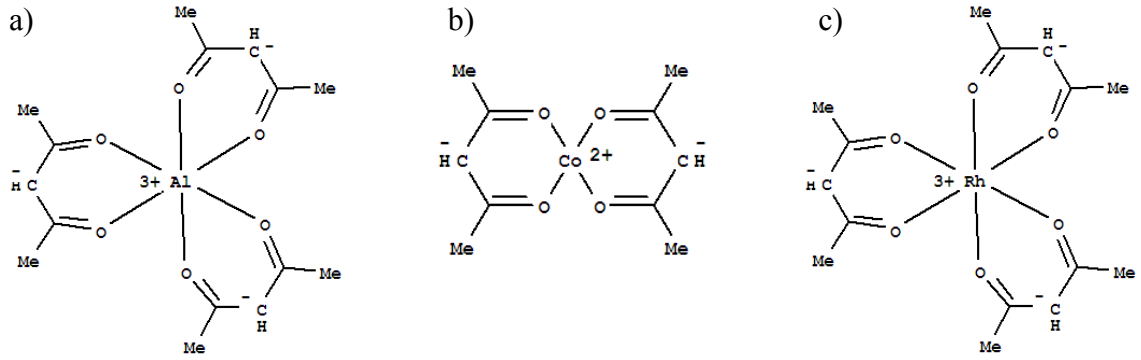

Fig. 5. Structural formulas of acetylacetonate complexes:
a) $Al(acac)_3$ (http://www.lookchem.com/Aluminum-acetylacetonate),
b) $Co(acac)_2$ (http://www.lookchem.com/cas-140/14024-48-7.html),
c) $Rh(acac)_3$ (http://www.lookchem.com/cas-142/14284-92-5.html).

The surface of supports covered by acac complexes can be estimated (Eq. 6) on the basis of metal loading determined by elemental analysis and monolayer capacity defined by Eq. 5.

$$\textbf{Theoretical surface coverage} = \frac{\textbf{metal loading}}{\textbf{monolayer capacity}} \qquad (6)$$

If the theoretical surface coverage is equal to 1, the monolayer capacity corresponds to the metal loading. At higher initial acac complex concentrations, a sudden increase in the coverage is observed suggesting that the adsorption is not monolayer (surface coverages > 1), (Baltes, 2001).

3.2.3 Metals grafting

Metal oxides are supported on the surfaces with high surface area by increasing their stability, ideally with no sintering and no loss of metal surface area. At very low concentrations, metal ions are isolated and the activity of catalysts per metal ion is very high. The activity decreases with increasing metal concentration and the metal ions form pairs or clusters leading to lower catalytic activity reflecting the behavior of pure oxides as reported for Cu, Fe, Co, Cr, Mn and Ni in oxide matrices in the study of N_2O decomposition (Kapteijn, 1996). The loading of metals is strongly dependent on the morphology of supports due to differences in accessibility of the internal porous network. The most accessible structures will have the highest loading of metals (Hanu, 2006).

The actual nature of the surface metal species will depend on several factors:

- Influence of metal loading

At low metal loadings, the metal species are isolated tetrahedral or octahedral units. With increasing metal loading, a fraction of supported metal species aggregate to form metal crystals on the support surface.

- Influence of synthesis method

The main difficulty in comparing various studies is that even when the same synthesis method is used, the experimental conditions may differ. The preparation method significantly determines the state of dispersion, and consequently the degree of polymerization and clustering of supported metal oxides.

- Influence of support properties

The nature of the supported metal oxide is mainly influenced by the support properties, such as the surface area, crystallinity and porosity of supports. Much higher metal loading without formation of microcrystals can be obtained on alumina, titania and zirconia in comparison to silica. Silica is relatively inert and the interaction with the metal phase is very weak which results in quite poor dispersion. In contrast, a strong interaction between metals and the support can result in the formation of mixed metal oxide compounds rather than stable surface metal oxide layers.

- Influence of additives

The presence of impurities or the addition of promoters affects the properties of supported metal catalysts. Interacting additives, e.g. alkali/alkaline earth oxides (e.g. K, Na, Ca), preferentially coordinate to the surface metal phase rather than to the oxide support. On the other hand, non-interacting additives, e.g. oxides of Mo, Ni, Co and Fe, preferentially coordinate to the oxide support rather than to the surface metal phase. They do not change the nature of supported metals at all or by lateral interactions leading to a forced aggregation of the metal phase. They are used to introduce additional characteristics (e.g. acidity) to the catalyst system (Baltes, 2001).

- **Aluminum**

The interaction of aluminum with the substrate is associated with the uptake of aluminum onto the surface of the silica framework and the direct formation of acid groups. Brönsted acid groups are preferential from the point of view of acid catalysis. The characterization of coordination of deposited aluminum atoms can be performed by Al-MAS-NMR analysis. Rather low affinities of aluminum oxides for the silicate surface lead to the occurrence of aluminum nanoclusters formed during calcination. These alumina clusters after the deposition of aluminum by MDD method did

not promote the formation of Brönsted groups, as described in Collart (2003). According to Loewenstein rule, the presence of two neighboring tetrahedral aluminum atoms is forbidden, forcing the aluminum to have octahedral symmetry. Opposite to this presumption, aluminum grafted by post synthesis method on MCM-41 (Park, 2002) and on SBA-15 (Xu, 2004) had both tetrahedral and octahedral species. The differences in coordination of species may be due to different aluminum precursors.

- Differences between theoretical and experimental loading

All complexes react with the surface only at lower complex concentrations. The difference between maximal theoretical and experimental loading suggests that at higher complex concentrations not all of the complexes interact with the surface. The result may be more difficult approach on the support surface due to octahedral configuration of complexes as in the case of aluminum acac complexes (Collart, 2003).

- **Cobalt**

Cobalt belongs to the group of transition metals with non-paired d-level electrons. Transition metals act as electron donor and acceptor centers so that they are great catalysts for catalytic oxidation/reduction reactions.

The supported cobalt phase exists in different surface configurations. The isolated cobalt species can be anchored to the surface in a tetrahedral or octahedral coordination with the oxidation state 2+ and/or 3+. They can be also present as polymeric condensed species with tetrahedral and octahedral coordination corresponding to Co_xO_y crystallites. The principal Co_xO_y oxides are CoO (the oxidation state of cobalt is 2+) and Co_3O_4 (the oxidation states of cobalt are 2+ and 3+) (Baltes, 2001, Urraca, 2006).

Bivalent complex $Co(acac)_2$ is characterized by a planar geometry presuming not strong steric hindrance and better adsorption on silica support in comparison with octahedral configuration of $Al(acac)_3$. The $Co(acac)_2$ complex belongs to the group of the acid and base sensitive complexes. As reported in the literature (van der Voort, 1997, Van Veen, 1989), these complexes react with both acidic and basic OH groups and their adsorption leads to the precipitation of oxides on alumina surface. On the other hand, the low stability of $Co(acac)_2$ can be beneficial to form a high loading of cobalt on silica surface avoiding the forming of an insoluble hydroxides. The unstable $Co(acac)_2$ complexes bond to the silica with rearrangement of loss of the acac ligands allowing to bind cobalt ions specially to the siloxides (Kenvin, 1991). Different cobalt precursors were applied as reported in Wang (2009). In the case of $Co(acac)_2$ complexes, they showed a high dispersion and the stability on ordered mesoporous silica materials.

- **Rhodium**

The rhodium center is a soft Lewis acid that usually binds soft bases very tightly. Rhodium (III) complexes are nearly always six-coordinate, octahedral compounds with an 18-electron configuration, while rhodium (I) compounds are typically four-coordinate, square planar compounds with a 16-electron configuration (http://chem.uaf.edu/howard/Rhodium.htm).
The $Rh(acac)_3$ complex belongs to the group of the acid sensitive complexes. As reported by Van Veen and co-authors (1989), it does not react with coordinatively unsaturated sites (c.u.s.) Al^{3+} neither with the acidic OH groups present on the alumina surface. In the case of silica, the reaction of $Rh(acac)_3$ complexes with the acidic OH groups occurred and a fine dispersion of rhodium metal on silica surface was achieved (van der Voort, 1997).

3.2.4 Aluminum grafting versus incorporation

- **Comparison of grafted and incorporated aluminum**

The Al-grafting on the silica surface or Al-incorporation within the framework is used in order to increase the acidity, ion exchange capacity, dispersion of metals on the surface support and their stability on the support (Cesteros, 2001, Xu, 2004). The incorporation or grafting of aluminum into mesoporous silica also strengthens the hydrothermal stability of mesoporous silica materials as reported in the literature (Hussain, 2014, Xia, 2004). The reason can be the increase of silica wall thickness and/or enhanced cross-linking within the silicate framework. However, it is important to choose the right Si/Al ratio for the incorporation of aluminum. When too much Al is incorporated, disruptions in the framework and collapse of pores and channels occur. According to Chen (1999), the advantage of post-synthesis grafted samples is better thermal stability. A side effect of aluminum incorporation is the loss of electroneutrality of the structure. Every change of tetravalent Si^{4+} ions by trivalent Al^{3+} ions creates a negative overcharge. Aluminum atoms are counterbalanced by protons creating acidic functional groups and sites for ion exchange on the surface (Weckhuysen, B.M., 2000).

- **Acidity of silica supports and its modification**

Pure siliceous MCM-41, SBA-15 and silicas have no Brönsted acidity. Brönsted acid sites can be generated by substitution of Si by Al by in-situ synthesis or by post synthesis Al-grafting (Xu, 2004). As presented in Chmielarz (2011), the modification of silica materials with aluminum resulted in the formation of acidic Brönsted as well as Lewis sites. To differentiate Brönsted and Lewis acidity, acetonitrile CH_3-CN is a good probe molecule. Higher deposition of Al created stronger Brönsted acidity compared to lower loading (Collart, 2001). However, the created alumina clusters did not promote the formation of Brönsted groups which are preferential for acid catalysis

(Collart, 2003). The total acidity created at the surface can be determined by titration with gaseous ammonia. Generally, the adsorption of ammonia occurs on weak (100–200 °C), moderate (200–350 °C) and strong acid sites (350–500 °C) (Karásková, 2010). For a similar concentration of aluminum, the total acidity of samples with Al-deposited and Al-incorporated was comparable as presented by Collart (2001). In contrary, the total acidity of the post-synthesis grafted samples was lower than the one at those samples prepared by direct hydrothermal alumination according to Chen (1999). The preferred sites for physisorption of ammonia on silica are expected to be hydroxyl groups. Considering the ammonia chemisorption, it proceeds by the reaction with siloxane Si-O-Si as well as hydroxyl Si-OH groups on the silica surface (Zamani, 2009).

3.2.5 Comparison of MDD with other methods

The first step is the choice of an appropriate support material. Then the principal technique of catalyst preparation involves: the fixation (e.g. by precipitation, impregnation, grafting or vapor deposition) and the activation step (by calcination or extraction).

The activation of the surface is preferential for surface reactions (such as catalysis, sorption and ion exchange) in comparison with the incorporation of heteroelements to the silicate framework. The activation preserves the homogeneity of inner framework and its stability (Collart, 2003). A wide range of methods has been developed in order to activate support materials by compounds such as organics, enzymes, metals and metal oxides. One of the most common methods is the impregnation with solutions of precursor salts.

The steps to prepare a catalyst by the impregnation technique are:

- The support undergoes a thermal treatment to clean its surface, without modifying its physicochemical properties;
- The support is in contact with a solution of a thermally unstable precursor salt which contains the compound to impregnate the support;
- After drying and calcination steps, the oxide metal particles remain on the support material.

The disadvantage of impregnation is long duration of deposition, uncontrolled distribution of species and the formation of large crystalline clusters on the surface (Urraca, 2006).

As presented by Chmielarz (2006), catalysts obtained by MDD method are more active and selective than catalysts prepared by the impregnation technique. The advantage of grafting (such as MDD method) is high degree of metal dispersion, use of non-aqueous solvents. The disadvantage is quite low loading on the support surface, use of toxic solvents (e.g. toluene) and release of toxic products.

The main difficulty in comparing various studies is that even when the same synthesis method is used, the reproducibility of some methods is difficult. In addition, the crystallinity, surface area and porosity features of the supports can vary significantly.

3.3 Catalytic activity

3.3.1 N_2O decomposition and reduction

- **Environmental issue of nitrous oxide and methods of its abatement**

The N_2O catalytic decomposition (Eq. 7) has been widely studied in the last four decades because this simple reaction was often chosen as the test reaction to find a correlation between structural and catalytic properties (Christopher, 1991).

$$N_2O \rightarrow N_2 + ½\ O_2 \quad (7)$$

Recently, the attention of N_2O is paid to its environmental effects such as the global warming and the destruction of stratospheric ozone layer. The decomposition of nitrous oxide has been studied as a possible method for abatement of the N_2O emissions in waste gases, e.g., from nitric acid plants, which have been indicated as the greatest industrial source of anthropogenic N_2O emissions (Pérez-Ramírez, 2003).

Several positions are possible for N_2O abatement in HNO_3 production plants: (i) high temperature homogeneous decomposition of N_2O downstream the ammonia burner (Galle, 2001, Watzenberger, 2001), (ii) high temperature catalytic decomposition situated immediately downstream of the ammonia burner (Granger, 2006, Ivanov, 2009, Schumacher, 2004) and (iii) low temperature catalytic N_2O decomposition upstream or downstream of the tail-gas expander and the NO_x emissions reduction technology ($DeNO_x$) (Schwefer, 2005, Hamon, 2007, Pieterse, 2008). While homogeneous N_2O decomposition requires a new design of the ammonia oxidation unit, catalytic decomposition is a cost-efficient process option easily applicable in any existing plant. Therefore, the catalytic N_2O decomposition has been intensively studied by many academic institutes and research teams. Regardless, it is still problematic to find a catalyst with sufficient activity and stability in real off-gas conditions because of water, oxygen and NO_x inhibition effect (Kapteijn, 1996). In this study, the main focus is on low-temperature ($\leq$ 450 °C) catalytic N_2O decomposition. It was found that catalysts containing rhodium or cobalt have been the most active among all tested catalysts (Kapteijn, 1996).

The mechanism of N_2O catalytic decomposition can be simply described by Eqs. 8–10. During the chemisorption of N_2O on the catalyst surface (Eq. 8), the active sites act as electron donors into the N_2O antibonding orbital. The desorption of O_2 from the catalyst surface is connected with transfer of electrons back to the active sites (Eqs. 9, 10). It is known as the rate determining step of N_2O

decomposition (Chmielarz, 2011). Therefore, the adsorption of N_2O and the desorption of O_2 are relatively easy in the presence of transition metals in two valence states, such as Co^{2+}/Co^{3+}, Rh^{+}/Rh^{3+} (Obalová, 2006). Transition metals possess non-paired d-level electrons which play a key role in catalytic behavior.

$$N_2O + * \rightarrow N_2 + O* \quad (8)$$

$$2O* \leftrightarrow O_2 + 2* \quad (9)$$

$$O* + N_2O \rightarrow N_2 + O_2 + * \quad (10)$$

- **Types of catalysts**

The range of catalytically active transition metal species on different supports for the decomposition of N_2O was widely studied (Chmielarz, 2005, Drago, 1997, Haber, 2008, Kawi, 2001). Supported oxides are better due to higher dispersion by combination with the large specific surface area of supports. Their behavior is compatible with the behavior of pure oxides. For instance, the activity of transition metals in spinels was in the order Co > Ni, Cu > Fe > Mn > Cr whereas the activity order in the zeolite ZSM-5 was Rh, Ru > Pd > Cu > Co > Fe > Pt > Ni > Mn (Kapteijn, 1996).

Recently, several papers dealing with the catalytic performance of mesoporous silica materials modified with rhodium in the N_2O decomposition have been published (Du, 2008, Hussain, 2012, Chmielarz, 2010, Piumetti, 2015, Xu, 2004). In the study of Hussain et al. (2012), rhodium was deposited on ordered mesoporous silica materials (namely MCM-41, SBA-15 and KIT-6) by different methods (ion-exchange, impregnation, precipitation and grafting). The temperatures at 50 % of N_2O conversion in an inert gas for MCM-41 impregnated with 1 wt% Rh (T_{50} = 396 °C) and for the conventional SBA-15 impregnated with 1 wt% Rh (T_{50} = 400 °C) were comparable (GHSV = 26500 h^{-1}). SBA-15 as the catalyst support for rhodium was used as well by Du et al. (2008). SBA-15 was impregnated by rhodium to obtain its concentration of 0.93–1.03 wt% and showed T_{50} from 372 to 447 °C (GHSV = 19000 h^{-1}) depending on rhodium precursors. Other silica supports than SBA-15, such as MCM-41, KIT-6, MCF, were used by Piumetti and co-authors (2015). The highest activity showed 0.9 wt% Rh-MCF (T_{50} = 335 °C at GHSV = 17 000 h^{-1}) reflecting the important role of 3D porous structure. The values of T_{50} for 1.2 wt% Rh-MCM-41 (T_{50} = 405 °C) and 1.4 wt% Rh-SBA-15 (T_{50} = 403 °C) were comparable.

The possible industrial application of mesoporous silica supports modified with Rh presented Hussain et al. (2014). The optimized Al-KIT-6 and Al-SBA-15-S supported Rh catalysts were deposited on the cordierite monolith showing a good catalytic activity, even in the presence of O_2, CO and H_2O.

- **Influence of aluminum on catalytic activity**

Aluminum was presented as an element generating acid sites by substitution of Si by Al in the structure of SBA-15, enhancing dispersion and stability of metals (such as Fe, Ru or Rh) on silica surface (Xu, 2004). The catalyst with 1 wt% Rh introduced by impregnation on SBA-15 grafted with aluminum exhibited slightly higher catalytic activity (T_{50} = 420 °C) than the catalyst with 1 wt% Rh impregnated on unmodified SBA-15 (T_{50} = 425 °C) at GHSV = 47368 h^{-1}. In agreement with this, Chmielarz et al. (2011) reported higher catalytic activity for Al-SBA-15 grafted with 0.89 wt% Rh (T_{50} = 380 °C) in comparison with SBA-15 grafted with 1.1 wt% Rh (T_{50} = 400 °C) at GHSV = 12000 h^{-1}.

It was reported by Rivallan and co-authors (2009) that the higher catalytic activity observed in the presence of aluminum is not due to a substantial decrement of the activation energy of the rate-determining step of N_2O decomposition. Another role of aluminum was analyzed by infrared spectroscopy on Fe-zeolites and Fe-silicalites. The N_2O molecules were weakly adsorbed on strong Brønsted sites by hydrogen-bonding interaction on the Fe-zeolite with the Si/Al ratio = 40 whereas there was no such interaction on the Fe-silicalite. In the study of Yakovlev et al. (1999) by the density functional calculations, it was demonstrated that Lewis sites containing aluminum are unlikely to decompose N_2O molecules since the formation of a weak Al-O bond does not compensate the rupture of N-O bond. Therefore, the active sites for N_2O decomposition are transition metals in different oxidation states.

3.3.2 CO oxidation

- **Environmental issue of carbon monoxide and methods of its abatement**

High amounts of carbon monoxide are emitted to the air mainly from transportation, power plants, industrial processes and domestic activities. Carbon monoxide is a precursor of ground-level ozone which can cause serious respiratory problems due to its high affinity with hemoglobin. It is a highly flammable gas, however, homogeneous CO combustion in polluted air (50–50 000 ppm) at the ambient conditions is impossible. It is also not very soluble in water. Therefore, the catalytic oxidation of CO into CO_2 (Eq. 11) is necessary for its abatement.

$$CO + ½\ O_2 \rightarrow CO_2 \quad (11)$$

The reaction of CO oxidation over unsupported platinum occurs according to Langmuir-Hinshelwood mechanism (Eqs 12–14), as reported by Engel and Ertl (1979).

$$CO(g) + Pt(surf) \rightarrow CO\text{-}Pt(surf) \quad (12)$$

$O_2(g) + Pt(surf)\text{-}Pt(surf) \rightarrow 2\ O\text{-}Pt(surf)$ (13)

$CO\text{-}Pt(surf) + O\text{-}Pt(surf) \rightarrow CO_2(g) + Pt(surf)\text{-}Pt(surf)$ (14)

The determining step of the reaction is the adsorption of CO and O_2 and their adsorption is different on the surface of noble metals. When CO is first adsorbed (Eq. 12), the O_2 adsorption is more difficult because O_2 molecule should find a pair of adjacent metal site (Eq. 13). Opposite to this, the O_2 adsorption is not supposed to be inhibited by the CO adsorption on cobalt oxides as reported by Thormählen et al. (1999).

For CO oxidation over cobalt oxides, Mars–van Krevelen mechanism has been proposed (Royer, 2011), Eqs 15–18:

$CO(g) + Co^{3+}(surf) \rightarrow OC\text{-}Co^{2+}(surf)$ (15)

$\frac{1}{2}\ O_2(g) + Co\text{-}Co(surf) \rightarrow Co\text{-}O\text{-}Co(surf)$ (16)

$OC\text{-}Co^{2+}(surf) + Co\text{-}O\text{-}Co(surf) \rightarrow (CO_2)\text{-}Co^{3+}(surf) + Co\text{-}Co(surf)$ (17)

$(CO_2)\text{-}Co^{3+}(surf) \rightarrow CO_2(g) + Co^{3+}(surf)$ (18)

Most of researchers assume that CO adsorbs on Co^{3+} sites of the Co_3O_4 surface (Eq. 15) abstracting the surface oxygen coordinated with three Co^{3+} cations. The partially reduced cobalt site as Co^{2+} cation with a neighboring oxygen vacancy (Eq. 17) is re-oxidized by a gas-phase oxygen molecule to the active Co^{3+} site (Eq. 18), (Xie, 2009). The others have reported that CO would be adsorbed on Co^{2+} sites, so that active oxygen species would be adsorbed on Co^{3+} sites concluding that a specific ratio between Co^{2+} and Co^{3+} is required. As reported by Lin et al. (Lin, 2003), two kinds of O species can participate in CO oxidation, either binuclear specie such as superoxide O_2^- adsorbed on CoO_x or O anions of cobalt spinel structure.

- **Types of catalysts**

The exceptional activity of noble metals (such as Au, Pt, Pd, Rh) for the catalytic reaction of CO oxidation has been widely described. However, due to the increasing price of noble metals, the interest is paid to the use of other transient metal oxide (such as Co, Cu, Ni, Cr) catalysts (Royer, 2011).

Activities in CO oxidation of different unsupported cobalt oxide catalysts were investigated (Yu Yao, 1974, Lin, 2003, Xie, 2010). The coexistence and a good balance between Co^{2+}-Co^{3+} ion pairs was reported as essential for the optimal catalytic activity in CO oxidation. Those oxides containing only Co^{3+} or the ion pairs Co^{3+}-Co^{4+} would be much less active. Another important

parameter is the cluster size of Co_3O_4 having a great impact on Co^{3+}/Co^{2+} ratio of the spinel structure.

Cobalt oxides on alumina Al_2O_3 can be very active catalyst for CO oxidation at low temperature. The cobalt oxide CoO_x supported on Al_2O_3 was the most active one among other supports (SiO_2, TiO_2) with T_{50} = 285 °C (5 wt% Co, GHSV = 2500 h^{-1}). However, the impregnation of acidic cobalt salts on alumina can cause a strong interaction with the formation of cobalt aluminate and decrease in activity (Wang, 2006). This effect would be prevented by using basic precursor salts. The surface reaction between adsorbed CO and O molecules occurred even below room temperature on pre-oxidized CoO_x/Al_2O_3 catalyst, however, carbonates were formed and blocked the surface on pre-reduced catalyst (Thormählen, 1999). Silica can avoid strong interactions with cobalt oxide; on the other hand, it may reduce the thermal stability of silica-supported catalysts. Thermal resistance was improved by inserting CoO_x into SBA-15 structure (Xu, 2006). The promising activity showed Co_3O_4 clusters inserted in the mesoporous SBA-15 (T_{50} equaled to 180 °C at GHSV = 20000 h^{-1} for Co-SBA-15 with the Co/Si ratio = 0.35) as reported by Lopes (2007). The presence of CoO_x on Au/SiO_2 or Au/SBA-15 promoted the catalytic activity of CO oxidation even at ambient temperature (Qian, 2007, Xu, 2006).

4 EXPERIMENTAL METHODS

4.1 Synthesis of mesoporous silica supports

4.1.1 MCM-41

MCM-41 material (further designated as MCM) was prepared by a direct interaction between an ionic, positively charged surfactant and a negatively charged silica source in a basic environment. The synthesis of MCM was performed according to Liu (2003) by using cetyltrimethylammonium bromide (99 % CTMABr, $C_{16}H_{33}(CH_3)_3NBr$, Sigma-Aldrich), aqueous ammonia (30 % NH_4OH, Acros Organics), tetraethyl ortosilicate (98 % TEOS, $Si(OC_2H_5)_4$, Sigma-Aldrich) and H_2O.
First, 5.45 g CTMABr was dissolved in 107.90 cm^3 of deionized H_2O and 34.30 cm^3 of aqueous ammonia by mixing for 15 min. Then 11.06 cm^3 TEOS was added and stirred for 2. The white precipitate was collected by filtration and washed with deionized H_2O. After drying at ambient air for 3 days, the samples were calcined at 550 °C with the heating rate of 1 °C.min^{-1} for 6 h at ambient air.
The batch molar ratio was 1 $Si(OC_2H_5)_4$: 0.3 $C_{16}H_{33}(CH_3)_3NBr$: 11 NH_3 : 144 H_2O (Liu, 2003).

4.1.2 SBA-15

SBA-15 material (further designated as SBA) was made by use of polymeric based surfactants that interact with the positively charged silica source in acid medium. SBA was synthesized as described in Meynen (2009) in acidic conditions using the template triblock copolymer poly (ethylene oxide)-poly (propylene oxide)-poly (ethylene oxide) ($EO_{20}PO_{70}EO_{20}$, P123, Sigma-Aldrich), hydrochloric acid (37 % HCl, Acros Organics), tetraethyl ortosilicate (98 % TEOS, $Si(OC_2H_5)_4$, Acros Organics) and H_2O.
The mass 8 g of P123 was added to 260 ml of deionized H_2O and 40 ml of HCl. Then the mixture was stirred until complete dissolution (for about 15 h). After that 17.5 ml of TEOS was added and stirred for 7.5 h at 45 °C. The ageing without stirring lasted for 15.5 h at 80 °C. Finally the mixture was cooled down, filtrated and washed by deionized H_2O (3 x 25 ml) and dried. The samples were calcined at 550 °C with the heating rate of 1 °C.min^{-1} for 6 h at ambient air.
The batch molar composition was 1 $Si(OC_2H_5)_4$: 0.018 $EO_{20}PO_{70}EO_{20}$: 6.12 HCl : 183 H_2O.

4.1.3 Al-MCM-41

Two approaches were applied to synthesis MCM-41 with aluminum incorporated within the silica structure.

Al-MCM-41 further designated as Al-MCM[a] was synthesized according to Stöcker (Meynen, 2009). Tetradecyltrimethylammonium bromide (99 % TDTMABr, $C_{14}H_{29}(CH_3)_3NBr$, Sigma-Aldrich), sodium aluminate ($NaAlO_2$, 54 % Al_2O_3, 41 % Na_2O, Riedel-de Haën), sodium silicate 5 hydrate ($Na_2SiO_3 \cdot 5H_2O$, 8.9 % Na_2O + 28 % SiO_2, VWR BDH) and sulfuric acid (10 % a 50 % H_2SO_4, Merck p.a. 95–97 %) were used. The 15 g of template TDTMABr was dissolved in 95 g of H_2O and stirred. The sodium aluminate (0.43, 0.21 or 0.14 g, depending on Si/Al ratio equal to 20, 40, 60) was added and stirred for 2 h. Sodium silicate of 18.7 g was added under stirring, followed by 5.6 g of 10 % sulphuric acid. The mass of 15 g of H_2O was added and the entire solution was stirred for 30 min. The pH was adjusted to 10 with 50 % of sulphuric acid. The final solution was transferred to teflon-lined autoclaves and heated for 24 h at 100 °C. After that the samples were filtered, washed with deionized H_2O and dried at ambient air for 3 days. The product was calcined at 550 °C with the heating rate of 5 °C.min^{-1} for 7 h in ambient air.
The batch molar composition was 1 $Na_2SiO_3 \cdot 5H_2O$: 0.06/0.03/0.02 $NaAlO_2$: 0.51 $C_{14}H_{29}(CH_3)_3NBr$: 69 H_2O.

Al-MCM-41 further designated as Al-MCM[b] was prepared according to Poladi (2002) by dissolving 0.8 g NaOH and 1.2 g cetyltrimethylammonium bromide (CTABr, $C_{16}H_{33}(CH_3)_3NBr$, Sigma-Aldrich) in 64 ml of deionized H_2O. After dissolution, 7.7 g of TEOS ($Si(OC_2H_5)_4$, Acros Organics) was added to the mixture. 0.74 g of aluminum sulphate ($Al_2(SO)_4.16\ H_2O$, Sigma Aldrich, Si/Al ratio equal to 32) was dissolved in 20 ml of deionized H_2O in a separate beaker and added to the reaction mixture and the stirring continued for 105 min. The mixture was heated at 80 °C for 20 min and stirred. After cooling to room temperature, the resulting mixture was stirred overnight. Finally, it was transferred to autoclave for crystallization at 150 °C for 6 h. Samples were collected by filtration, dried and calcined at 550 °C at the heating rate 2 °C.min^{-1} for 12 h.
The batch molar composition was 1 $Si(OC_2H_5)_4$: 0.03 $Al_2(SO)_4.16\ H_2O$: 0.54 NaOH : 0.09 $C_{16}H_{33}(CH_3)_3NBr$: 126 H_2O.

4.2 Deposition of metals by MDD

The catalysts with different loadings of metals (Al, Co and Rh) were prepared by MDD method on four prepared different ordered mesoporous silica materials (MCM, Al-MCM[a, b] and SBA). The silica supports calcined at 550 °C for 6 h in the ambient air were dried overnight in an oven at 200 °C in the air atmosphere. The appropriate amounts of $Al(acac)_3$, $Co(acac)_2$ or $Rh(acac)_3$ according to previously reported and expected mass concentrations of metals were dissolved in zeolite dried toluene. Afterwards, the calculated amounts of silica supports were added to 100 ml of toluene and the solution was stirred for1 h at room temperature. After the reaction, the modified supports were filtered off, washed three times with toluene (1 washing cycle: 25 ml of toluene per 1 g of

support) and dried under vacuum at the room temperature. Finally, the samples were calcined in air at 550 °C with the heating rate of 1 °C.min^{-1} in the period of 6 h (Fig. 6). After the deposition of aluminum by MDD, the same procedure of MDD followed for the deposition of cobalt or rhodium. In detail, the support MCM grafted by aluminum calcined at 550 °C was dried in an oven at 200 °C prior to MDD and finally cobalt or rhodium was grafted.

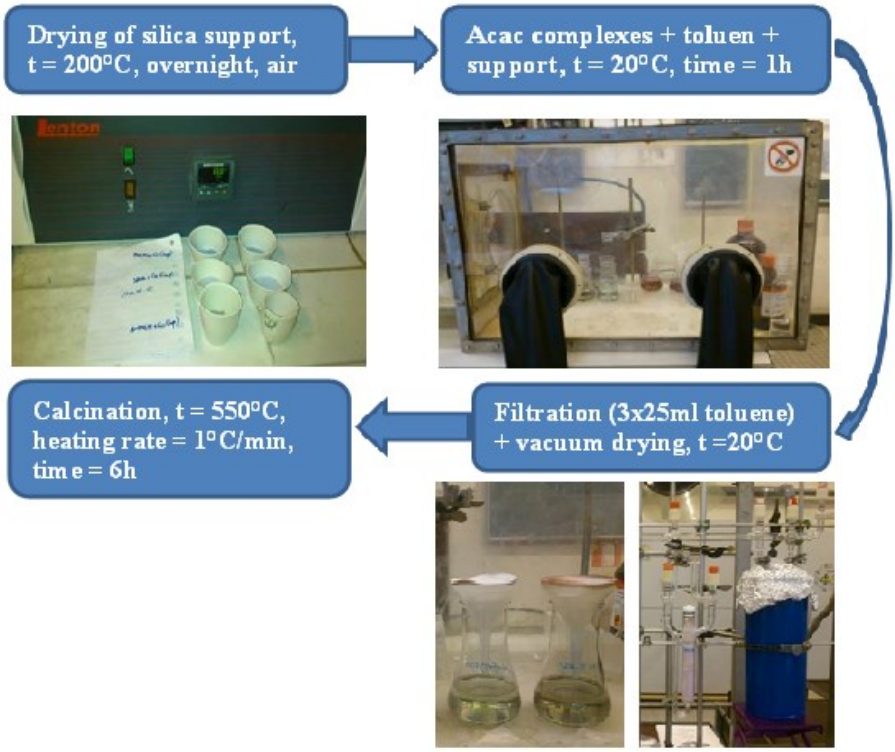

Fig. 6. The scheme of MDD method with the applied laboratory equipment.

The designations of prepared samples are:

i) MCM+Co, resp. MCM+Rh(wt%), meaning that cobalt, resp. rhodium, were deposited by MDD method on MCM; MCM+Al+Co, resp. MCM+Al(wt%)+Rh(wt%), meaning that aluminum and cobalt, resp. rhodium, were deposited by MDD method on MCM;

ii) Al-MCM+Co, resp. Al(wt%)-MCM+Rh(wt%), meaning that cobalt, resp. rhodium, was deposited by MDD method on Al-MCM;

iii) SBA+Co, resp. SBA+Rh(wt%), meaning that cobalt, resp. rhodium, were deposited by MDD method on SBA and SBA+Al+Co meaning that aluminum and cobalt were deposited by MDD method on SBA.

4.3 Characterization of catalysts

The first characteristic that needs to be known after the synthesis of catalyst support is its structure and texture properties. After the activation of support, its chemical composition and active metal concentrations need to be defined. In correlation with the activity of catalyst, the coordination and oxidation states of active metals are studied. The size and distribution of metal nanoparticles and their aggregates on the catalyst surface are described as well as the reactivity of catalyst defined by its reducibility and acid-base properties.

- **Chemical composition and metal concentration: Electron probe microanalysis (EPMA), electron dispersive X-ray (EDX), X-ray photoelectron spectroscopy (XPS) and atomic absorption spectroscopy (AAS)**

The surface metal loadings were determined by microprobe analysis using JEOL JXA 733 Super Probe electron probe microanalyzer (EPMA) at the Laboratory of Adsorption and Catalysis, University of Antwerp or an electron dispersive X-ray (EDX) analyzer XL30 Phillips at the Nanotechnology Centre, VŠB-TU Ostrava.

In the case of rhodium grafted ordered mesoporous silica materials, X-ray photoelectron spectra (XPS) of the catalysts were measured on a Prevac photoelectron spectrometer equipped with a hemispherical VG SCIENTA R3000 analyzer at the Department of Chemical Technology, Jagiellonian University, Krakow. The samples were placed in a holder of 6 mm in diameter and 0.3 mm in depth. XPS spectra are obtained by irradiating a solid surface with a beam of X-rays while simultaneously measuring the kinetic energy and electrons that are emitted from the top (1–10 nm) of the sample. The areas and binding energies of Si 2p, O 1s, Rh $3d_{5/2}$, Al 2p and C 1s photoelectron peaks were investigated.

The metal composition in the whole sample volume was determined by atomic absorption spectroscopy (AAS) using a Spectr AA880 (Varian) at the Institute of Chemical Process Fundamentals of the ASCR, v.v.i., Prague and the Department of Solid State Chemistry, University of Chemistry and Technology, Prague. For AAS analysis of cobalt, the catalysts were dried, dissolved in 3 ml HCl and heated up. Before AAS analysis of rhodium, the catalysts were dried at 105 °C, dissolved under microwave radiation in mixture of concentrated acids (3 ml HNO_3, 3 ml H_2SO_4 and 1ml HF) and diluted by deionized H_2O to 25 ml.

- **Texture properties of catalysts: N_2 sorption**

Textural properties of the samples were determined by nitrogen sorption measurements at -196 °C using a QuadraSorb SI MP Station at the Laboratory of Adsorption and Catalysis, University of Antwerp. Prior to the measurements, the samples were degassed under vacuum at 200 °C for 16 h.

The mesopore diameter was determined from the maximum of pore size distribution curve of BJH method. The microporosity was evaluated by t-plot method using de Boer for oxidic silicas.

- **Bonding mechanism of acetylacetonate complexes: infrared spectroscopy (DRIFT), thermogravimetric analysis (TGA)**

The samples were measured on the infrared spectroscope Nicolet 6700 with DTGS detector (bench: gain 8, aperture 100, optical velocity 0.63, no. of scans 200) Laboratory of Adsorption and Catalysis, University of Antwerp. KBr was used as non-adsorbing matter in ratio 98:2 with the sample. The spectra were evaluated in the program OMNIC.

Thermogravimetric analysis measurements were performed on a Mettler Toledo TGA/SDTA851e Laboratory of Adsorption and Catalysis, University of Antwerp. Samples were heated from 30°C to 550°C with a heating rate of 5°C.min^{-1} under an oxygen flow (60–70 ml.min^{-1}).

- **Nature and structure of catalysts: X-ray diffraction (XRD), infrared spectroscopy (ATR-FTIR), Raman spectroscopy, scanning electron microscopy (SEM)**

The XRD patterns in *2θ* range from 0.5 to 5° were recorded under CuKα irradiation (λ = 1.540598 Å) using the Ultima IV RIGAKU diffractometer at the Nanotechnology Centre, VŠB-TU Ostrava. Measurements were carried out in the reflection mode, powder samples were pressed in a rotational holder, goniometer with the Bragg-Brentano geometry in *2θ* range from 0.5 to 5°, step size 0.01° (scintillation counter). The XRD patterns in *2θ* range from 10 to 80° were recorded under CoKα irradiation (λ = 1.789 Å) using the Bruker D8 Advance diffractometer (Bruker AXS) equipped with a fast position sensitive detector VÅNTEC 1. Measurements were carried out in the reflection mode, powder samples were pressed in a rotational holder, goniometer with the Bragg-Brentano geometry in 2 θ range from 5 to 60°. Phase composition was evaluated using database PDF-2 Release 2011 (International Centre for Diffraction Data).

Mid-infrared spectra (4000–400 cm^{-1}) were measured by Nicolet 6700 FT-IR spectrometer (Thermo Nicolet, USA) at the Nanotechnology Centre, VŠB-TU Ostrava using single reflection ATR technique with a diamond crystal and 32 scans.

Raman spectra were measured by Smart Raman Microscopy System XploRA™ (HORIBA Jobin Yvon, France) at the Nanotechnology Centre, VŠB-TU Ostrava. Raman spectra were acquired with 532 nm excitation laser source, and 2400 groove.mm^{-1} grating in the range 150–1100 cm^{-1}. The intensity of the laser beam was set on 10 % of the laser signal. As the Raman system is coupled with a microscope, the powder samples were measured with a 50x objective of the optical microscope Olympus BX41/51. The acquisition time was set at 240 s and 600 s with

2 accumulations depending on sample signal. Raman spectra were acquired at each of at least 5 points.

The catalysts morphology was investigated by a scanning electron microscope XL30 Phillips at the Nanotechnology Centre, VŠB-TU Ostrava. It was operating at accelerating voltage of 25 kV, using the detector ETD and the parameters mode SE, magnification 30 000x and scale 4 μm.

- **Coordination and oxidation state of metal species: visible and ultraviolet spectroscopy (DR UV-Vis), Raman spectroscopy**

Diffuse reflectance UV–Vis spectra of the powder samples were recorded in the range 190–900 nm (11111–50000 cm^{-1}) at room temperature on the Cintra 303 equipped with a diffuse reflectance attachment at the Department of Physical Chemistry, University of Pardubice. The diffuse reflectance was recalculated to Kubelka-Munk function (Eq. 19), (Ewing, 2005).

$$f(R_\infty) = \left(\frac{1-R_\infty}{2 \cdot R_\infty}\right)^2 \tag{19}$$

- **Total surface acidity: temperature programmed desorption of ammonia (TPD-NH_3)**

The surface acidity of the rhodium catalysts was determined by temperature programmed desorption of ammonia in a fixed bed microreactor in AutochemII 2920 instrument equipped with a TCD detector at the Institute of Environmental Technology, VŠB-TU Ostrava. Prior to the TPD-NH_3 measurements, samples (50 mg) were outgassed in the flow of pure helium (50 $ml.min^{-1}$) at 500 °C for 60 min. Subsequently, the samples were cooled down to 100 °C and saturated at this temperature in the flow of 5 % NH_3/He (50 $ml.min^{-1}$) for 60 min. Then, the samples were purged in helium flow for 30 min to remove physisorbed ammonia. The desorption of chemisorbed ammonia was carried out in the temperature range of 100–500 °C with the heating rate of 20 $°C.min^{-1}$ in the flow of He (50 $ml.min^{-1}$).

- **Reducibility of metals: temperature programmed reduction by hydrogen (TPR-H_2)**

Temperature programmed reduction by hydrogen on cobalt catalysts was carried out on the powder samples (50 mg) of the grain 0.160–0.315 mm. The TPR runs were performed in the flow of 10 vol% H_2/Ar (50 $ml.min^{-1}$) with the heating rate 20 $°C.min^{-1}$in the temperature range 25–900 °C. Hydrogen concentrations were detected with a mass spectrometer Omnistar 300 (Pfeiffer Vakuum) at the Institute of Chemical Process Fundamentals of the ASCR, v.v.i., Prague.

Temperature programmed reduction by hydrogen on rhodium catalysts was proceeded on AutochemII 2920 at the Institute of Environmental Technology, VŠB-TU Ostrava. Prior to the TPR

experiments, the samples were outgassed in the flow of pure helium (50 ml.min^{-1}) at 500 °C for 60 min and afterwards oxidized in the flow of 10 vol% O_2/He (50 ml.min^{-1}) with the heating rate of 20 °C.min^{-1} in the temperature range 25–500 °C. The TPR runs were performed in the flow of 10 vol% H_2/Ar (50 ml.min^{-1}) with the heating rate 20 °C.min^{-1} in the temperature range 25–500 °C. The TPR experiments of silica supports were proceeded without the activation and oxidation prior to TPR measurements. Water vapor formed during TPR was captured in a cold trap. The hydrogen consumption was monitored on-line by a thermal conductivity detector (TCD) connected to the reactor outlet by a heated line.

- **Dispersion of metals on the surface: pulsed chemisorption of H_2**

The dispersion of rhodium on catalyst surfaces was determined by AutochemII 2920 at the Institute of Environmental Technology, VŠB-TU Ostrava on reduced samples by pulsed chemisorption of 10 vol% H_2/Ar in intervals 90 s by the loop volume 0.5 ml at the room temperature. The stoichiometric factor is assumed to be as Rh/H_2 ratio equaled to 2 according to literature (Nakai, 2003, Webb, 2003).

4.4 Catalytic tests

4.4.1 Experimental conditions

Catalytic tests were performed in an integral fixed bed stainless steel reactor of 5 mm internal diameter from the temperature 450 °C up to 210 °C for N_2O decomposition and from 450 °C up to 120 °C for CO oxidation and atmospheric pressure. The catalyst bed contained 0.1 g of the sample with the particle size of 0.160–0.315 mm. The weight hourly space velocity (WHSV) of 60 000 l.h^{-1}.kg^{-1} (GHSV 15648 h^{-1}) corresponding to the total flow 100 ml.min^{-1} was applied. Before each run, the catalyst was pre-treated by heating it in the nitrogen flow at 450 °C and maintained at this temperature for 1 hour. Then the feed gases were added and the reaction was stabilized for 7 hours. The feed introduced to the reactor contained (i) 0.1 mol% N_2O in nitrogen (for N_2O decomposition), (ii) 0.1 mol% N_2O and 0.1 mol% CO in nitrogen (for N_2O reduction), (iii) 0.1 mol% N_2O, 0.1 mol% CO and 5 mol% O_2 in nitrogen (for N_2O reduction in the presence of oxygen), (iv) 0.1 mol% N_2O, 5 mol% O_2, 200 ppm NO and 1.8–2.3 mol% of water vapor in nitrogen (for N_2O decomposition in the presence of inhibiting compounds) and (v) 0.1 mol% CO with 5 mol% O_2 in nitrogen (for CO oxidation).

4.4.2 Experimental set-up and analytical instrumentation

The applied apparatus containing the laboratory reactor placed in the furnace, the gas mass flow rate controllers (Aaborg, Elmet), gas bottles (N_2, O_2 and He from the central gas substation; 3 mol% N_2O/N_2, 1 mol% NO/N_2, 2 mol% CO/He) and the refrigerator for condensation of water vapors are shown in Fig. 7.

Infrared spectrometer SICK S800 was used for N_2O analysis and the calibration gas mixtures 97 ppm N_2O/He (SIAD Czech spol. s.r.o.) and 995 N_2O/He (SIAD Czech spol. s.r.o.) was used for two-point calibration. IR spectrometer Ultramat 6 with NO_2/NO converter was utilized for NO analysis and it was calibrated by the calibration gas mixture 777 ppm NO/N_2 (SIAD Czech spol. s.r.o.) for one-point calibration.

The gas chromatograph with thermal conductivity detector (GC-TCD) (Agilent Technologies 7890A) and the chromatographic columns (i) HP-PLOT MoleSieve 5A (dimensions: 30 m x 530 μm x 25 μm, oven program: 80 °C for 4 min then 50 °C/min to 250 °C for 4 min) and (ii) GS-Carbonplot (dimensions: 30 m x 320 μm x 3 μm, oven program: 40 °C for 7 min then 75 °C/min to 250 °C for 3 min) were applied for the N_2O analyses. The GC-TCD (Agilent Technologies 7890A) with the chromatographic column HP-PLOT MoleSieve 5A (dimensions: 30 m x 530 μm x 25 μm, oven program: 80 °C for 4 min then 40 °C/min to 250 °C for 3 min) was used for the analysis of CO concentrations. The software Agilent GC Chemstation was utilized for the data evaluation.

The concentrations of CO and CO_2 were detected by Fourier transform infrared (FTIR) analyzer (Nicolet Antaris IGS, Thermo Scientific). The spectral resolution was 0.5 cm^{-1}, the length of metal cell was 10 meters with ZnSe beam splitter and the type of detector was MCT-A.

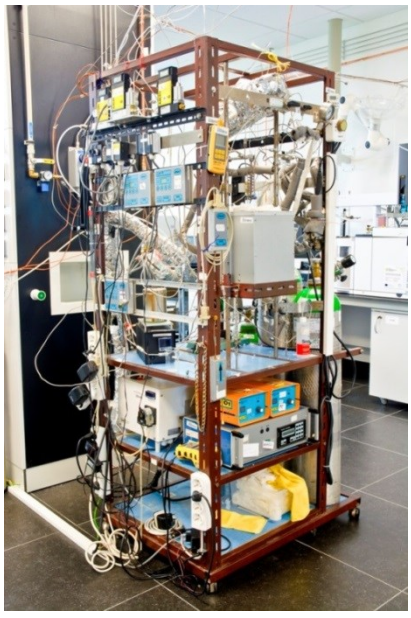

Fig. 7. The photo of apparatus applied for catalytic tests.

4.4.3 Elimination of macro-kinetic properties

For the comparison of catalysts, it is important to eliminate macro-kinetic properties of experiments and to focus on micro-kinetic properties of the catalysts. The catalytic reaction must be the slowest and the rate controlling step whereas mass and heat transfer must be fast steps. The laboratory reactor should have the parameters of isothermal tubular reactor with ideal plug flow at the constant pressure (Kapteijn, 1997).

The **ideal plug flow** can be expected according to the ratio D_t / d_p > 15, where D_t – internal diameter of reactor (mm), d_p – particle diameter (mm), therefore d_p should be smaller than 0.3 mm for the laboratory reactor of D_t = 5 mm.

It is important that the bed length of catalyst is much higher than the particle diameter for the **elimination of axial dispersion**, according to Eq. 20.

$$\frac{L_b}{d_p} > \frac{20}{Pe_p} \cdot \ln\left(\frac{1}{1-X}\right) \tag{20}$$

where L_b – bed length (mm), d_p – particle diameter (mm), Pe_p – Peclet number (-), and X – conversion of reactive gas (-).

As an example, the experimentally measured bed density of catalysts on basis of MCM is about 0.27 g.cm^{-3} and the calculated bed length of catalyst equals to about 19 mm for the diameter 5 mm of the reactor. The bed length was increased by addition of inert glass material (0.3 g) up to 29 mm. The value of Peclet number is equal to 0.5 for low Reynolds numbers. The conversions, for which the axial dispersion is possible to eliminate, should be below 0.9 for the limit value of particle diameter 0.315 mm and for the bed length 29 mm.

The maximal **adiabatic increase of temperature ΔT_{ad}** in the catalyst bed length was calculated according to Eq. 21:

$$\Delta T_{ad} = \frac{(-\Delta H_r) \cdot c_{A0}}{c_p \cdot \rho} \tag{21}$$

where ΔT_{ad} – adiabatic increase of temperature (K), ΔH_r – reaction heat (J.mol^{-1}), c_{A0} – inlet N_2O concentration (mol.m^{-3}), c_p – specific heat capacity of N_2 (J.kg^{-1}.K^{-1}), and ρ – density of N_2 (kg. m^{-3}).

The ΔT_{ad} value is estimated for nitrogen due to the low molar fraction of N_2O (1000 ppm of N_2O/N_2, specific heat capacity of N_2 at 450 °C = 1100 J.kg^{-1}.K^{-1}, density of N_2 at 450 °C = 0.47 kg.m^{-3}):

$$\Delta T_{ad} = \frac{14091 \cdot 0.017}{1100 \cdot 0.47} = 0.5K$$

The **pressure drop** ***Δp*** was calculated according to Ergun equation (Eq. 22, Fogler 1999):

$$\frac{p_1}{p_2} = (1 - \frac{2 \cdot \beta_0 \cdot L_b}{p_0})^{1/2} \tag{22}$$

where Δp – pressure drop (Pa), $\Delta p = p_1 - p_2$, β_0 – parameter (kg.s^{-2}.m^{-2}), $\beta_0 = \frac{G \cdot (1-\varepsilon)}{\rho \cdot d_p \cdot \varepsilon^3} \cdot \left[\frac{150 \cdot \mu \cdot (1-\varepsilon)}{d_p} + 1.75 \cdot G \right]$, G – superficial mass velocity (kg.s^{-1}.m^{-2}), ε – porosity (-), μ – dynamic viscosity (Poise), and p_0 – atmospheric pressure (Pa).

The total flow = 100 ml.s^{-1}, the reactor diameter = 5 mm, the particle diameter = 0.16 mm, and the catalyst bed length = 19 mm and the dynamic viscosity of N_2 at 450 °C = 3.5·10^{-4} P are known experimental parameters. The porosity of bed is estimated to be 0.5.

$$\frac{p_1}{p_2} = (1 - \frac{2 \cdot 350092 \cdot 0.019}{101325})^{1/2} = 0.993$$

It is estimated that the reactor operates in isothermal (the adiabatic increase of temperature equals to 0.5 K) and isobaric state (the pressure drop is 0.7 kPa).

The rate of catalytic reaction can be influenced by flow of reacting gases, particle size of catalyst and geometry of reactor, however, the aim is to avoid them. Four criteria of transport phenomena: i) external diffusion, ii) external heat transfer, iii) internal diffusion, and iv) internal heat transfer were calculated and the influence of transport phenomena on the reaction rate can be omitted for the reaction conditions as defined in Section 4.4.1 according to the experiments reported in literature (Obalová, 2003). For the calculation, it was presumed that the reaction of N_2O decomposition (Eq. 7) is the 1st order reaction.

4.4.4 Calculations of conversion

The N_2O, resp. CO, concentration in steady state was used for determination of N_2O, resp. CO, conversion (X) according to Eq. 23 with the presumption that the total volumetric flow along the reactor is considered to be constant for low N_2O, resp. CO, concentration.

$$X = \frac{x^o - x}{x^o} \tag{23}$$

where X – conversion of gas molecules, x^o – gas mole fraction at the reactor inlet and x – gas mole fraction at the reactor outlet.

5 RESULTS AND DISCUSSION

5.1 Characterization of different silica supports

5.1.1 Textural properties

The shapes of all adsorption-desorption isotherms correspond to IV type isotherm (according to IUPAC classification), which is typical for mesoporous materials (Fig. 8). All prepared supports of MCM and Al-MCM[a, b] present a sharp inflection in the relative pressure range of 0.2–0.4 indicating mesopore filling and capillary condensation in mesopores. The isotherms of calcined SBA exhibit a sharp inflection at significantly higher relative pressure (p/p_0 = 0.65–0.8), which designate the uniform mesoporous structure of SBA with wider pore diameters compared to MCM. Total pore filling is apparent from the isotherms of MCM and SBA (at relative pressure p/p_0 = 0.99–1.0). The isotherms for Al-MCM[a] include a hysteresis loop (hysteresis H3) at higher relative pressures indicating the presence of disordered mesopores. A hysteresis loop (hysteresis H1) also appeared in the isotherm of SBA confirming cylindrical shape of pores.

Textural properties of the calcined silica supports used for aluminum, cobalt and rhodium grafting are presented in Table 1. Among the prepared silica materials, MCM has the highest surface area whereas SBA has the smallest surface area with the presence of micropores interconnecting the mesopore structure. Measured points of adsorbed volume were extrapolated by linear plot going through the origin of t-plot in the case of silica supports MCM and Al-MCM[a, b] (not shown). This fact corresponds to zero micropore volume and micropore area. The y-intercepts of linear t-plots were positive in the case of SBA supports (not shown) resulting in the presence of micropores. The syntheses of silica supports can be assumed as reproducible according to the values of textural properties presented in Table 1 (not shown for more Al-MCM[a,b] samples).

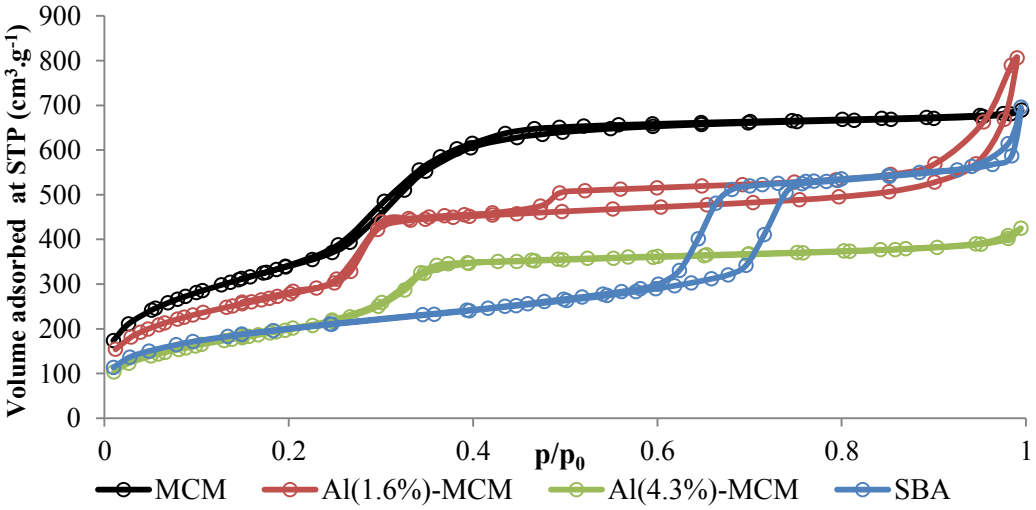

Fig. 8. Nitrogen adsorption-desorption isotherms of prepared supports, MCM[2], Al(1.6 %)-MCM[a], Al(4.3 %)-MCM[b] and SBA[2].

Table 1. Textural properties of silica supports applied for cobalt and rhodium grafting.

Sample	S_{BET} $m^2.g^{-1}$	S_{micro} $m^2.g^{-1}$	V_{total}* $cm^3.g^{-1}$	V_{micro} $cm^3.g^{-1}$	d_{pore} nm
MCM[1]	1271	-	1.10	-	2.7
MCM[2]	1259	-	1.07	-	2.7
MCM[3]	1144	-	1.00	-	2.5
Al(1.6 %)-MCM[a]	1011	-	1.25	-	2.5
Al(4.3 %)-MCM[b]	762	-	0.66	-	2.7
SBA[1]	633	196	0.92	0.11	5.4
SBA[2]	706	263	1.08	0.12	6.1
SBA[3]	625	231	0.85	0.10	5.6

[1, 2, 3] Designation of different batches of silica supports MCM and SBA.

[a, b] Designation of two different approaches in synthesis of Al-MCM.

* Total pore volume was defined at $p/p_0 = 0.99–1.0$.

Typical X-ray diffraction patterns of MCM, Al-MCM[a] and SBA show the 2D hexagonally structured pores (space group: p6m) at low angles (see Fig. 9). It typically contains three main reflection lines (d100, d110, and d200) at low angles. The values of d-spacings for MCM[2] are (100) = 3.61 nm, (110) = 2.08 nm, (200) = 1.80 nm; for Al(1.4 %)-MCM[a] are (100) = 3.60 nm, (110) = 2.08 nm, (200) = 1.81 nm; for Al(4.3 %)-MCM[b] are (100) = 3.96 nm, (110) = 2.27 nm, (200) = 1.96 nm and for SBA[2] are (100) = 9.19 nm, (110) = 5.39 nm, (200) = 4.69 nm. A broad maximum at 2θ about 25 ° corresponds to amorphous silica (Huo, 2014), see Fig. 10.

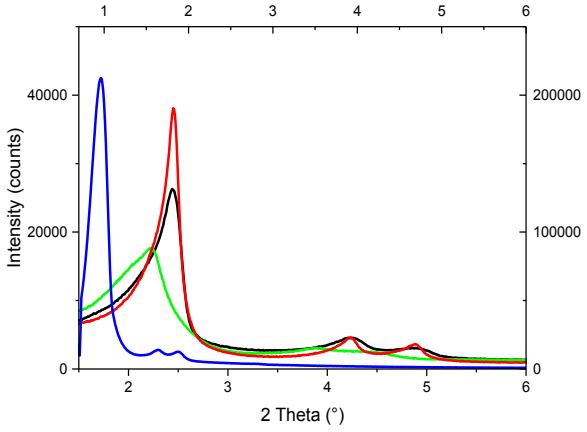

Fig. 9. XRD patterns of supports at low angles (2θ = 0.5–6 °), MCM[2] (black), Al(1.6 %)-MCM[a] (red), Al(4.3 %)-MCM[b] (green), SBA[2] (blue).

Note: Top x and right y axes corresponds to SBA.

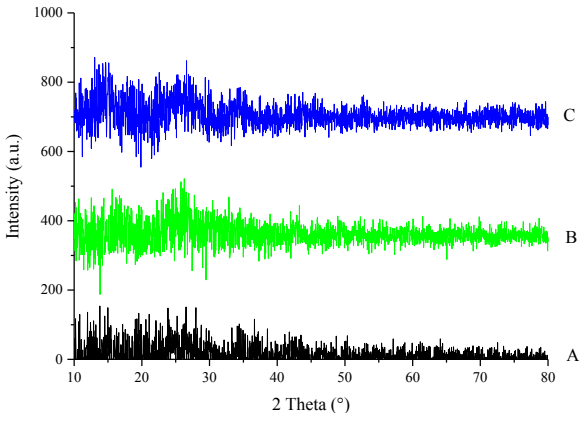

Fig. 10. XRD patterns of supports at high angles (2θ = 10–80 °), A) MCM[2], B) Al(4.3 %)-MCM[b], C) SBA[2].

5.1.2 Morphology

Figs. 11–13 from the scanning electron microscopy show that MCM forms more uniform and compatible particles in comparison with Al-MCM[a]. However, both silica materials form compact agglomerates consisting of individual spherical particles in comparison with SBA particles which have fiber-like morphology.

The surface defects are apparent in the SEM image of supports Al-MCM[a] (Fig. 12) and SBA (Fig. 13). As reported by Limnell et al. (2011), the surface of SBA contains more surface defects than MCM defined as the reason for stronger interaction of reactive molecules via hydrogen bonding into SBA than in MCM causing better chemical stability.

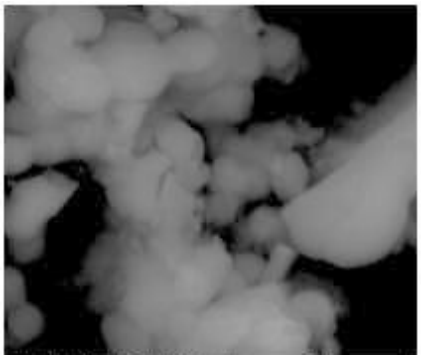

Fig. 11. SEM image of MCM.

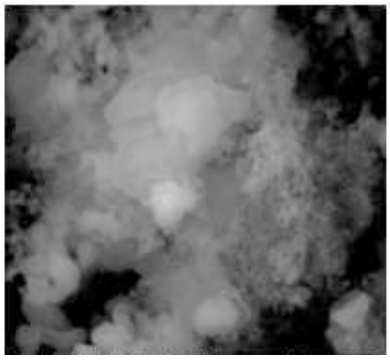

Fig. 12. SEM image of Al(1.6 %)-MCM[a].

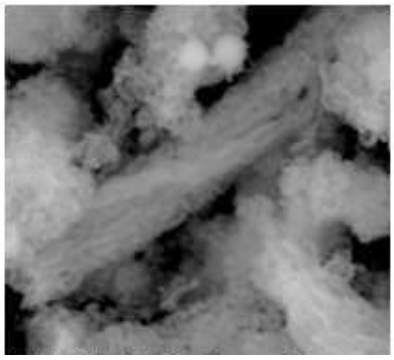

Fig. 13. SEM image of SBA.

5.1.3 Grafting of aluminum

To compare aluminum incorporated in the silica matrix Al-MCM[a] with the theoretical Si/Al ratio equals to 20, 40 and 60 and Al-MCM[b] with the theoretical Si/Al ratio 32, it was necessary to find the appropriate $Al(acac)_3$ loadings with the desired Si/Al ratios.

As reported by Collart (2001), the loading of 0.45 mmol Al/g MCM-48 showed a complete accessibility of the surface and well dispersion of aluminum. In another study of Al grafting by MDD, the concentration 0.4 mmol Al/g SBA-15 was equal to about 1 wt% of Al (Chmielarz, 2011). Therefore, the same loading of $Al(acac)_3$ complex was used as the initial concentration. Fig. 14 shows aluminum concentrations measured by EPMA and experimental Si/Al ratios in dependency on initial $Al(acac)_3$ loadings.

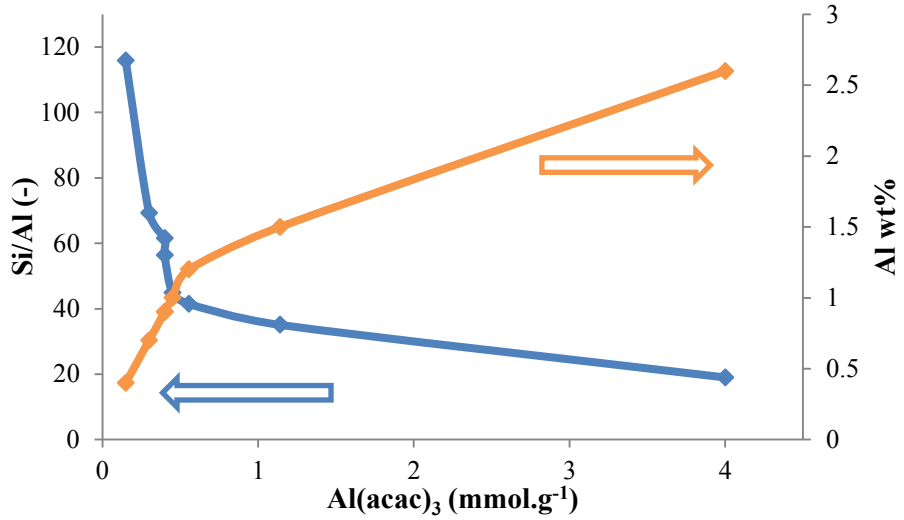

Fig. 14. Measured Al concentrations (orange) and defined Si/Al ratios according to elemental analyses (blue) in dependency on initial $Al(acac)_3$ loadings on MCM.

Theoretical Si/Al ratios 20, 40 and 60 according to batch compositions of Al-MCM[a] with the relevant initial $Al(acac)_3$ concentrations in solution and experimental Si/Al ratios are summarized in Table 2.

Table 2. Theoretical Si/Al ratios 20, 40 and 60 with relevant experimental Si/Al ratios, initial $Al(acac)_3$ concentrations and Al concentrations (in parentheses) on MCM measured by EPMA.

Sample	Si/Al (theor)	Si/Al(exp)	$Al(acac)_3$ $mmol.g_{support}^{-1}$
MCM+Al(2.6%)	20	19	4.0
MCM+Al(1.2%)	40	41	0.6
MCM+Al(0.9%)	60	62	0.4

The maximal loading capacity of Al according to applied Al precursor ($Al(acac)_3$) can be estimated by the simple calculation of monolayer capacity (Eq. 5). The variables in the calculation of monolayer capacity are: A_m ($Al(acac)_3$) = 0.89 nm^2, $Al(acac)_3$ was modelled by the program NWChem 6.3; S_{BET} = 1135 $m^2.g^{-1}$, the average value from the MCM supports applied for $Al(acac)_3$ grafting as presented in Fig. 14.

$$V_m = \frac{\mathbf{1135 \cdot 10^{-3}}}{0.89 \cdot 10^{-18} \cdot 6.022 \cdot \mathbf{10^{23}}} = \mathbf{2.1}\ \text{mmol.g}^{-1}$$

The presented results are in agreement with the results of $VO(acac)_2$ modifying silica gel (Kieselgel 60, Merck) presented by Baltes (2001). The variance from the linear dependence of final Al concentration on initial $Al(acac)_3$ loading below the calculated monolayer capacity is apparent in Fig. 14. The loading of aluminum increases almost linearly with the increase of $Al(acac)_3$

concentrations in solution up to about 0.6 mmol.g^{-1}. From this point, steeper increase in Al concentrations (wt%) is observed. This fact may be explained by the formation of multilayers, aggregates and clusters before a complete monolayer is formed.

5.2 Characterization and catalytic activity of catalysts grafted by cobalt

There is no detail study of cobalt grafted on the ordered mesoporous silicas by MDD method and the determination of the limited cobalt loading corresponding to monolayer surface coverage on the ordered mesoporous silica supports. Therefore, different loadings of $Co(acac)_2$ were applied for cobalt deposition. From theoretical and experimental values of cobalt loading capacity, the same initial concentration of 3.2 $mmol_{Co(acac)2}.g_{support}^{-1}$ was applied for the further grafting of cobalt. Five types of catalysts were prepared by MDD with the same initial concentration of cobalt precursor. They are divided in three groups for the clarity of their comparison:

(i) MCM and SBA grafted with cobalt studying the effect of different silica supports,

(ii) MCM modified by aluminum (incorporated or grafted) and further grafted with cobalt studying the effect of aluminum and its different location,

(iii) MCM and SBA grafted with aluminum and cobalt compared with MCM and SBA grafted only with cobalt studying the presence of grafted aluminum.

They were further characterized and tested in the catalytic reaction of N_2O decomposition in the inert atmosphere or by using CO as the reducing agent and tested in CO catalytic oxidation. The aim is to find the relation among physicochemical properties of cobalt grafted on different supports and the performance of these materials in the above mentioned catalytic reactions. The main interest is focused on the differences in (i) textural and structural properties of catalysts supports, (ii) coordination and oxidation state of cobalt cations and (iii) reducibility of catalysts.

5.2.1 Grafting of cobalt and its monolayer surface coverage on MCM

The initial concentration of $Co(acac)_2$ was 0.4 $mmol.g_{support}^{-1}$ whereas multiples of 0.4 were used (1.2, 1.6, 3.2 $mmol.g_{support}^{-1}$). Fig. 15 shows cobalt concentrations on MCM support measured by elemental analyses and experimental Si/Co mass ratios in dependency on initial $Co(acac)_2$ loadings. The concentrations of cobalt increase almost linearly with the increase of $Co(acac)_2$ concentrations in solution.

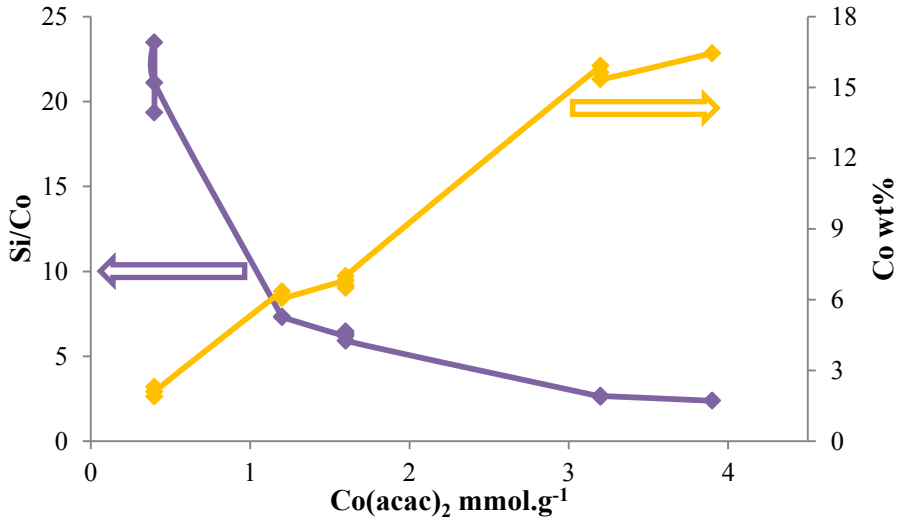

Fig. 15. Measured Co concentrations (yellow) and defined Si/Co ratios according to elemental analyses (purple) in dependency on initial $Co(acac)_2$ loadings on MCM.

The data presented in Fig. 15 are summarized in Table 3. The support MCM was grafted by Al of different concentrations previous to cobalt grafting by MDD. The presence of Al in different concentrations does not have an influence on final Si/Co ratios within the same initial cobalt loadings. The differences in Si/Co mass ratios for the initial concentration 0.4 $mmol_{Co(acac)2}.g_{support}^{-1}$ can be due to the experimental error. According to these values, the repeated syntheses showed a good reproducibility of MDD technique for the applied initial $Co(acac)_2$ concentrations.
The theoretical concentration of Co (wt%(Co)) was calculated according to Eq. 24.

$$wt\%(Co) = \frac{m_{Co(acac)2} \cdot M_{Co}}{m_{support} \cdot M_{Co(acac)2}} \cdot 100 \qquad (24)$$

where $m_{Co(acac)2}$ – weight of cobalt acetylacetonate (g), M_{Co} – molecular weight of cobalt ($g.mol^{-1}$), $M_{Co(acac)2}$ – molecular weight of cobalt acetylacetonate ($g.mol^{-1}$), $m_{support}$ – weight of silica support (g).

The differences between theoretical and final cobalt concentrations are more apparent with increasing initial $Co(acac)_2$ concentrations which can be attributed to the fact that not all $Co(acac)_2$ complexes in solution interacted with MCM support during the synthesis.

Table 3. Initial $Al(acac)_3$ and $Co(acac)_2$ loadings with experimental Al and Co concentrations and Si/Co ratios defined by elemental analyses EPMA and/or EDX.

	Initial $Al(acac)_3$ conc. mmol.g^{-1}	**Final Al conc.** wt%	**Initial $Co(acac)_2$ conc.** mmol.g^{-1}	**Theoretical Co conc.** wt%	**Final Co conc.** wt%	**Si/Co*** -	**Analysis**
MCM+Al(0.4)+Co(0.4)	0.4	1.0	0.4	2.4	2.3	19	EPMA
MCM+Al(0.6)+Co(0.4)	0.6	1.2	0.4	2.4	1.9	24	EPMA
MCM+Al(1.1)+Co(0.4)	1.1	1.5	0.4	2.4	2.1	21	EPMA
MCM+Al(0.2)+Co(1.2)	0.2	1.0	1.2	7.1	6.4	7	EDX
MCM+Al(0.4)+Co(1.2)	0.4	1.5	1.2	7.1	6.1	7	EDX
MCM+Al(0.3)+Co(1.6)	0.3	0.7	1.6	9.4	6.8	6	EPMA
MCM+Al(0.4)+Co(1.6)	0.4	1.0	1.6	9.4	6.5	6	EPMA
MCM+Al(1.0)+Co(1.6)	1.0	1.3	1.6	9.4	6.6	6	EPMA
MCM+Al(2.0)+Co(1.6)	2.0	1.4	1.6	9.4	7.0	6	EPMA
MCM+Co(3.2)	0.0	0.0	3.2	18.8	15.9	3	EDX
MCM+Al(3.1)+Co(3.2)	3.1	2.5	3.2	18.8	15.6	3	EDX
MCM+Al(6.2)+Co(3.2)	6.2	3.1	3.2	18.8	15.3	3	EDX
MCM+Co(3.9)	0.0	0.0	3.9	22.9	16.4	2	EDX

* Si/Co values are mass ratios.

It was important to find the limited cobalt loading corresponding to monolayer surface coverage of silica support eliminating the formation of cobalt aggregates and clusters. The simple calculation of the loading capacity is defined as **monolayer capacity** (Eq.5).

As an example for the calculation of monolayer capacity according to Eq. 5 is taken MCM grafted with $Co(acac)_2$: $A_m(Co(acac)_2)$ = 0.56 nm^2, $Co(acac)_2$ was modelled by the program NWChem 6.3 (Section 3.2.2); S_{BET} = 1100 $m^2.g^{-1}$.

$$V_m = \frac{\mathbf{1100 \cdot 10^{-3}}}{0.56 \cdot 10^{-18} \cdot 6.022 \cdot \mathbf{10^{23}}} = \mathbf{3.26}\ \text{mmol.g}^{-1}$$

The calculated values of monolayer capacity and the concentrations of cobalt depend on the differences in BET surface area of silica supports which is, in general, twice lower in the case of SBA than MCM. Other parameters are cross-sectional area of acetylacetonate complex such as $Co(acac)_2$ and silanol number ($OH.nm^{-2}$) which may differ within different mathematical models and experiments as reported in literature (Kozlova, 2010, Limnell, 2011).

The sample MCM+Co(16 %) with the initial $Co(acac)_2$ loading higher than 3.2 $mmol_{Co(acac)2}.g_{MCM}^{-1}$ was prepared by MDD with the mass ratio 1 g $Co(acac)_2$ to 1 g MCM. The initial $Co(acac)_2$ loading equals to 3.9 $mmol_{Co(acac)2}.g_{MCM}^{-1}$. Free OH groups band at 3740 cm^{-1} analyzed by IR spectroscopy (Fig. 16) disappeared at this cobalt concentration. The theoretical concentration of cobalt in solution equals to 23 wt% whereas the concentration of cobalt measured by EDX analysis was 16 wt%. The phase CoO (PDF 89-8398) overlapped by broad peaks of amorphous silica was analyzed by XRD (Fig. 17).

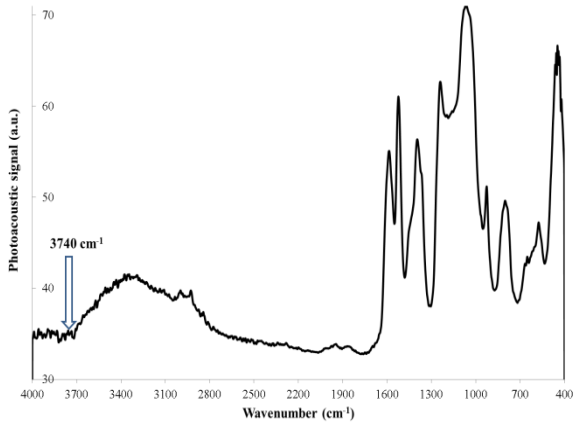

Fig. 16. IR spectra of MCM+Co(16%).

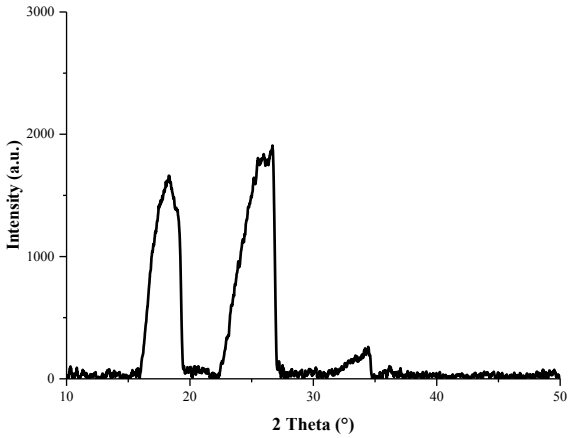

Fig. 17. XRD analysis of MCM+Co(16%)

Another approach to define limited cobalt loading corresponding to theoretical surface coverage equal to 1 can be done by using silanol number. **Silanol number α_{OH}** is defined as the number of hydroxyl groups per nm^2 (Eq. 25).

$$\boldsymbol{\alpha_{OH}}=\frac{\boldsymbol{\delta_{OH}}\cdot N_A}{\boldsymbol{S_{BET}}} \quad (25)$$

where α_{OH} – silanol number (OH.nm^{-2}), δ_{OH} – concentration of hydroxyl groups (mmol.g^{-1}), S_{BET} – BET surface area (m^2.g^{-1}), N_A – Avogadro´s number, 6.022.10^{23} mol^{-1}; (Vansant, 1995).
The experimentally determined silanol number of fully hydroxylated silicas (pretreated by vacuum drying at 200 °C) was 0.9 OH.nm^{-2} for MCM-48, 0.9–1.0 OH.nm^{-2} for SBA-15 (Urraca, 2006).
As an example of the calculation of hydroxyl groups concentration is taken SBA grafted with $Co(acac)_2$:

$$\delta_{OH}=\frac{\alpha_{OH}\cdot S_{BET}}{N_A}=\frac{0.9\cdot 1100\cdot 10^{18}\cdot 10^3}{6.023\cdot 10^{23}}=1.6 \text{ mmol.g}^{-1}$$

The concentration of cobalt reacting with the calculated concentration of hydroxyl groups according to Eq. 26:

$$\boldsymbol{w_{Co}}=\boldsymbol{\delta_{OH}\cdot M_{Co}\cdot 100} \quad (26)$$

where w_{Co} – weight percent of cobalt (%), M_{Co} – molecular weight of cobalt (g.mol^{-1}).

$$w_{Co}=0.0016\cdot 58.93\cdot 100=9.4\ \%$$

From theoretical (the calculation of monolayer capacity) and experimental (Fig. 15) values of cobalt loading capacity, the same initial concentration of 3.2 $mmol_{Co(acac)2}.g_{support}^{-1}$ was further applied for grafting of cobalt by MDD on three different silica supports (MCM, Al-MCM^b and SBA).

5.2.2 Elemental analysis

Initial loadings of $Al(acac)_3$ and $Co(acac)_2$ complexes in solution and final concentrations of Al and Co determined by EDX and AAS analyses are displayed in Table 4.

Table 4. Initial concentrations of $Al(acac)_3$ and $Co(acac)_2$ complexes in solution, final concentrations of Al and Co, Si/Al and Co/Si ratios on the different supports.

Sample	**Initial $Al(acac)_3$ conc.** $mmol.g_{support}^{-1}$	**Initial Co $(acac)_2$ conc.** $mmol.g_{support}^{-1}$	**Final Al conc.** * wt%	**Si/Al** * -	**Final Co conc.** ** wt%	**Co/Si** * -
MCM+Co	-	3.2	-	-	11.3	0.38
MCM+Al+Co	3.1	3.2	2.5	16	11.3	0.38
Al-MCM[b]+Co	-	3.2	4.3	9	9.9	0.33
SBA+Co	-	3.2	-	-	12.2	0.31
SBA+Al+Co	3.1	3.2	1.8	23	9.5	0.23

[b] Designation of Al-MCM synthesized according to Poladi (2002).

* EDX analysis, ** AAS analysis. Co/Si and Si/Al are mass ratios.

The theoretical concentration of cobalt in solution was the same (19 wt%), the theoretical concentration of Al in solution during MDD synthesis was 8.3 wt%, calculated according to Eq. 24. The differences in Si/Al ratio may be due to the experimental error of EDX analysis, however, it is not an important fact for the comparison of catalysts divided in groups i) and iii) as defined in the introduction of Section 5.2. The different location of aluminum within MCM framework is important for the group ii) and it is possible to compare MCM+Al+Co and Al-MCM^{b}+Co. The cobalt concentrations measured by AAS are in the range 9.5–12.2 and their difference is the most obvious for SBA+Co and SBA+Al+Co. The experimental cobalt concentrations are lower of about 36–50 % than the theoretical cobalt concentration (19 %).

5.2.3 Bonding mechanism of cobalt acetylacetonate

The results of TGA/DTA of prepared Co-grafted catalysts are summarized in Table 5 and selected profiles (MCM+Co, Al-MCM^{b}+Co, SBA+Co) are depicted in Fig. 18. The decomposition of $Co(acac)_2$ occurs at similar temperatures and similar manner for all presented catalysts. First weight loss at temperatures 74–85 °C is caused by adsorbed water from the ambient air (Collart, 2003). The second weight loss at temperatures 104–140 °C can be ascribed to the release of Hacac converting the hydrogen bonded $Co(acac)_2$ into covalently bonded species (Baltes, 2001). This weight loss is the highest for Al-MCM+Co which indicate that more Hacac is released within the temperature at 115 °C. The different bonding mechanism of $Cr(acac)_3$ complexes on MCM-41 and Al-MCM-41 was presented by Weckhuysen et al. (2000). The H-bonding was the only type of interaction between $Cr(acac)_3$ complexes and MCM-41 whereas the deposition of $Cr(acac)_3$ complexes onto Al-MCM-41 occurred either through H-bonding or ligand exchange mechanism. Further weight losses at temperatures above 200 °C is likely caused by oxidative decomposition of covalently bonded -Co(acac) complexes, which proceeds intensively at the temperature range 282–294 °C for all presented catalysts (Collart, 2003). At the used cobalt loading (3.2 $mmol_{Co(acac)2}.g_{support}^{-1}$ in the solution), multilayers and microcrystals of cobalt oxide can be formed.

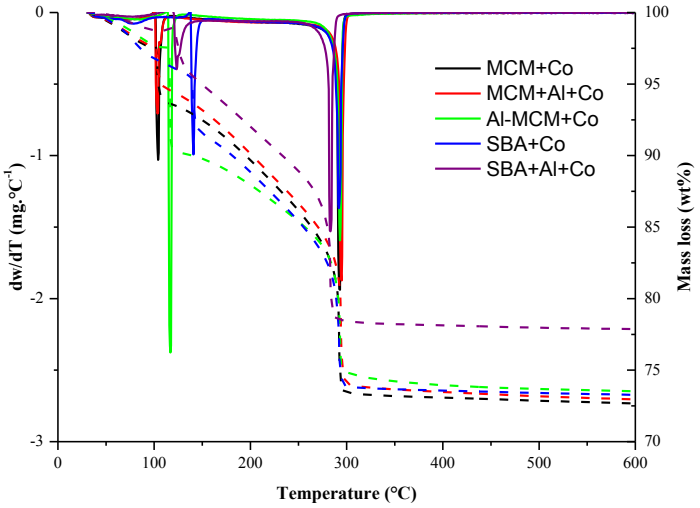

Fig. 18. TGA/DTG profiles of Co-grafted catalysts.

Table 5. Temperatures and mass losses of decomposition of $Co(acac)_2$ complexes.

Sample	**Temperatures of mass losses** °C				**Water loss** %	**Total mass loss** %
MCM+Co	74	104	208	293	2	27
MCM+Al+Co	74	103	206	294	2	27
Al-MCM^b+Co	85	115	220	293	2	26
SBA+Co	78	140	208	292	4	27
SBA+Al+Co	78	123	200	282	1	22

5.2.4 Textural properties

The isotherms of N_2 adsorption-desorption on Co-grafted on supports MCM, Al-MCM^b and SBA are shown in Fig. 19. Different batches of MCM and SBA (designated as 1, 2) were prepared for cobalt grafting. The samples MCM+Co, MCM+Al+Co and Al-MCM^b+Co show a sharp inflection in a relative pressure range of 0.2–0.4 indicating mesopore filling and capillary condensation in mesopores. The isotherms of SBA+Co and SBA+Al+Co also exhibit a sharp inflection but at significantly higher relative pressures (p/p_0 = 0.65–0.8), which designate the presence of uniform mesoporous structure with wider pore diameters compared to others. The isotherms of SBA+Co and SBA+Al+Co exhibit parallel adsorption and desorption branches (hysteresis H1) confirming a cylindrical shape of mesopores. Similar shapes of isotherms before (Fig. 8) and after (Fig. 19) cobalt grafting step suggest that the uniform mesoporous structure obtained for the silica supports remained almost unchanged after the grafting.

The evaluated textural properties of prepared supports and corresponding Co-grafted catalysts are summarized in Table 6. The catalysts MCM+Co and MCM+Al+Co have the highest surface areas

whereas SBA+Co and SBA+Al+Co have the highest mesopore diameters with the presence of micropores in the mesopore structure. Measured points of adsorbed volume were extrapolated by linear plot and went through the origin of t-plot in the case of the Co-grafted on MCM and Al-MCM[b] supports (not shown). This fact corresponds to their micropore volume and micropore area equal to zero. The BET surface area and total pore volume of MCM and Al-MCM[b] decreased by more than 20 % after the deposition of $Co(acac)_2$ complexes by MDD followed by calcination whereas there is almost no change in the case of SBA[1]. The reason can be their mesopores blocking and the densification of MCM and Al-MCM[b] structures which did not happen in such extent in SBA[1] due to larger mesopore diameter. As presented by Hanu et al. (2006), the most accessible structure of MCM-41 (spherical and gyroidal in comparison to irregular MCM-41) had the highest loading of vanadium dispersed by MDD method using $VO(acac)_2$ complexes. In this study, the SBA structure is expected to be the most accessible one for the deposition of $Co(acac)_2$ complexes.

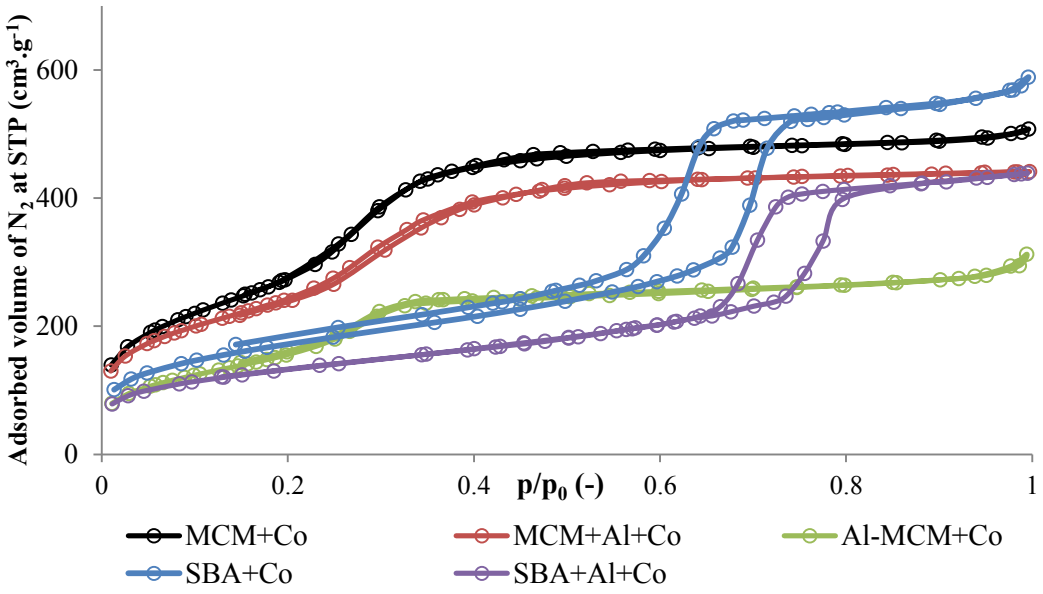

Fig. 19. Nitrogen adsorption-desorption isotherms of Co-grafted catalysts.

Table 6. Textural properties of silica supports and Co-grafted catalysts.

Sample	S_{BET} $m^2.g^{-1}$	ΔS_{BET} %	S_{micro} $m^2.g^{-1}$	V_{total} $cm^3.g^{-1}$	ΔV_{total} □ %	V_{micro} $cm^3.g^{-1}$	d_{pore} nm	Δd_{pore} %
MCM[1]	1271		-	1.10		-	2.7	
MCM[1]+Co	1004	21*	-	0.79	28*	-	2.4	11*
MCM[2]	1259		-	1.07		-	2.7	
MCM[2]+Al+Co	882	30*	-	0.68	37*	-	2.5	7*
Al-MCM[b]	762		-	0.66		-	2.7	
Al-MCM[b]+Co	571	25*	-	0.48	27*	-	2.5	7*
SBA[1]	633		196	0.92		0.11	5.4	
SBA[1]+Co	614	3*	125	0.91	1*	0.06	5.7	6**
SBA[2]	706		263	1.08		0.12	6.1	
SBA[2]+Al+Co	469	34*	115	0.68	37*	0.05	6.9	13**

[1, 2] Designation of different batches of silica supports MCM and SBA.

[b] Designation of Al-MCM synthesized according to Poladi (2002).

□ Total pore volume V_{total} was defined at $p/p_0 = 0.99–1.0$.

* Relative decrease of S_{BET}, V_{total} and d_{pore} after cobalt grafting, ** Relative increase of d_{pore} after cobalt grafting.

5.2.5 Phase analysis

Due to the amorphous silica nature of the pore walls of MCM, Al-MCM[b] and SBA, they have no crystallinity at the atomic level and no reflections can be observed at higher angle degrees *2θ* for the catalysts MCM+Co, MCM+Al+Co, SBA+Co and SBA+Al+Co. As depicted in Fig. 20, the peak of amorphous SiO_2 is apparent at the maximum *2θ* about 26 ° in the case of Al-MCM[b]+Co.
The cobalt spinel phase was detected in the catalyst Al-MCM[b]+Co. Due to the similar reflection angles and intensities in XRD, it is not possible to distinguish between Co_3O_4 (PDF number 65-3103), $CoAl_2O_4$ (PDF number 03-0896) and Co_2AlO_4 (PDF number 02-1410). The Na^+ ions introduced in the synthesis solution might form the phase $NaCo_2O_4$ (PDF number 73-0133) after the grafting of cobalt on Al-MCM[b]. The intensities at high angles are much lower (max. about 500 counts) in comparison with the intensities at low angles (max. about 220,000 counts, Fig. 9), thus the crystallinity is much lower in comparison with their amorphous nature. For the rest of the catalysts, there was no detection of phases as it is apparent from the XRD patterns A), B), C) and D) in Fig. 20.

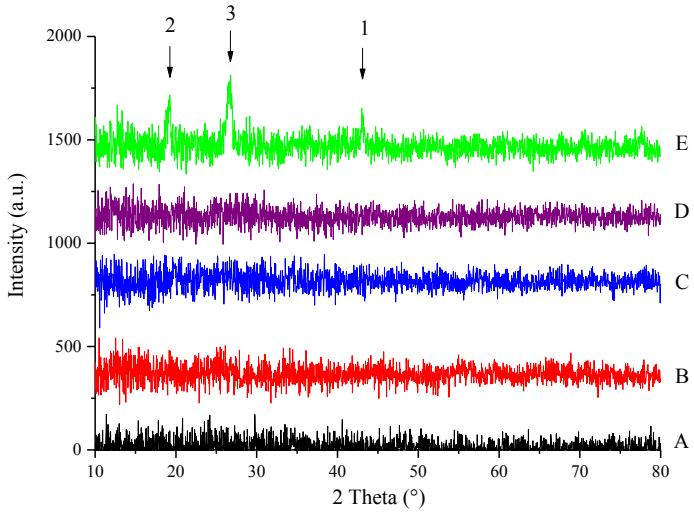

Fig. 20. XRD patterns of catalysts A) MCM+Co, B) MCM+Al+Co, C) SBA+Co, D) SBA+Al+Co and E) Al-MCM^{b}+Co.

The phases are: 1 – cobalt spinel, 2 – $NaCo_2O_4$, 3 –amorphous SiO_2.

5.2.6 Coordination and oxidation state of cobalt

- **DR UV-Vis spectroscopy**

The DR UV-Vis spectra are used for the characterization of the nature and the coordination of cobalt oxide species (Table 7, Fig. 21). Triplet absorption bands at around 15650, 17035, 19080 cm^{-1} are assigned to $^{4}A_2(F) \rightarrow {}^{4}T_1(P)$ transition of Co(II) species anchored to the support surface in tetrahedral coordination (Bhoware, 2006, Janas, 2007, Zhang, 2007). Before calcination, the color of samples was pink, after calcination the color turns to blue (from very light to deep blue in correlation with the concentration of cobalt). Blue color is characteristic for tetrahedral Co(II) ions (Bhoware, 2006, Mwenesongole, 2008).

The absorption band at 13210 and 23260 cm^{-1} can be attributed to non-specified oxide Co_xO_y (Szegedi, 2009, Zhang, 2007). These bands are evident in the Al-MCM^{b}+Co. The color of this catalyst was green, characteristic for the oxidized Co_xO_y species dispersed in the pores as well as the presence of tetrahedral Co(II) ions and Co(III) ions in octahedral position in the presence of Al(III) in the lattice (Mwenesongole, 2008, Šponer, 2000). The color of samples changes from blue or green to pink with longer exposition into the air whereas it turns to blue or green again upon heating, dehydration and therefore the catalytic tests as well.

Table 7. Wavenumbers of bands from DR UV-Vis spectra corresponding to the coordination of cobalt.

Sample	Wavenumber cm^{-1}			Interpretation
MCM+Co	15650	17035	19080	tetrahedral Co(II)
MCM+Al+Co	15650	17035	19080	tetrahedral Co(II)
Al-MCM^{b}+Co	13210			Co_xO_y
	15650	17035	19080	tetrahedral Co(II)
	23260			Co_xO_y
SBA+Co	15625	17035	19120	tetrahedral Co(II)
SBA+Al+Co	15625	17035	19120	tetrahedral Co(II)

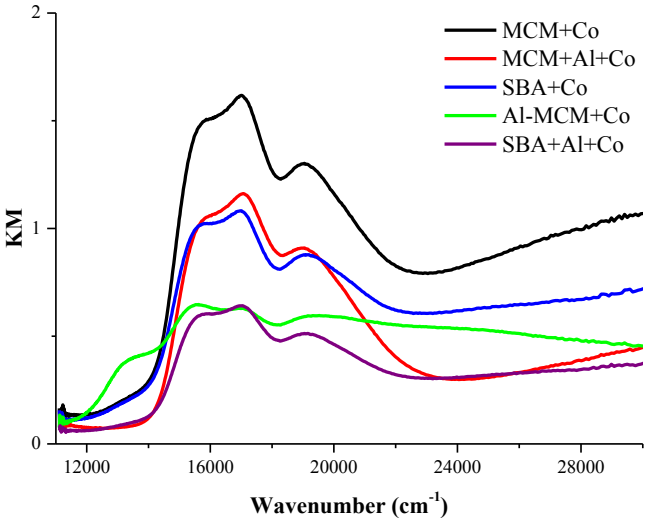

Fig. 21. DR UV-Vis spectra of Co-grafted catalysts.

From the point of view of oxidation and coordination state of cobalt, the catalysts MCM+Co, MCM+Al+Co, SBA+Co and SBA+Al+Co are comparable and the main difference shows Al-MCM^{b}+Co with the presence of non-specified oxide Co_xO_y.

➢ FTIR and Raman spectroscopy

FTIR spectra of the supports SBA^{1}, Al-MCM^{b}, and MCM^{1} are shown in Fig. 22. These spectra are very similar to each other. The broad absorption band around 3400 cm^{-1} may be attributed to stretching vibration of water adsorbed on the surface and/or of H-bridged silanol groups (Si-OH). The band corresponding to the O-H deformation vibration is located at 1627 cm^{-1}. These bands do not significantly shift their position in all measured spectra (see Figs. 22, 23) (Albuquerque, 2008). In SBA samples, their intensities are lower than in samples MCM. In case of SBA+Co (Fig. 23b), these bands almost missing, thus the SBA+Co catalyst contain less water and/or H-bridged silanol

groups. The most intensive band around 1050 cm^{-1} (Fig. 23) is apparent in all spectra and corresponds to the vibration of siloxane groups (Si-O-Si) (Albuquerque, 2008). The position of the band in the Al-MCM[b] spectrum is shifted to the lower wavenumbers (1042 cm^{-1}) against the position of the band in MCM spectrum (1050 cm^{-1}). This shift may be caused by incorporation of Al atoms to the MCM structure. This statement may be confirmed by missing band 976 cm^{-1} in the spectrum Al-MCM[b] (Fig. 22b) which corresponds to the stretching vibrations of the surface Si-O^- groups (Huo, 2014). The remaining bands in the MCM[1] spectrum (1239, 804 and 440 cm^{-1}) are assigned to the asymmetric and symmetric stretching and deformation vibration of the Si-O groups, respectively (Huo, 2014). The band at 1239 cm^{-1} is apparent in the spectra of Al-MCM[b] and SBA[1] as a shoulder.

Measured FTIR spectra of the prepared catalysts are shown in the Fig. 23. It is clearly visible, that only bands corresponding to the supports are presented in the spectra no other bands are visible, due to the strongest signal of the supports. Thus, determination of the presented cobalt phase in the sample is not possible from FTIR measurements.

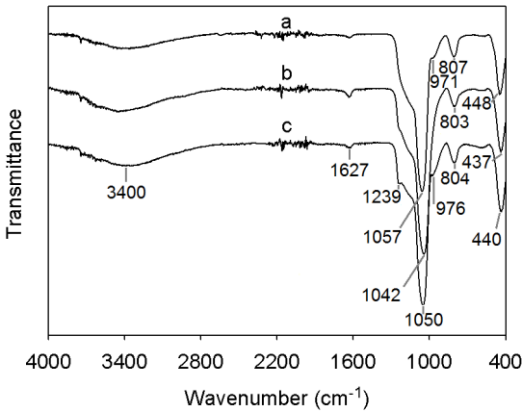

Fig. 22. FTIR spectra of SBA[1] (a), Al-MCM[b] (b), and MCM[1] (c) supports.

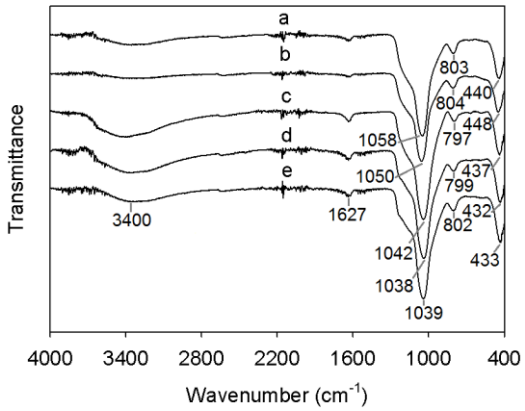

Fig. 23. FTIR spectra of SBA+Al+Co (a), SBA+Co (b), Al-MCM[b]+Co (c), MCM+Al+Co (d), and MCM+Co (e) catalysts.

The measured Raman spectra of the cobalt standards Co_3O_4, CoO, and $CoAl_2O_4$ are shown in the Fig. 24. Raman spectra of the SBA[1], Al-MCM[b] and MCM[1] supports are shown in Fig. 25 where only one band (479 cm^{-1}) is clearly noticeable and belongs to the Si-O vibration. This band is only slightly visible in case of the Al-MCM[b].

Raman spectra of the prepared catalysts are shown in the Fig. 26. In case of the sample Al-MCM[b]+Co (Fig. 26c), bands at 194, 479, 520, 612, and 682 cm^{-1} corresponding to the symmetric vibrational modes F_{2g}, E_g, F_{2g}, F_{2g}, and A_{1g} are clearly visible and predict the spinel structure of the Co_3O_4 as reported in the literature (Na, 2012). The Raman A_{1g} mode is assigned to characteristics of the octahedral sites and the E_g and F_{2g} modes corresponds to the combined vibrations of

tetrahedral site and octahedral oxygen motions (Na, 2012). In other samples only the most intensive band is visible and shifted to the higher wavenumbers (692 cm^{-1}). These Raman spectra are noisier what may be caused by the background of the MCM and SBA. The band at position 480 cm^{-1} refers to the initial MCM and SBA matrixes as well as the band at 271 cm^{-1} which may not be clearly seen in the Fig. 25 due to the fluorescence background.

After comparison of spectra of catalysts (Fig. 26) with standards (Fig. 24), it is clearly evident that the phase $CoAl_2O_4$ is not present in the catalysts as well as Co_2AlO_4 and $NaCo_2O_4$ according to the literature (Lee, 2015). The determination of the presence of CoO and/or Co_3O_4 is very difficult due to the similar spectra of these two compounds and the position of the bands could be also affected by the presence of supports. Raman bands of CoO sample are shifted to lower wavenumbers compared to the bands of Co_3O_4 sample. Thus, the main band (680 cm^{-1}) of Al-MCM^b+Co (Fig. 26c) better corresponds to CoO position of the main band (675 cm^{-1}). The main band in other samples is in higher wavenumbers (692 cm^{-1}) so better corresponds to Co_3O_4 position of the main band (688 cm^{-1}), however, in these samples other bands are not visible, thus the confirmation of the present phase is difficult. Probably, both phases (CoO and Co_3O_4) are present in the samples.

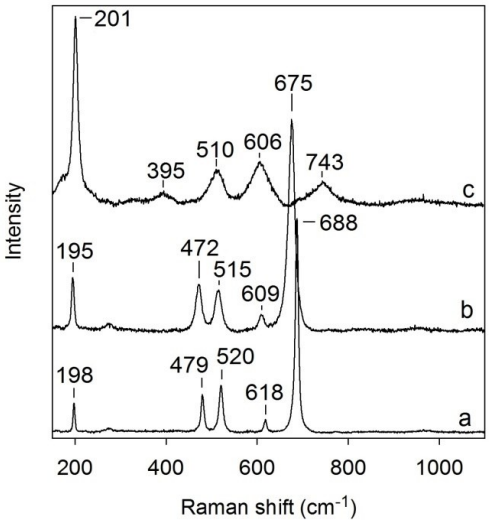

Fig. 24. Raman spectra of the standards Co_3O_4 (a), CoO (b), and $CoAl_2O_4$ (c).

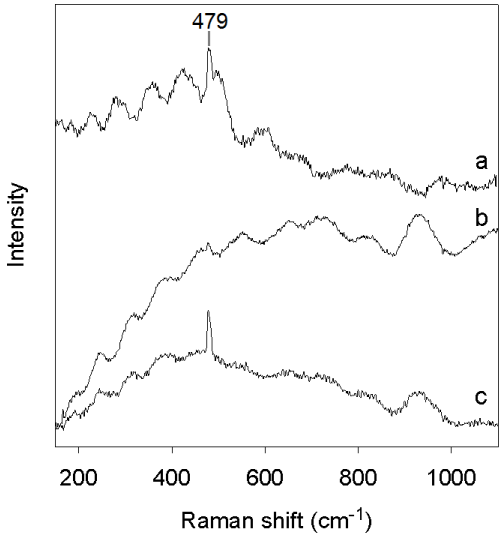

Fig. 25. Raman spectra of SBA[1] (a), Al-MCM[b] (b), and MCM[1] (c) supports.

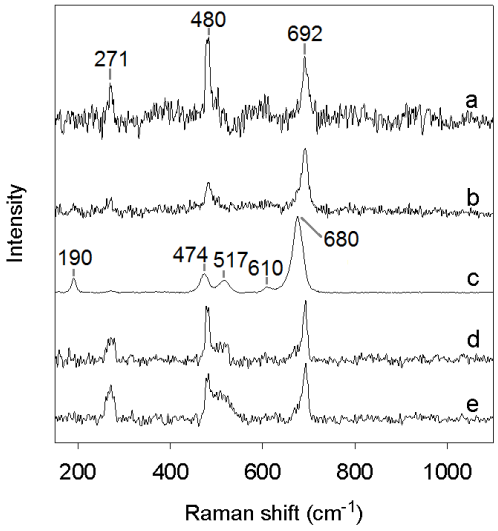

Fig. 26. Raman spectra of SBA+Al+Co (a), SBA+Co (b), Al-MCM[b]+Co (c), MCM+Al+Co (d), and MCM+Co (e) catalysts.

The presence of cobalt oxide crystallites (CoO or Co_3O_4) is clearly visible from the spectra of Al-MCM[b]+Co as characterized by Raman spectroscopy. The catalysts MCM+Co, MCM+Al+Co, SBA+Co and SBA+Al+Co are comparable and the confirmation of CoO and/or Co_3O_4 phases is difficult. These Raman spectra are noisier what may be caused by the background of the MCM and SBA.

5.2.7 Reducibility of catalysts

TPR profiles corresponding to reduction of the standards Co_3O_4 and $CoAl_2O_4$ are depicted in Fig. 27. The maxima temperature of reduction about 400 °C was measured for the standard Co_3O_4 (Alfa Aesar, CAS: 1308-06-1, purity 99.7 %) and $CoAl_2O_4$ (Alfa Aesar, CAS: 12672-27-4, Co 39–41 %). The low-temperature reduction peaks correspond to the reduction of $Co^{III} \rightarrow Co^{II}$ and/or $Co^{II} \rightarrow Co^0$ in cobalt spinel phase. The standard $CoAl_2O_4$ exhibits the reduction above 800 °C attributed to the reduction of cobalt surrounded by aluminum ions in a spinel-like phase (Obalová, 2009).

TPR profiles of all prepared Co-grafted catalysts are shown in Fig. 28, Table 8. All catalysts exhibit very low amount of easily reducible compounds strongly apparent in TPR profiles of cobalt oxides standards (reduced at temperatures lower than 600 °C). The results are in accordance with data published earlier by Wang (2009), who declare that cobalt grafted on the MCM and SBA materials show intensive reduction peak with T_{max} in the temperature range of 710–860 °C indicating high reduction stability. The catalyst SBA+Co shows even higher reduction temperature than MCM+Co, suggesting that cobalt ions in SBA formulate a similar or even more stable

distribution than those ones in MCM. As reported by Simionato et al. (2003), the reduction peaks within the maxima at 700 °C are assigned to well-dispersed surface Co^{2+} ions and the peaks at the maxima about 800 °C are described as Co^{2+} ions interacting strongly with the support. The reduction peak around 797 °C was attributed to the reduction of surface Co silicate in the study of Wang (2013) using $Co(acac)_2$ as the cobalt precursor for its impregnation on SiO_2. The reduction of Al-MCM^b+Co catalyst substantially differed from reduction of other catalysts. The broad reduction peak starting at temperature ca. 500°C up to 850 °C is clearly observed indicating less uniform cobalt ion distribution in the Al-MCM^b framework (Wang, 2009). XRD, IR and Raman spectroscopy analyses and DR UV-Vis confirmed presence of cobalt spinel phase in Al-MCM^b+Co. In accord with Simionato et al., the reduction within the maxima temperature at 600–630 °C can be attributed to Co^{3+} ions in crystallites.

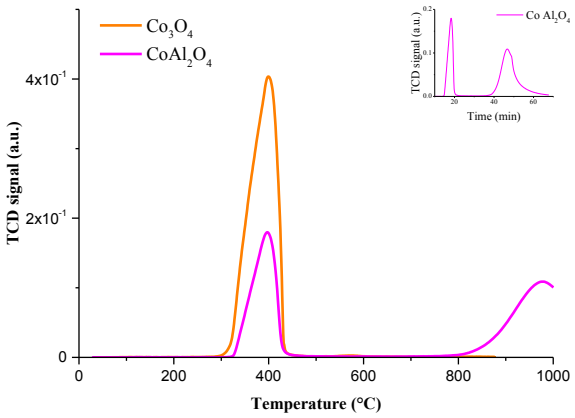

Fig. 27. TPR-H_2 profiles of cobalt standard materials.

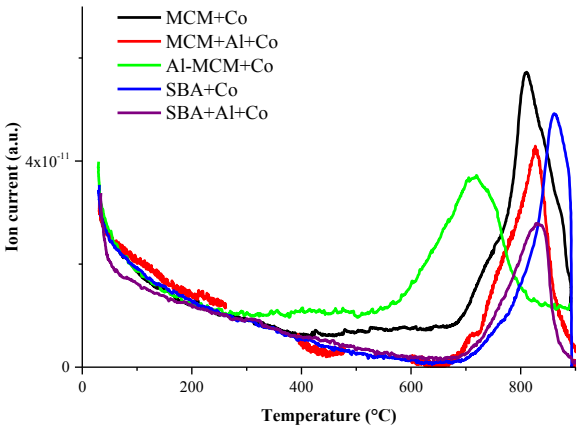

Fig. 28. TPR-H_2 profiles of Co-grafted catalysts.

Table 8. Temperatures of reduction maxima and consumed hydrogen obtained from TPR.

Sample	T_{max1} °C 25–600°C	H_2 consumed mmol.g^{-1} 25–600°C	T_{max2} °C 600–900°C	H_2 consumed mmol.g^{-1} 25–900°C
MCM+Co	483	0.10	810	2.66
MCM+Al+Co	290; 344	0.16	828	2.98
Al-MCM^b+Co	413	0.36	716	2.90
SBA+Co	-	0.00	862	2.01
SBA+Al+Co	537	0.06	834	1.49
Co_3O_4	400	15.37	-	0.00
$CoAl_2O_4$	397	2.63	977	4.59

In summary of TPR experiments, the catalyst Al-MCM^b+Co has less uniform cobalt ion distribution presuming the presence of Co^{2+} as well as Co^{3+} ions. The other catalysts show similar TPR profiles presuming the presence of well-dispersed Co^{2+} ions interacting with the support

attributed to surface Co silicate. It is suggested that the catalyst SBA+Co has more uniform cobalt ion dispersion on SBA support than the other catalysts. All catalysts showed very low amount of easily reducible compounds whereas cobalt spinel standards are easily reducible at low temperatures with the maxima at about 400 °C.

5.2.8 Catalytic activity

- **N_2O decomposition and reduction**

The Co-grafted catalysts were tested in the reaction of N_2O decomposition. The N_2O conversion at 450 °C did not exceed 14 % as shown in Table 9. The similar results were achieved by Chmielarz and co-authors (2005) for the catalysts based on mesoporous silicas modified with chromium and iron. The catalytic activities demonstrated in Table 9 are in agreement with TPR study (Section 5.2.7) as the tested Co-grafted catalysts show almost no H_2 consumption within the temperature range of catalytic tests. As presented by Obalová (2008), the presence of cation active sites reducible and able to transfer electrons in the temperature range of catalytic N_2O decomposition is important parameter for the activity of catalysts.

Table 9. The conversions X_{N2O} at 450 °C and the temperatures T_{50} at 50 % and T_{90} at 90 % of CO conversion on the silica support and Co-grafted catalysts.

Conditions: N_2O decomposition: 0.1 mol% N_2O in nitrogen, N_2O reduction: 0.1 mol% N_2O and 0.1 mol% CO in nitrogen, CO oxidation: 0.1 mol% CO and 5 mol% O_2 in nitrogen; 0.1 g of catalyst, 100 ml.min^{-1}.

Sample	N_2O decomposition	N_2O reduction		CO oxidation	
	X_{N2O} %	X_{N2O} %	X_{CO} %	T_{50} °C	T_{90} °C
MCM+Co	14	22	26	255	292
MCM+Al+Co	3	13	8	274	344
Al-MCM+Co	n.d.	9	8	207	234
SBA+Co	2	24	30	164	198
SBA+Al+Co	5	26	28	226	286
MCM-41[1]	n.d.	9	9	352	384
SBA-15[2]	n.d.	n.d.	n.d.	347	400

The rate determining step of catalytic decomposition of N_2O is supposed to be the reduction of active sites to remove adsorbed oxygen species which is left on the surface after dissociation of N_2O molecule.

Therefore, the reducing agent (e.g. H_2, hydrocarbons or CO) could facilitate the desorption of oxygen species and hence the increase of the reaction rate of N_2O decomposition. Carbon monoxide was used as the reducing agent in this work and the reduction of N_2O according to Eq.

27 was tested. The temperature dependences of N_2O reduction on Co-grafted catalysts are displayed in Fig. 29. At first, the reduction of N_2O was measured on the support MCM[1] (as designated in Table 6) getting the negligible conversion of N_2O at 450 °C (9 %) with the same conversion of CO. Therefore, the activities of the catalysts with similar conversions are insignificant. The reducing agent increased the activity, however, the N_2O conversion did no exceed 26 % at 450 °C.

The N_2O reduction by CO in the presence of oxygen was studied on the catalyst MCM+Co and the N_2O conversion decreased to 6 % at 450 °C due to competitive CO oxidation to CO_2. The conversion of CO was 100 % in tested temperature range 300–450 °C. Based on this result, it was concluded that prepared catalysts would be active in CO oxidation and decided to verify this assumption experimentally.

$$N_2O + CO \rightarrow N_2 + CO_2 \quad (27)$$

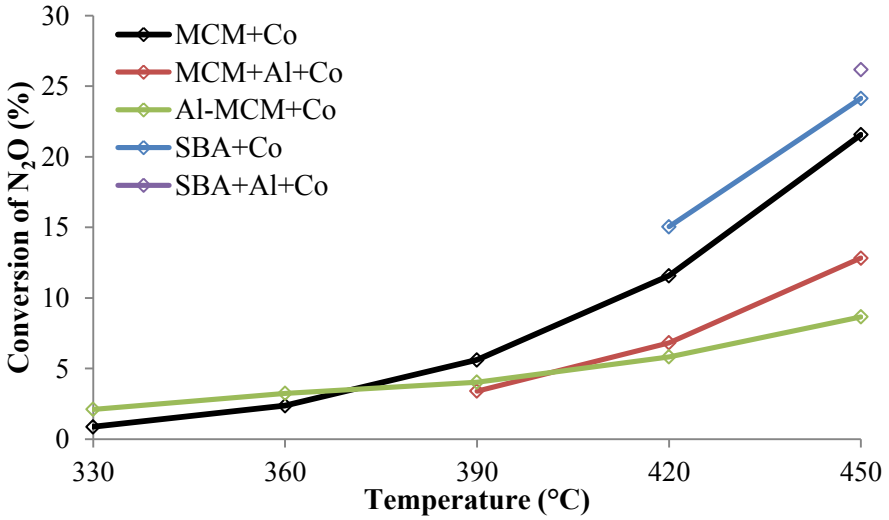

Fig. 29. The N_2O conversions in catalytic reduction of N_2O by carbon monoxide on Co-grafted catalysts.

Conditions: 0.1 mol% N_2O and 0.1 mol% CO in nitrogen, 0.1 g of catalyst, 100 $ml.min^{-1}$.

- **CO oxidation**

The CO conversions on silica supports and Co-grafted catalysts are summarized in Table 9 and in Fig. 30.

The CO oxidation was tested on the catalysts as well as silica supports (MCM[1] and SBA[2], as designated in Table 6). The CO conversion 9 % at 450 C was observed on MCM[1] with no presence of oxygen in the gas phase. The same conversion was found for N_2O, therefore, CO molecules

were consumed for the reduction of N_2O molecules. However, such low conversion is expected to be insignificant.

Higher conversion of CO molecules was reached in the presence of oxygen in the gas phase, however, the CO conversion was 5 times less on SBA[2] and 3 times less on MCM[1] at the temperature 300 °C in comparison with 100 % conversion of CO on Co-grafted catalysts, except of the catalyst MCM+Al+Co. The gas-phase homogeneous oxidation of CO requires higher temperatures (above 730 °C) and the oxidation rate can be enhanced with a thermal reactor (Flagan, 2013). It was confirmed by the reaction of CO oxidation in the empty reactor where the conversion of CO was 79 % at 450 °C. In the experiments on the silica surface prepared by the sol-gel method reported by Matsumura (1992), the CO oxidation was catalyzed over lattice oxygen atoms at the temperatures 580 °C or higher. The essential role of surface hydroxyl groups in low-temperature CO oxidation is shown for instance in the study over a model Pd catalyst (Parker, 2011). According to the composition of silica supports, the role of lattice oxygen atoms and hydroxyl groups is expected in the oxidation of CO, however, not confirmed by other analyses in this study.

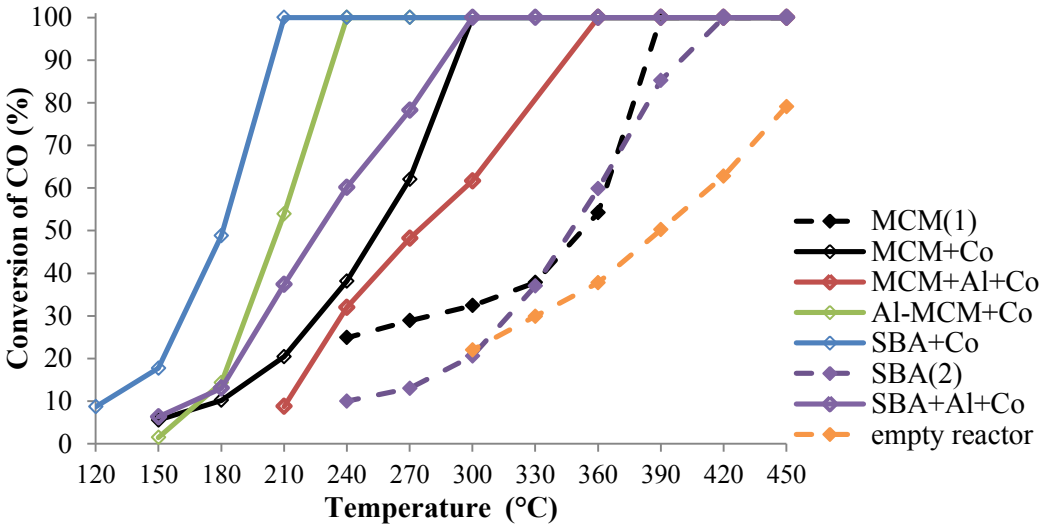

Fig. 30. The CO conversions in catalytic oxidation of CO on silica supports and Co-grafted catalysts.

Conditions: 0.1 mol% CO + 5 mol% O_2 in nitrogen, 0.1 g of catalyst, 100 ml.min^{-1}

The catalytic activities of Co-grafted catalysts increased in comparison with the activities of silica supports and are in the order: SBA+Co > Al-MCM+Co > SBA+Al+Co > MCM+Co > MCM+Al+Co. The temperatures T_{50} at 50 % and T_{90} at 90 % of CO conversion are summarized in Table 9 and are in the same order as in the previous sentence.

After the catalytic tests of N_2O decomposition and CO oxidation, the color of samples did not change: (i) blue (for MCM, MCM+Al+Co, SBA+Co, SBA+Al+Co), so that cobalt(II) ions were in

tetrahedral coordination whereas (ii) green (for Al-MCM^{b}+Co) meaning the presence of tetrahedral cobalt(ii) ions as well as non-specified oxide Co_xO_y.

From obtained results we can evaluate:

(i) The effect of supports (MCM and SBA) on the CO oxidation at the same theoretical content of Co (the catalysts MCM+Co and SBA+Co). From the results of catalytic activity it is clear that the CO conversion is the highest for SBA+Co. As it is apparent from DR UV-Vis and TPR-H_2 study, the catalysts SBA+Co and MCM+Co contain highly stabilized cobalt ions in tetrahedral(II) coordination state. It is obvious from Fig. 31 expressing the catalytic activity as converted CO molecules per unit BET surface area that more active sites are distributed on SBA per unit specific surface area than on MCM. This can be related to higher number of silanol groups as presented in Section 3.1.2. Higher activity of SBA+Co may be also attributed to better accessibility of cobalt precursors in bigger mesopore diameters of SBA during the synthesis and higher density of catalytically active cobalt sites on SBA per unit surface area.

As reported by Salek and co-authors (2014), the catalyst with the formula CoO(OH) having larger pore volume by 25 % performed better activity at high conversion rate and better accessibility of CO molecules than the catalyst CoO(OH) synthesized by different cobalt precursor. The bigger and more accessible pores of SBA-15 as well as channel interconnections were beneficial for the diffusion and better accessibility of ions such as apatite or indomethacin in the studies of Harris (2008) or Limnell (2011) and their co-authors. However, the pore diameters of the ordered mesoporous silicas used in this study are much bigger than the reacting molecules of CO and O_2 in CO oxidation. Therefore, it is assumed that the reaction rate within the applied reaction conditions is the controlling step and is not influenced by transport phenomena.

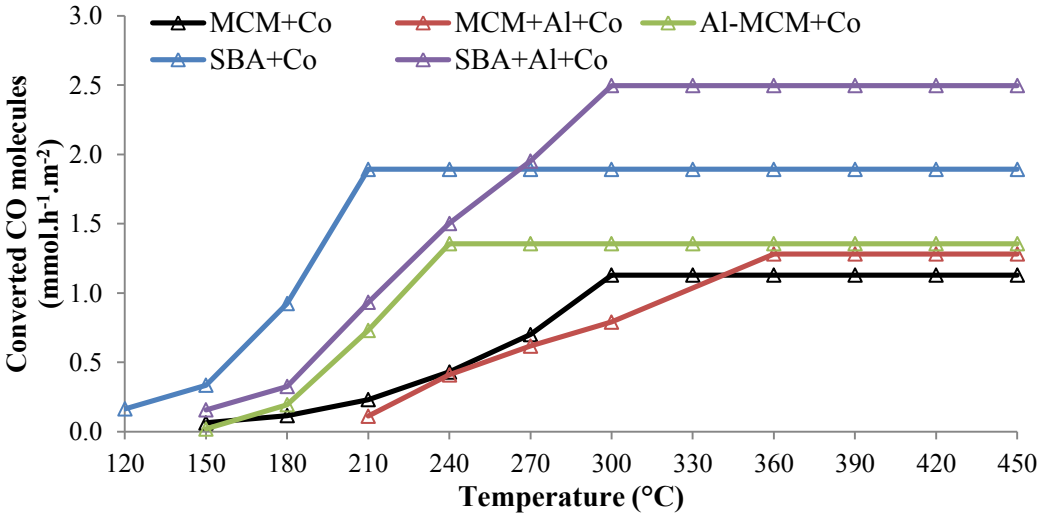

Fig. 31. The converted CO molecules per BET surface area versus temperature on Co-grafted catalysts.

(ii) The effect of modification of MCM by aluminum (incorporated or grafted) at the same theoretical content of Co. The conversion of CO was in the order: Al-MCM+Co > MCM+Co > MCM+Al+Co, see Fig. 30. The catalytic activity of Al-MCM+Co can be influenced by the presence of cobalt aluminate as the inactive phase in CO oxidation. However, its presence was not confirmed by Raman spectroscopy analysis. On the other hand, the presence of crystalline cobalt spinel phase was identified by XRD analysis confirmed by DR UV-Vis and Raman spectroscopy attributed either to CoO or Co_3O_4 phase. The shift of TPR profile to lower temperatures of Al-MCM+Co catalyst supports the presumption that Co^{2+} as well as Co^{3+} ions are present in Al-MCM+Co. As mentioned in Section 3.3.2, a specific ratio between Co^{2+} and Co^{3+} is required for the catalytic CO oxidation. Therefore, the presence of Co^{2+} as well as Co^{3+} ions seems to be beneficial for higher catalytic activity of Al-MCM+Co in comparison with the catalysts MCM+Co and MCM+Al+Co.

(iii) The effect of aluminum grafted on MCM and SBA at the same theoretical content of Co. The conversion of CO was in the order: SBA+Co > SBA+Al+Co > MCM+Co > MCM+Al+Co, see Fig. 30. Interestingly, the catalysts MCM+Co, MCM+Al+Co, SBA+Co and SBA+Al+Co are comparable from the point of view of oxidation and coordination state of cobalt. The amount of hydrogen consumed in TPR-H_2 experiments do not correspond to the differences in catalytic activities. Therefore, there has to be another reason of different catalytic performance. As it is obvious from Fig. 31, less catalytic active sites are distributed on the catalysts with aluminum grafted on MCM, resp. SBA, per unit specific surface area than on MCM, resp. SBA, with no aluminum. It is expected that the dispersion of cobalt on silica supports is the main reason for different catalytic activities. The density of catalytic active sites is planned to be investigated by pulse chemisorption technique and temperature programmed reduction by carbon monoxide in future study.

5.3 Characterization and catalytic activity of catalysts grafted by rhodium

In this section, the catalysts with rhodium grafted on ordered mesoporous silica supports (MCM, MCM with incorporated and grafted aluminum and SBA) were prepared and tested in the N_2O catalytic decomposition. The catalytic activity was measured under the nitrogen atmosphere as well as in the presence of typical inhibiting compounds such as oxygen, water vapor and nitric oxide. These compounds are common in waste gases together with N_2O and can have a great impact on the catalytic activity in the N_2O decomposition (Obalová, 2009). The aim presented in this section is to find the relation among physic-chemical properties of rhodium grafted on different supports and the performance of these materials in the N_2O catalytic decomposition. The main interest is focused on the presence of aluminum and its different location within the support structures and on different textural properties of catalysts supports. Three series of catalysts were prepared in which only one parameter is studied:

i) the effect of supports (SBA and MCM) at the same Rh content on catalytic activity,
ii) the effect of different Rh loadings on SBA on catalytic activity,
iii) the effect of modification of MCM by aluminum (incorporated or grafted) at the same content of Rh on catalytic activity.

5.3.1 Grafting of rhodium

As reported by Hussain et al. (2012), the activity of catalysts in the N_2O decomposition is increasing with rhodium loading from 0.1 wt% to 1.5 wt%. Furthermore, the N_2O conversion was negligible for the rhodium concentration lower than 0.1 wt%. On the other hand, the rhodium loading till 1.5 wt% is appropriate from the economic point of view. Therefore, the maximal initial concentration of rhodium was defined according to the initial concentration of $Rh(acac)_3$ (0.2 $mmol.g_{support}^{-1}$) presumed to be about 1 wt% Rh as demonstrated by Chmielarz and co-authors (2011).

5.3.2 Elemental analysis

Two series of rhodium containing catalysts were prepared, (i) the catalysts with the same rhodium content grafted on different mesoporous silica supports to obtain information about support effect on catalytic activity in N_2O decomposition and (ii) the catalysts with different rhodium loading grafted on SBA to optimize rhodium content. Initial loadings of Al and Rh acetylacetonate complexes and theoretical concentrations of rhodium in solution and their final concentrations determined by EDX and AAS analyses are displayed in Table 10.

The final concentrations of Al measured by EDX are comparable for the catalysts MCM+Al+Rh(2.7 %) and Al-MCM[a]+Rh(2.7 %). The final concentrations of Rh measured by EDX analysis are comparable for the catalysts with the same initial $Rh(acac)_3$ concentration 0.2 $mmol.g_{support}^{-1}$. The difference in final rhodium concentrations measured by AAS for these catalysts may be due to low amount of catalysts used for the analysis. There is a great difference between theoretical and final rhodium concentration defined by EDX for the catalyst SBA+Rh(1.4 %) which is caused by the experimental error of EDX for such low rhodium concentration. However, its final rhodium concentration defined by AAS is in a good agreement with theoretical rhodium concentration.

5.3.3 Bonding mechanism of rhodium acetylacetonate

The infrared spectroscopy as well as thermal analysis can provide the information on the interaction between the support and the acetylacetonate (acac) complexes during the synthesis of rhodium catalysts by MDD.

After modification with acac complexes, the intensity of free silanol band at 3745 cm^{-1} in IR spectra decreases as depicted in Fig. 32. The fraction of the surface silanol groups is in H-bond interaction with the acac complexes between 3600–3200 cm^{-1}. The H-bonding mechanism of silanol groups corresponds as well to the band at 1625 cm^{-1}. There is almost no change of this band before and after calcination meaning that acac complexes anchor by ligand exchange mechanism with silanol groups of SBA in the case of SBA+Rh(1.7 %). A broad band between 1600–1200 cm^{-1} shows the characteristic acac bands.

The thermolysis of covalently bonded Rh(acac) complexes occurs in three steps in depicted TGA/DTG profiles of SBA+Rh(1.7 %) and SBA+Rh(1.4 %), Fig. 33: i) the water loss happens at 42 °C, ii) the release of Hacac occurs at 111 °C, iii) the rest of covalently bonded complexes are converted to Si-O-Rh + acetone + CO_x at about 270 °C.

Table 10. Initial concentrations of $Al(acac)_3$ and $Rh(acac)_3$ and theoretical concentration of Rh in solution and final concentrations of Al and Rh on the different supports.

Sample	Initial Al $(acac)_3$ conc. $mmol.g_{support}^{-1}$	Initial Rh $(acac)_3$ conc. $mmol.g_{support}^{-1}$	Theoretical Rh conc. wt %	Final Al conc. [a] wt %	Final Rh conc. [a, b] wt %
MCM+Rh(2.7 %)	-	0.20	2.0	-	2.6 [a], 1.1 [b]
MCM+Al+Rh(2.7 %)	0.4	0.20	2.0	1.8	2.8 [a], 2.3 [b]
Al-MCM[a]+Rh(2.7 %)	-	0.20	2.0	1.6	2.9 [a], 2.5 [b]
SBA+Rh(2.7 %)	-	0.20	2.0	-	2.6 [a], 1.8 [b]
SBA+Rh(1.7 %)	-	0.10	1.0	-	1.7 [a], 1.1 [b]
SBA+Rh(1.4 %)	-	0.01	0.1	-	1.4 [a], 0.1 [b]

[a] EDX analysis, [b] AAS analysis.

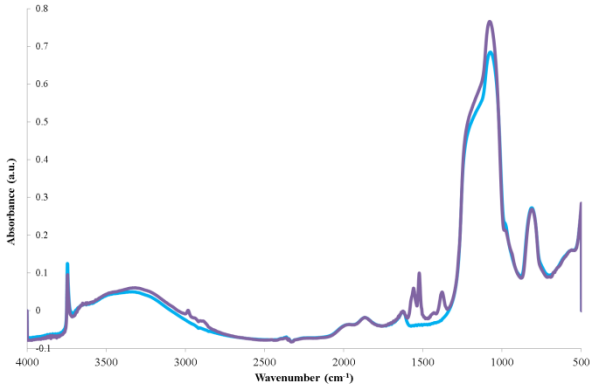

Fig. 32. IR spectra of SBA+Rh(1.7 %) before (purple) and after (blue) calcination.

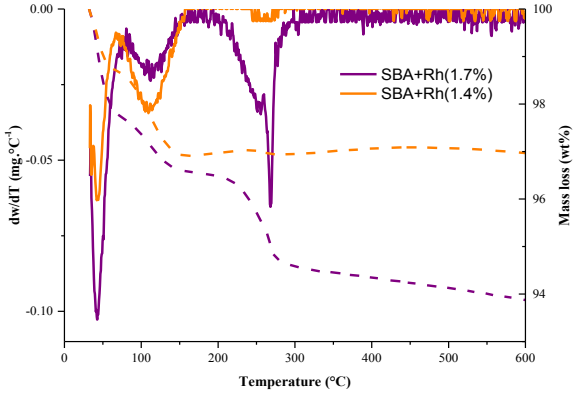

Fig. 33. TGA/DTG profiles of SBA+Rh(1.7 %) and SBA+Rh(1.4 %).

5.3.4 Textural properties

The isotherms of N_2 adsorption-desorption on Rh-grafted on supports MCM, Al-MCM[a] and SBA are shown in Fig. 34. Similar shapes of isotherms before (not shown) and after rhodium grafting step suggest that the uniform mesoporous structure obtained for the silica supports remained almost unchanged after the grafting. The detailed description of textural features from the isotherms is given in Section 5.1.

The evaluated textural properties of prepared supports and corresponding Rh-grafted catalysts are summarized in Table 11. The catalysts MCM+Rh(2.7 %) and MCM+Al+Rh(2.7 %) have the highest surface area whereas SBA+Rh(2.7 %), SBA+Rh(1.7 %) and SBA+Rh(1.4 %) have the highest mesopore diameter with the presence of micropores in the mesopore structure. Measured points of adsorbed volume were extrapolated by linear plot and went through the origin of t-plot in the case of the Rh-grafted on MCM and Al-MCM[a] supports (not shown). This fact corresponds to micropore volume and micropore area equal to zero. The total pore volume of Al-MCM[a] support decreased after the deposition of $Rh(acac)_3$ complexes whereas it increased in the case of MCM and SBA which may be caused by the densification of silica structure after its modification and calcination.

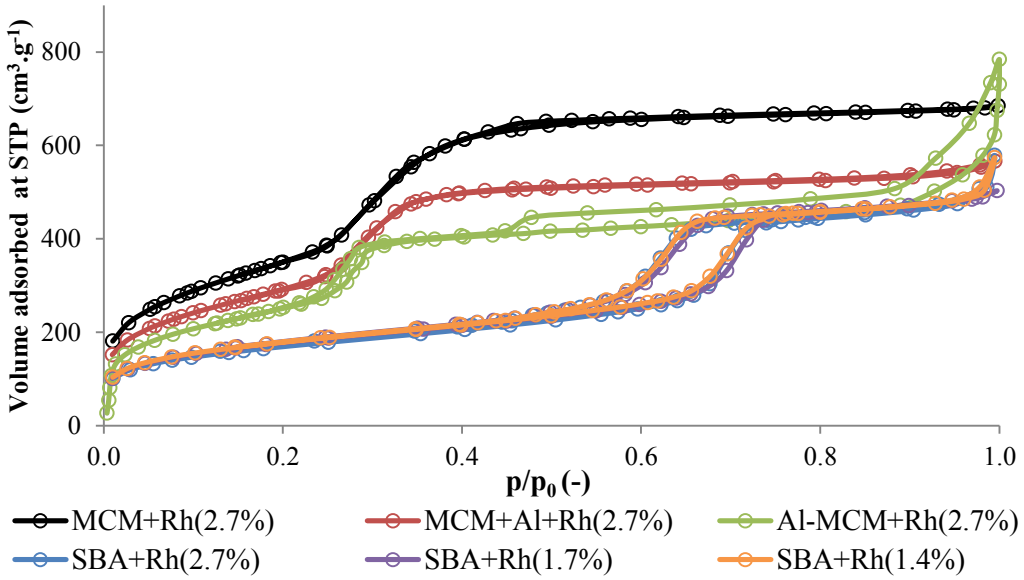

Fig. 34. Nitrogen adsorption-desorption isotherms of prepared Rh-grafted catalysts.

Table 11. Textural properties of silica supports and Rh-grafted catalysts.

Sample	S_{BET}	S_{micro}	V_{total} p/p_0 = 0.99-1.0	V_{micro}	d_{pore}
	$m^2.g^{-1}$	$m^2.g^{-1}$	$cm^3.g^{-1}$	$cm^3.g^{-1}$	nm
MCM[3]	1144	-	1.00	-	2.5
MCM[3]+Rh(2.7 %)	1288	-	1.06	-	2.5
MCM[4]+Al+Rh(2.7 %)	1071	-	0.88	-	2.5
Al-MCM[a]	1011	-	1.25	-	2.5
Al-MCM[a]+Rh(2.7 %)	913	-	0.96	-	2.5
SBA[3]	625	231	0.85	0.10	5.6
SBA[3]+Rh(2.7 %)	609	202	0.90	0.09	5.4
SBA[4]+Rh(1.7 %)	625	213	0.78	0.10	5.7
SBA[4]+Rh(1.4 %)	628	225	0.89	0.10	5.7

[3, 4] Designation of different batches of silica supports MCM and SBA; N_2 sorption analysis of the supports MCM[4] and SBA[4] was not performed.

[a] Designation of Al-MCM synthesized according to Meynen (2010).

5.3.5 Acidity of catalysts surface

The values of total acidity expressed as a total amount of consumed NH_3 in the temperature range 100–500 °C are shown in Table 12. The lowest amount of chemisorbed NH_3 was detected on the pure MCM. The ammonia chemisorption proceeds by the reaction with siloxane Si-O-Si as well as hydroxyl Si-OH groups on the silica surface as described by Zamani et al. (2009). Brønsted acid sites are not expected on surfaces of pure silica materials due to the fact that Brønsted acid sites are generated by the substitution of Si with Al (Chen, 1999). After the grafting and incorporation of aluminum into the MCM structure, the total acidity of MCM significantly increased. The percentage of reactive aluminum sites calculated as a total amount of chemisorbed NH_3 to aluminum concentration from elemental analysis equals to 63 % for Al-MCM[a] and 51 % for MCM+Al. The maxima of temperature peaks of desorbed NH_3 are in the range of weak and moderate acid sites for the catalysts containing rhodium. The total acidity within the non-modified supports and the supports grafted with rhodium increased by 15 % for the support MCM+Al whereas it decreased by 8 % for the support Al-MCM[a]. These differences are within the experimental error and are comparable for the catalysts MCM+Al+Rh(2.7 %) and Al-MCM[a]+Rh(2.7 %).

Table 12. The amount of chemisorbed NH_3 and the maximal temperature of NH_3 desorption for Rh-grafted catalysts.

Sample	T_{max} °C	Chemisorbed NH_3 mmol.g^{-1}
MCM[3]	-	0.02
MCM+Rh(2.7 %)	173	0.04
MCM+Al(1.8 %)	159	0.34
MCM+Al(1.8 %)+Rh(2.7 %)	167	0.39
Al(1.6 %)-MCM[a]	162	0.37
Al(1.6 %)-MCM[a]+Rh(2.7 %)	183	0.34
SBA[3]	-	0.06
SBA+Rh(2.7 %)	223	0.11

5.3.6 Reducibility and dispersion of rhodium on catalysts surface

TPR-H_2 patterns of all the catalysts show sharp reduction peaks with the maximum temperatures in the range 60–95 °C (Fig. 35). According to the literature (Hwang, 1999, Martin, 1995), it corresponds to the reduction of rhodium oxides. The shift of peak maximum to higher temperatures is attributed to smaller Rh particle size and higher dispersion which was described in previous TPR studies (Guerrero-Ruiz, 1997, Pitkaaho, 2012). It is apparent from Fig. 35 that with decreasing rhodium concentration grafted on SBA, there is the shift of T_{max} to higher values presuming higher dispersion of rhodium. The silica supports do not perform any reduction peaks within the tested temperature range (Fig. 36) indicating that the supports do not contribute to the reducibility of catalysts.

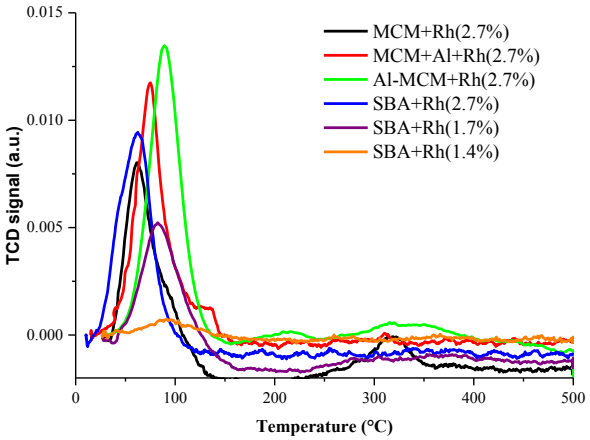

Fig. 35. TPR-H_2 profiles of Rh-grafted catalysts.

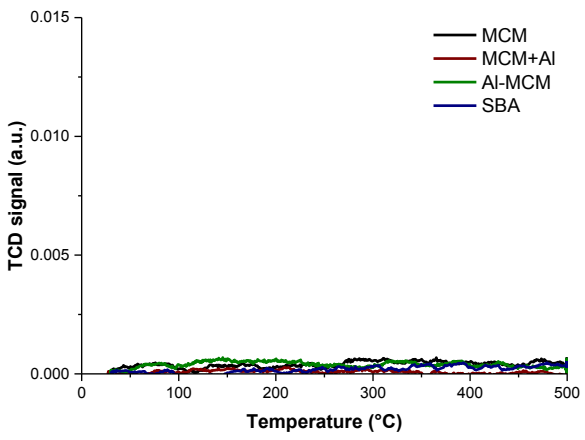

Fig. 36. TPR-H_2 profiles of all prepared supports.

Table 13 demonstrates the results of rhodium dispersion on the catalyst surfaces, particle diameters and metallic surface areas. The presence of aluminum has the promoting effect on rhodium dispersion, the highest dispersion showed Al-MCM[a]+Rh(2.7 %) whereas the percentages of Rh dispersion are comparable for other studied catalysts. However, the values for rhodium dispersion were expected to be higher within the used MDD method. The reason could be that the values of rhodium concentration from EDX analysis are higher than expected. Therefore, the dispersion of rhodium was calculated from the theoretical amount of rhodium as well.

5.3.7 Composition of catalysts surface

The results of XPS experiments are summarized in Table 14. Three different oxidation states of rhodium (Rh^0, Rh^+ and Rh^{3+}) were defined from the values of binding energy (BE). Metallic rhodium shows its peak at 307.1 eV, rhodium oxide with a non-stoichiometric state or Rh^+ at 308.4–308.6 eV, and Rh^{3+} species at 310.0 eV (Brinen, 1975, Wang, 1999). It is apparent from the ratio of each rhodium oxidation state that the addition of aluminum enhanced the oxidation state of rhodium. It is related to higher consumption of H_2 as confirmed by TPR experiments comparing MCM+Al+Rh(2.7 %) and Al-MCM[a]+Rh(2.7 %). In the case of MCM+Al+Rh(2.7 %), the most represented state was Rh^+, whereas Rh^{3+} played a dominant role in the Al-MCM[a]+Rh(2.7 %).

Table 13. The results from TPR-H_2 such as the maximum temperature and consumed hydrogen and from pulsed chemisorption of H_2 such as dispersion, particle diameter and metallic surface area of Rh.

Sample	T_{max} at TPR	H_2 consumed [a]	Dispersion of Rh		Particle diameter of Rh [c]	Metallic surface area [c]
	°C	$mmol.g_{sample}^{-1}$	%		nm	$m^2.g_{metal}^{-1}$
MCM+Rh(2.7 %)	62	0.083	46 [b]	35 [c]	3.1	156
MCM+Al+Rh(2.7 %)	74	0.258	48 [b]	34 [c]	3.3	148
Al-MCM[a]+Rh(2.7 %)	90	0.277	69 [b]	48 [c]	2.3	211
SBA+Rh(2.7 %)	62	0.248	41 [b]	32 [c]	3.5	139
SBA+Rh(1.7 %)	82	0.102	47 [b]	28 [c]	3.9	123
SBA+Rh(1.4 %)	95	0.010	n.d. [b]	n.d. [c]	n.d.	n.d.

[a] H_2 consumed within the temperature region up to 200 °C.

[b] According to theoretical Rh concentration.

[c] According to EDX analysis.

Table 14. Binding energies and the ratios of Rh concentration for each state of Rh (Rh^0, Rh^+ and Rh^{3+}) from the total Rh concentrations.

Sample	Rh^0		Rh^+		Rh^{3+}		Total Rh conc.
	BE	$Rh^{0(a)}$	BE	$Rh^{+(a)}$	BE	$Rh^{3+(a)}$	
	eV	%	eV	%	eV	%	at%
MCM+Rh(2.7 %)	307.1	44	308.5	36	310.0	20	0.50
MCM+Al+Rh(2.7 %)	307.1	14	308.6	53	310.0	33	0.57
Al-MCM[a]+Rh(2.7 %)	307.1	11	308.4	38	310.0	51	0.37
SBA+Rh(2.7 %)	307.1	11	308.5	42	310.0	47	0.19

[(a)] Atomic ratio of Rh concentration for each state to the total Rh concentration (Rh^0, Rh^+ and Rh^{3+}).

5.3.8 Catalytic activity

- **N_2O decomposition in the inert gas**

The temperature dependence of N_2O conversions on the different silica supports with or without aluminum and with various rhodium loadings are displayed in Fig. 37.

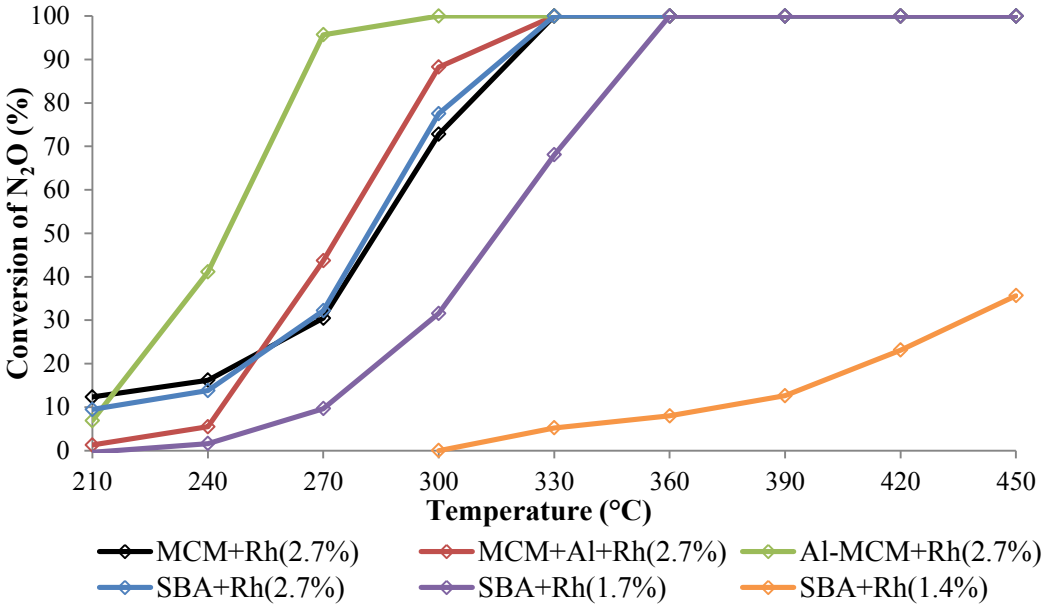

Fig. 37. The N_2O conversions in catalytic decomposition of N_2O on Rh-grafted catalysts.
Conditions: 0.1 mol% N_2O in nitrogen, 0.1 g of catalyst, 100 ml.min^{-1}

From obtained results it can be evaluated:
(i) The effect of supports (SBA, MCM) on the N_2O conversion at the same content of Rh (2.7 %). It is obvious that the catalytic activity of MCM and SBA at the same initial $Rh(acac)_3$ loading (0.2 mmol.$g_{support}^{-1}$) is comparable. It is apparent from Fig. 38 expressing the catalytic activity as the turnover frequency (TOF). TOF is defined as the number of N_2O molecules converted per time per rhodium concentration, Eq. 28 (Abdul-Wahab, 2013).

$$TOF = \frac{n_{N_2O,reacted}}{n_{Rh}} \tag{28}$$

However, the difference is obvious from the comparison of converted N_2O molecules per BET surface area in Fig. 39. More catalytic active sites per unit specific surface area are distributed on SBA with almost twice lower BET surface area than MCM, within the same rhodium concentration (2.7 %). Even though, BET surface area of SBA is high enough for good rhodium dispersion and is not a limiting factor in the catalytic activity of the N_2O decomposition.

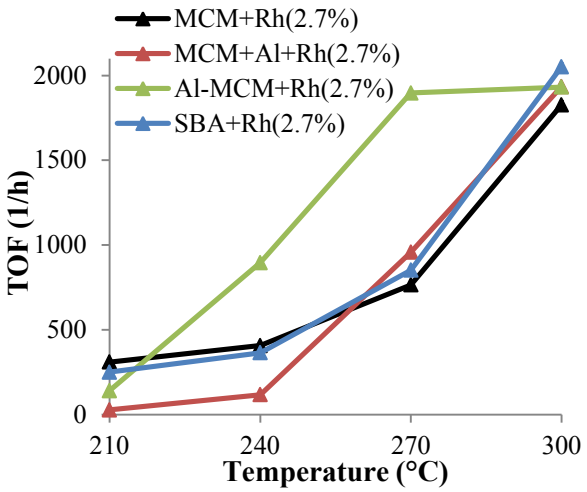

Fig. 38. TOF versus temperature.

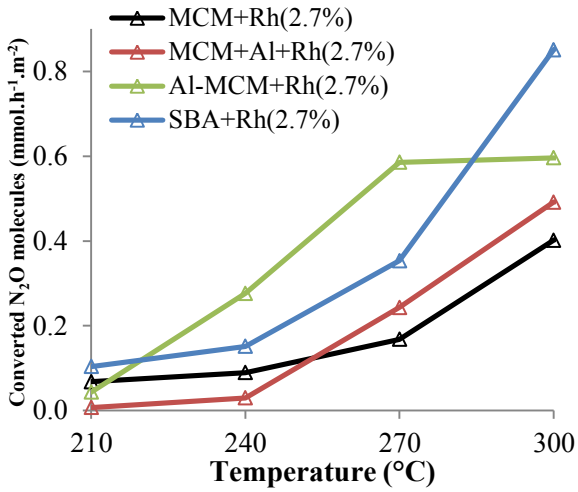

Fig. 39. Converted N_2O molecules per BET surface area versus temperature.

- Elimination of internal diffusion effect

The result of nearly the same catalytic activities of MCM+Rh(2.7 %) and SBA+Rh(2.7 %) supports the fact that differences in mesoporous-microporous structures of MCM and SBA do not play key role within the applied amount of rhodium and experimental conditions of N_2O decomposition.

As mentioned in Section 4.4.2, the rate of catalytic reaction of N_2O decomposition should be governed by the catalytic reaction with the elimination of internal diffusion effect. It can be confirmed by the calculation of the internal effectiveness factor η valid for 1st order reaction in a spherical catalyst pellet according to the article (Klyushina, 2015). The parameters needed for the calculation are: the porosity/tortuosity of catalyst particle (= 0.1), the pore radius (Table 11), the density of N_2 in dependence on the reaction temperature, the pressure at the inlet (=102000 Pa) and the bulk densities of supports which were measured (MCM = $267 \cdot 10^3$ g.m^{-3}, Al-MCM^a = $285 \cdot 10^3$ g.m^{-3}, Al-MCM^b = $394 \cdot 10^3$ g.m^{-3}, SBA = $280 \cdot 10^3$ g.m^{-3}). The kinetic constants k (Table 15) were estimated according to Eq. 29 obtained by integration and linearization of the equation of experimental reactor mass balance and the kinetic equation for N_2O conversions on Rh-grafted catalysts below the value of 1. It is assumed that the reaction of N_2O decomposition (Eq. 7) is the 1st order reaction.

$$k = \frac{\ln\left(\frac{1}{1 - X_{N2O}}\right) \cdot \dot{V}}{m_{catalyst}} \tag{29}$$

where k – kinetic constant, 1st order rate law (m^3.s^{-1}.g^{-1}), X_{N2O} – conversion of N_2O molecules (-), $\dot{V}$ – volume flow of gas reaction mixture (m^3.s^{-1}), $m_{catalyst}$ – weight of catalyst (g).

Temperature dependence of the internal effectiveness factor in Rh-grafted catalysts for the N_2O conversions below the value of 1 is depicted in Fig. 40. The value of internal effectiveness factor close to 1 represents none or negligible effect of internal diffusion which is estimated for Rh-grafted catalysts within the applied experimental conditions.

(ii) The effect of different rhodium loading on SBA. It is obvious that with decreasing rhodium concentration, the N_2O conversion decreased. The choice of appropriate concentration of rhodium is apparent in the case of the catalyst SBA+Rh(1.4 %). Its initial concentration of Rh was 20 times lower than SBA+Rh(2.7 %) while the conversion of N_2O at 450°C decreased by 64 % showing low catalytic activity. At the temperature 330 °C is the catalytic activity in following order: 100 % for SBA+Rh(2.7 %) > 68 % for SBA+Rh(1.7 %) > 5 % for SBA+Rh(1.4 %).

(iii) The effect of modification of MCM by aluminum (incorporated or grafted) at the same content of Rh (2.7 %). The conversion of N_2O was in the order: Al-MCM^{a}+Rh(2.7 %) > MCM+Al+Rh(2.7 %) > SBA+Rh(2.7 %) ≈ MCM+Rh(2.7 %). The aluminum improved the catalytic activity which is in agreement with literature (Xu, 2004, Chmielarz, 2011). However, there has been no previous comparison of different location of aluminum within the structure of mesoporous ordered silica materials and its influence on rhodium dispersion measured by pulsed chemisorption of hydrogen. As it is shown in Table 13, aluminum incorporated within the support structure increased rhodium dispersion on catalyst surface which was confirmed by catalytic tests as to be beneficial for the catalytic activity in N_2O decomposition.

The reaction of N_2O decomposition is governed by the presence of both oxidation states of rhodium (Rh^{+} and Rh^{3+}) rather than the metallic state of rhodium. However, there is no clear evidence which of the oxidation states play the key role in the catalytic activity.

The formation of NO and NO_2 is possible during N_2O decomposition which was analyzed for the catalyst Al-MCM^{a}+Rh(2.7 %) by converting the NO_2 to NO and measure the sum NO+NO_2 (NO_x) by IR spectrometer Ultramat 6. The NO_x was the highest at the temperature 450 °C, however, still negligible (16 ppm)

.

Table 15. The kinetic constants *k* evaluated from the N_2O conversions on Rh-grafted catalysts.

	Temperature (°C)								
	450	420	390	360	330	300	270	240	210
MCM+Rh(2.7 %)	-	-	-	-	-	$4.5 \cdot 10^{-5}$	$1.2 \cdot 10^{-5}$	$5.5 \cdot 10^{-6}$	$3.9 \cdot 10^{-6}$
MCM+Al+Rh(2.7 %)	-	-	-	-	-	$7.4 \cdot 10^{-5}$	$1.9 \cdot 10^{-5}$	$1.7 \cdot 10^{-6}$	$3.8 \cdot 10^{-7}$
Al-MCM[a]+Rh(2.7 %)	-	-	-	-	-	-	$1.0 \cdot 10^{-4}$	$1.6 \cdot 10^{-5}$	$2.1 \cdot 10^{-6}$
SBA+Rh(2.7 %)	-	-	-	-	-	$5.2 \cdot 10^{-5}$	$1.3 \cdot 10^{-5}$	$4.6 \cdot 10^{-6}$	$2.9 \cdot 10^{-6}$
SBA+Rh(1.7 %)	-	-	-	-	$4.2 \cdot 10^{-5}$	$1.3 \cdot 10^{-5}$	$3.3 \cdot 10^{-6}$	$5.1 \cdot 10^{-7}$	-
SBA+Rh(1.4 %)	$1.9 \cdot 10^{-5}$	$1.1 \cdot 10^{-5}$	$5.4 \cdot 10^{-6}$	$3.2 \cdot 10^{-6}$	$2.0 \cdot 10^{-6}$	-	-	-	-

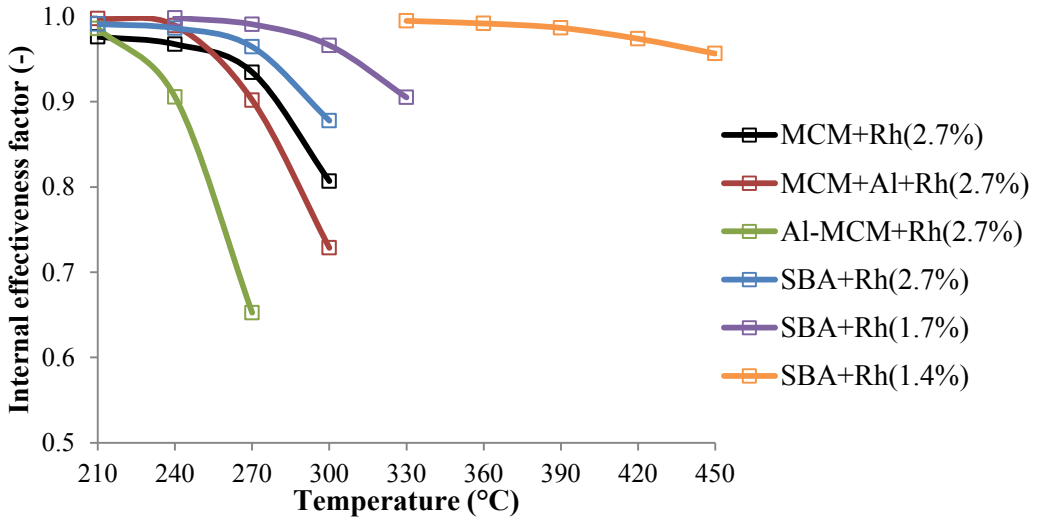

Fig. 40. Temperature dependence of the internal effectiveness factor calculated for Rh-grafted catalysts.

➢ Catalytic tests in the presence of inhibiting compounds (O_2, H_2O, NO)

The highest catalytic activity remained for Al-MCM[a]+Rh(2.7 %) even within the presence of O_2, H_2O and NO. In comparison with other catalysts, Al-MCM[a]+Rh(2.7 %) showed the highest resistance to water vapor, the decrease of catalytic activity was about twice lower than for other catalysts. The result of nearly the same catalytic activities of MCM+Rh(2.7 %) and SBA+Rh(2.7 %) in the presence of inhibiting compounds supports the fact that differences in mesoporous-microporous structure do not play key role in the presented experiments of N_2O decomposition (Table 16). High resistance to water vapor inhibition is important for potential practical application. Since NO presence in reaction mixture caused shift of T_{50} to significantly higher value, the Al-MCM[a]+Rh(2.7 %) catalyst is suitable for N_2O decomposition downstream the DeNOx technology where only traces of NO_x are present. Quite low value of T_{90} (340 °C) in the presence of oxygen and water vapor makes this catalyst comparable with others published in scientific literature, however, in practical applications, preheating of waste gases prior to the N_2O decomposition reactor would be necessary.

Table 16. Temperatures of 50 % (T_{50}) and 90 % (T_{90}) N_2O conversions for Rh-grafted catalysts.
Conditions: N_2O decomposition in inert conditions: 0.1 mol% N_2O in nitrogen, N_2O decomposition in real conditions: 0.1 mol% N_2O, 5 mol% O_2, 200 ppm NO, 1.8–2.3 mol% of water vapor in nitrogen, 0.1 g of catalyst, 100 ml.min^{-1}.

Sample	N_2, N_2O T_{50} °C	N_2, N_2O T_{90} °C	+ O_2, H_2O T_{50} °C	+ O_2, H_2O T_{90} °C	+ O_2, H_2O, NO T_{50} °C	+ O_2, H_2O, NO T_{90} °C
MCM+Rh(2.7 %)	284	319	385	418	419	448
MCM+Al+Rh(2.7 %)	274	304	406	437	424	454
Al-MCM[a]+Rh(2.7 %)	245	267	305	340	388	416
SBA+Rh(2.7 %)	282	317	393	429	420	449
SBA+Rh(1.7 %)	315	351	409	442	442	474
SBA+Rh(1.4 %)	485	581	n.d.	n.d.	n.d.	n.d.

➢ Stability of catalysts during catalytic tests

The stability of catalysts was checked by two tests of N_2O decomposition at reference conditions (in inert gas) which were performed (i) at the beginning of catalytic runs and (ii) after the catalytic experiments in the presence of oxygen, water vapor and NO simulating process conditions in waste gas from nitric acid production. The catalysts after test in the presence of inhibiting compounds (O_2, H_2O and NO) were regenerated in nitrogen flow at 450 °C for 1 h. They showed a good agreement within the evaluated measurement error (5 %) with the catalytic tests performed in nitrogen atmosphere (Fig. 41). The significant influence on the stability of the catalysts on basis of

mesoporous ordered silicas is expected to be due to water vapor as their low hydrothermal stability is widely known. The duration of catalytic tests in the presence of water vapor was 40 h in average. However, the catalytic activities did not decrease after the exposure to water vapor.

The reason of stability control was the fact that it is generally known that mesoporous silica materials often suffer by dealumination. Dealumination as the removal of aluminum causing the structural collapse was described in detail in literature (Xia, 2003). These results regarding the stability of catalysts are in agreement with the study of Hussain and co-authors (2013), reporting that the catalysts showed good stability which indicated that the dealumination process is very slow.

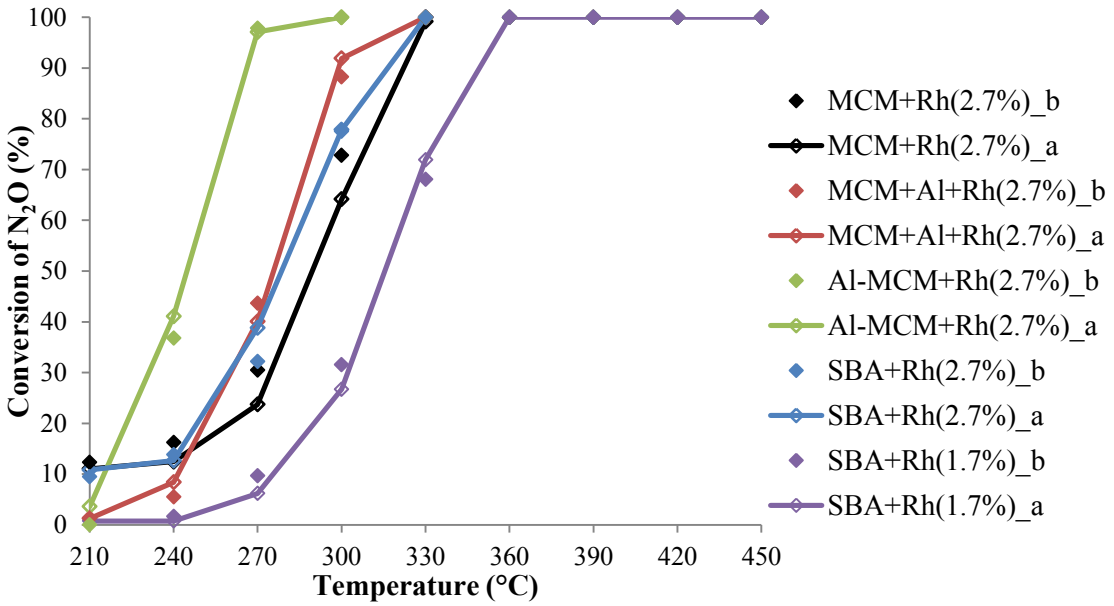

Fig. 41. The N_2O conversions in catalytic decomposition of N_2O on Rh-grafted catalysts before (b) and after (a) exposure to inhibiting compounds.

Conditions: 0.1 mol% N_2O in nitrogen, 0.1 g of catalyst, 100 $ml.min^{-1}$

6 CONCLUSIONS

The aim of this doctoral dissertation was to contribute to surface activation of ordered mesoporous silica materials and their application for the catalytic reactions (N_2O decomposition and reduction by carbon monoxide and CO oxidation at low temperatures).

Three different types of ordered mesoporous silica materials, such as MCM-41 (designated as MCM), aluminum incorporated into the silica framework MCM-41 (designated as Al-MCM) and SBA-15 (designated as SBA), were prepared. Apart from elemental composition, they differed in textural and structural properties. MCM had the highest surface area whereas SBA had the smallest surface area with the presence of micropores interconnecting mesopores with the diameter almost twice bigger than the diameters of MCM and Al-MCM. Different position of aluminum within silica framework was compared according to different syntheses either by aluminum incorporation during the synthesis of MCM or by aluminum grafting on as-prepared MCM or SBA by the Molecular Designed Dispersion (MDD) method. Furthermore, the MDD technique was applied for the surface activation of ordered mesoporous silicas by the deposition of catalytically active metal species (cobalt or rhodium).

Initial concentrations of aluminum acetylacetonate complexes as the precursors for MDD synthesis were determined experimentally in correlation with prepared Al-MCM samples of specific Si/Al ratio (20, 40, 60 or 32) according to two different approaches in their syntheses. The obtained values were applied in further preparation of catalysts. According to the calculation of monolayer capacity and experimental values, aggregates and multilayers of aluminum might be formed on MCM support before a complete monolayer was formed.

Different loadings of cobalt and repeated syntheses showed a good reproducibility of MDD technique. According to obtained experimental values of cobalt loading capacity and theoretical calculation of monolayer capacity, the same initial concentration of $Co(acac)_2$ equal to 3.2 $mmol_{Co(acac)2} \cdot g_{support}^{-1}$ was used. Five mesoporous silica supports were used for the syntheses of Co-grafted catalysts assigned as MCM+Co, MCM+Al+Co, Al-MCM^b+Co, SBA+Co and SBA+Al+Co. The cobalt concentrations measured by AAS analysis were comparable (in the range 9.5–12.2 wt%).

The results of the characterization of Co-grafted catalysts can be summarized as follows:

- It was identified that the grafting of cobalt by MDD caused the decrease of BET surface area and total pore volume of MCM and Al-MCM^b supports which could be due to their mesopores blocking and the densification of their structures. There was not such significant change in the case of SBA which can be attributed to bigger mesopore diameter.

- The presence of Co spinel phase was detected in the Al-MCM^{b}+Co by XRD, nevertheless, it was not possible to distinguish between Co_3O_4, $CoAl_2O_4$ and $Co_2Al_2O_4$ phases. The phases $CoAl_2O_4$ and $Co_2Al_2O_4$ were excluded by Raman spectroscopy, however, the resolution of CoO and Co_3O_4 phases was not ultimate for all Co-grafted catalysts. The occurrence of non-specified oxide Co_xO_y was confirmed in the catalyst Al-MCM^{b}+Co by DR UV-vis spectroscopy as well. This analysis identified the presence of tetrahedral Co(II) species in all prepared catalysts.
- High reduction stability of Co^{2+} ions interacting strongly with the support was confirmed for the catalysts MCM+Co, MCM+Al+Co, SBA+Co and SBA+Al+Co showing the maxima temperatures (810–862 °C) in TPR-H_2 profiles. The highest temperature during TPR-H_2 performed the catalyst SBA+Co assuming the most uniform cobalt dispersion on SBA than on other catalysts. The shift of temperature maxima to lower temperature in the case of Al-MCM^{b}+Co was related to the presence of Co^{2+} as well as Co^{3+} ions. All Co-grafted catalysts performed very low amount of easily reducible compounds below the temperature 600 °C.

From the catalytic tests performed on Co-grafted catalysts can be concluded:

- The Co-grafted catalysts showed poor activity (14 %) in catalytic N_2O decomposition in the inert condition at 450 °C and at GHSV 15648 h^{-1}. This was in agreement with TPR-H_2 study as Co-grafted catalysts showed very low H_2 consumption within the temperature range of catalytic tests of N_2O decomposition. The reduction of transition metal (such as cobalt) is connected with desorption of oxygen from the catalysts surface known as the rate determining step of the catalytic N_2O decomposition. Thus, the use of carbon monoxide as the reducing agent can facilitate the desorption of O_2 which was confirmed as the N_2O conversion increased up to 26 % at 450 °C (at GHSV 15648 h^{-1}). The catalytic reduction of N_2O by CO was studied in the presence of O_2 as well and the conversion of CO was 100 % on MCM+Co in the range 300–450 °C. Hence, the Co-grafted catalysts were further tested in the reaction of CO oxidation.
- The catalytic activities in the oxidation of CO were found in the order: SBA+Co > Al-MCM^{b}+Co > SBA+Al+Co > MCM+Co > MCM+Al+Co. The highest amount of crystalline Co_xO_y in Al-MCM^{b}+Co structure in comparison with other catalysts contained both cobalt ions, Co^{2+} as well as Co^{3+}, which appeared to be beneficial for its higher catalytic activity opposite to MCM+Co and MCM+Al+Co. On the other hand, it is assumed that a specific ration between Co^{2+} and Co^{3+} ions is not definitely required as the other Co-grafted catalysts active in CO oxidation were comparable from the point of view of oxidation and coordination state of cobalt. By expressing the catalytic activity as converted CO molecules per unit BET surface area, more active sites were distributed on SBA+Co per unit surface area than on other catalysts. Better accessibility of $Co(acac)_2$

complexes in bigger mesopore diameters of SBA during MDD synthesis could lead to higher density of catalytically active cobalt sites on SBA. It is expected that the dispersion of cobalt on silica supports was the main reason for different catalytic activities. The density of catalytic active sites is planned to be investigated by pulse chemisorption and temperature programmed reduction by CO in future study.

The MDD method was applied for the deposition of rhodium on four different mesoporous silica supports: MCM, MCM with aluminum incorporated into the silica framework (Al-MCM[a]), MCM grafted with aluminum (MCM+Al) and SBA. The initial concentrations of $Rh(acac)_3$ complexes (0.2–0.01 $mmol_{Rh(acac)3}.g_{support}^{-1}$) were applied according to previous studies reported in literature.
The results of the characterization of Rh-grafted catalysts can be summarized as follows:

- Total volume of Al-MCM[a] support decreased whereas it increased in MCM and SBA supports after rhodium grafting by MDD which could be caused by the densification of their silica structures.
- It was identified by TPD-NH_3 measurements that the total acidity after grafting or incorporation of aluminum significantly increased, however, their differences were within the experimental error and were comparable for MCM+Al+Rh(2.7 %) and Al-MCM+Rh(2.7 %). Thus, it is estimated that the total acidity did not play a key role in the reaction of N_2O decomposition.
- The addition of aluminum enhanced the oxidation state of rhodium as determined by XPS analysis. The state Rh^+ was the most dominant in MCM+Al+Rh(2.7 %) whereas the state Rh^{3+} was the most represented one in Al-MCM+Rh(2.7 %). Nevertheless, there is no clear evidence which of the oxidation states (Rh^+/Rh^{3+}) had the main influence in N_2O decomposition.
- The reduction of all Rh-grafted catalysts occurred in a similar manner and similar temperature range (60–95 °C). The reduction peak with higher maxima showed Al-MCM+Rh(2.7 %) attributed to higher dispersion of rhodium. This was confirmed by pulsed chemisorption of hydrogen.

From the catalytic tests performed on Rh-grafted catalysts can be concluded:

- The catalytic activities of Rh-grafted catalysts with the same rhodium concentration were in the order: Al-MCM+Rh(2.7 %) > MCM+Al+Rh(2.7 %) > SBA+Rh(2.7 %) ≈ MCM+Rh(2.7 %). The same order in catalytic activities was found by testing the catalytic activities in N_2O decomposition either in the absence or in the presence of inhibiting compounds (O_2, H_2O and NO). So far, it was proven that aluminum incorporated into the structure enhanced rhodium dispersion on the catalyst support as to be beneficial for its catalytic activity in the reaction of N_2O decomposition.

- The choice of appropriate rhodium concentration is also important for the design of catalytically active material. It was obvious that with decreasing rhodium concentration on SBA, the N_2O conversion decreased, in the following order at 330 °C: 100 % for SBA+Rh(2.7 %) > 68 % for SBA+Rh(1.7 %) > 5 % for SBA+Rh(1.4 %) showing very low catalytic activity.
- The result of nearly the same catalytic activities of MCM+Rh(2.7 %) and SBA+Rh(2.7 %) supports the fact that their surface areas were high enough for good and comparable rhodium dispersion for applied rhodium concentration. The reaction rate of N_2O catalytic decomposition is estimated to be governed by the catalytic reaction with none or negligible effect of internal diffusion. Therefore, the differences in pore volume or pore diameter of ordered mesoporous silica supports should not have the effect on the rate of catalytic reaction under the applied reaction conditions.
- The significant influence on the stability of the catalysts on basis of mesoporous ordered silicas was expected to be due to water vapor. Despite of this fact, the catalytic activities did not decrease after the exposure to water vapor (40 h in average) as showed the stability tests of the catalysts.

7 LIST OF REFERENCES

ABDUL-WAHAB, M.I., JACKSON, S.D. Hydrogenation of 3-nitroacetophenone over rhodium/silica catalysts: Effect of metal dispersion and catalyst support. *Applied Catalysis A: General*. 2013, 462–463, 121–128.

AHENAH, J., COOL, P., VANSANT, E.F. Enhanced Brönsted acidity created upon Al-grafting of porous clay heterostructures via aluminium acetylacetonate adsorption. *Physical Chemistry Chemical Physics*. 2000, 2, 5750–5755.

ALBUQUERQUE, M.C.G. et al. CaO supported on mesoporous silicas as basic catalysts for transesterification reactions. *Applied Catalysis A: General*. 2008, 334 (1–2), 35–43.

BALTES, M. et al. Synthesis and characterization of alumina-supported vanadium oxide catalysts prepared by the MDD of $VO(acac)_2$ complexes. *Physical Chemistry Chemical Physics.* 2000, 2, 2673–2680.

BALTES, Michael. *Synthesis and characterization of vanadium oxide catalysts*. Belgium, 2001. PhD Dissertation. Universitaire Instelling Antwerpen. Promoter E. F. Vansant.

BECK, J.S. et al. A new family of mesoporous molecular sieves prepared with liquid crystal templates. *Journal of the American Chemical Society*. 1992, 114 (27), 10834–10843.

BEYER, H. et al. Decomposition of nitrous oxide by rhodium catalysts: Effect of rhodium particle size and metal oxide support. *Applied Catalysis A: General.* 2011, 391, 411–416.

BHOWARE, S.S. et al. Cobalt-containing hexagonal mesoporous molecular sieves (Co-HMS): Synthesis, characterization and catalytic activity in the oxidation reaction of ethylbenzene. *Journal of Molecular Catalysis A: Chemical*. 2006, 255, 123–130.

BHOWARE, S.S., SINGH, A.P. Characterization and catalytic activity of cobalt containing MCM-41 prepared by direct hydrothermal, grafting and immobilization methods. *Journal of Molecular Catalysis A: Chemical*. 2007, 266, 118–130.

BHOWARE, S.S., KAMBLE, K.R. Catalytic activity of cobalt containing MCM-41 and HMS in liquid phase oxidation of diphenylmethane. *Catalysis Letters*. 2009, 133, 106–111.

BOISSEL, V., TAHIR, S., KOH C.A. Catalytic decomposition of N_2O over monolithic supported noble metal-transition metal oxides. *Applied Catalysis B: Environmental*. 2006, 64, 234–242.

BOIX, A.V., ASPROMONTE, S.G., MIRÓ, E.E. Deactivation studies of the SCR of NOx with hydrocarbons on Co-mordenite monolithic catalysts. *Applied Catalysis A: General.* 2008, 341 (1–2), 26–34.

BRINEN, J.S. et al. X-ray photoelectron spectroscopy studies of the rhodium on charcoal catalyst: II. Dispersion as a function of reduction. *Journal of Catalysis*. 1975, 40 (3), 295–300.

CESTEROS, Y., HALLER, G.L. Several factors affecting Al-MCM-41 synthesis. *Microporous and Mesoporous Materials*. 2001, 43, 171–179.

CHEN, L.Y. et al. A comparison of post-synthesis alumination and sol-gel synthesis of MCM-41 with high framework aluminum content. *Microporous and Mesoporous Materials*. 1999, 27, 231–242.

CHEN, Y.-J., WU D.-e., YEH, C.-t. Oxidation of carbon monoxide over nanoparticles of cobalt oxides. *Reviews on Advanced Materials Science*. 2003, 5, 41–46.

CHI, Y.-S., LIN, H.-P., MOU, C.-Y. CO oxidation over gold nanocatalyst confined in mesoporous silica. *Applied Catalysis A: General.* 2005, 284, 199–206.

CHIANG, C.-W., WANG, A., MOU, C.-Y. CO oxidation catalyzed by gold nanoparticles confined in mesoporous aluminosilicate Al-SBA-15: Pretreatment methods. *Catalysis Today*. 2006, 117, 220–227.

CHMIELARZ, L. et al. Nitrous oxide reduction with ammonia and methane over mesoporous silica material modified with transition metal oxides. *Journal of Porous Materials*. 2005, 12, 183–191.

CHMIELARZ, L. et al. Catalytic performance of various mesoporous silicas modified with copper or iron oxides introduced by different ways in the selective reduction of NO by ammonia. *Applied Catalysis B: Environmental*. 2006, 62, 363–380.

CHMIELARZ, L. et al. SBA-15 mesoporous silica modified with metal oxides by MDD method in the role of $DeNO_x$ catalysts. *Microporous and Mesoporous Materials*. 2010, 127, 133–141.

CHMIELARZ, L. et al. SBA-15 mesoporous silica modified with rhodium by MDD method and its catalytic role for N_2O decomposition reaction. *Journal of Porous Materials*. 2011, 18, 483–491.

CHRISTOPHER, J., SWAMY, C.S. Studies on the catalytic decomposition of N_2O on $LnSrFeO_4$ (Ln, La, Pr, Nd, Sm and Gd). *Journal of Molecular Catalysis*. 1991, 68 (2), 199–213.

COLLART, Olivier. *Nanodesign of an (alumino)silicate framework into a mesoporous MCM-48 architecture*. Belgium, 2003. PhD Dissertation. Universitaire Instelling Antwerpen. Promoter E. F. Vansant.

COLLART, O. et al. A controlled dispersion of Al^{3+} onto a silica mesoporous material. A comparative study with Al^{3+} incorporation. *Studies in Surface Science*. 2001, 135, 179.

COOL, P., AHENAH, J., COLLART, O., VANSANT, E.F. Al-modified porous clay heterostructures with combined micro and mesoporosity. *Studies in Surface Science and Catalysis*. 2000, 129, 409–416.

DITL, Pavel. *Chemické reaktory*. Ed. 2. Praha: ČVUT, Strojní fakulta, 2000. 193 p. ISBN 80-010-2207-2.

DRAGO, R.S., JURCZYK, K., KOB, N. Catalyzed decomposition of N_2O on metal oxide supports. *Applied Catalysis B: Environmental*. 1997, 13, 69–79.

DRY, M.E. The Fischer-Tropsch process: 1950–2000. *Catalysis Today*. 2002, 71, 227–241.

DU, J. et al. The influence of precursors on Rh/SBA-15 catalysts for N_2O decomposition. *Applied Catalysis B: Environmental*. 2008, 84, 490–496.

ENGEL, T., ERTL, G. Elementary steps in the catalytic oxidation of carbon monoxide on platinum metals. *Advances in Catalysis and Related Subjects*. 1979, 28, 1–78.

CAZES, J. *Ewing´s analytical instrumentation handbook*. Ed. 3. New York : Marcel Dekker, 2005. 1033 p. ISBN 0-8247-5348-8.

FARRIS, T.S. et al. Method for decomposing N_2O utilizing catalysts comprising calcined anionic clay minerals. United States Patent 5,472,677 A. Date of patent December 5, 1995.

FARZANEH, F., JALALIAN, M. and TALEBI, L. Epoxidation of alkenes with molecular oxygen catalyzed by immobilized $Co(acac)_2$ and $Co(bpy)_2Cl_2$ complexes within nanoreactors of Al-MCM-41. *E-Journal of chemistry*. 2012, 9 (4), 2205–2212.

FLAGAN, R.C., SEINFELD, J.H. *Fundamentals of air pollution engineering*. Courier Corporation, 2013. 576 p. Corrected republication of the work originally published in 1988 by Prentice-Hall.

FOGLER, H.S. *Elements of Chemical Reaction Engineering*. 3rd edition. New Jersey : Prentice Hall PTR, 1999.

GALLE, M., AGAR, D.W. WATZENBERGER, O. Thermal N_2O decomposition in regenerative heat exchanger reactors. *Chemical Engineering Science.* 2001, 56, 1587–1595.

GRANGER, P. et al. Effect of yttrium on the performances of zirconia based catalysts for the decomposition of N_2O at high temperature. *Applied Catalysis B: Environmental*. 2006, 62, 236–243.

GUERRERO-RUIZ, A. et al. Preparation, characterization, and activity for n-hexane reactions of alumina-supported rhodium-copper catalysts. *Journal of Catalysis*. 1997, 171, 374–382.

HABER, J. et al. Alkali-metal promoted rhodium-on-alumina catalysts for nitrous oxide decomposition. *Applied Catalysis B: Environmental*. 2008, 77, 278–283.

HAMDY, M.S. et al. Fe, Co and Cu-incorporated TUD-1: Synthesis, characterization and catalytic performance in N_2O decomposition and cyclohexane oxidation. *Catalysis Today*. 2005, 110, 264–271.

HAMON, C. et al. Catalyst based on ferrierite/iron for catalytic reduction of nitrous oxide. United States Patent, 7,238,641 B2. Date of patent July 3, 2007.

HANU, A.-M. et al. Influence of the MCM-41 morphology on the vanadia deposition by a molecular designed dispersion method. *Microporous and Mesoporous Materials*. 2006, 95, 31–38.

HANU, A.-M. et al. Influence of the MCM-41 silanol number on vanadia deposition by molecular designed dispersion method. *Revista De Chimie*. 2007, 10, 1004–1005.

HARRIS, K.D.M., EDWARDS, P.P. *Turning points in solid-state, materials and surface state*. Royal Society of Chemistry, 2008.

HUAKKA, S., LAKOMAA, S.H., SUNTOLA, T. Chemisorption of chromium acetylacetonate on porous high surface area silica. *Applied Surface Science*. 1994, 75, 220–227.

HLAVÁČ, J. *Základy technologie silikátů*. SNTL – Nakladatelství technické literatury. Praha, 1981.

HOTTA, M. et al. Decomposition catalyst for nitrous oxide, process for producing the same and process for decomposing nitrous oxide. United States Patent, 2006/0008401. Date of patent January 12, 2006.

HUO, C., OUYANG, J., YANG, H. CuO nanoparticles encapsulated inside Al-MCM-41 mesoporous materials via direct synthetic route. *Scientific Reports 4*. 2014, 3682. doi:10.1038/srep03682.

HUSSAIN, M., FINO, D., RUSSO, N. N_2O decomposition by mesoporous silica supported Rh catalysts. *Journal of Hazardous Materials*. 2012, 211–12, 255–265.

HUSSAIN, M. et al. Modified KIT-6 and SBA-15-sperical supported metal catalysts for N_2O decomposition. *Journal of Environmenal Chemical Engineering*. 2013, 1, 164–174.

HUSSAIN, M., FINO, D., RUSSO, N. Development of modified KIT-6 and SBA-15-sperical supported Rh catalysts for N_2O abatement: From powder to monolith supported catalysts. *Chemical Engineering Journal*. 2014, 238, 198–205.

HWANG, C.-P., YEH, C.-T., ZHU, Q. Rhodium-oxide species formed on progressive oxidation of rhodium clusters dispersed on alumina. *Catalysis Today*. 1999, 51, 93–101.

IVANOV, D.V. et al. Influence of oxygen mobility on catalytic activity of La-Sr-Mn-O composites in the reaction of high temperature N_2O decomposition. *Journal of Catalysis*. 2009, 267, 5–13.

JANA, S.K. et al. Aluminium incorporation in mesoporous MCM-41 molecular sieves and their catalytic performance in acid-catalyzed reactions. *Applied Catalysis A: General*. 2003, 245, 33–41.

JANAS, J. et al. Effect of Co content on the catalytic activity of CoSiBEA zeolite in the selective catalytic reduction of NO with ethanol: Nature of the cobalt species. *Applied Catalysis B: Environmental*. 2007, 75, 239–248.

KAPTEIJN, F., RODRIGUEZ-MIRASOL, J., MOULIJN, J. A. Heterogenous catalytic decomposition of nitrous oxide. *Applied catalysis B: Environmental*. 1996, 9, 25–64.

KAPTEIJN, Freek et al. *Laboratory Reactors, in Handbook of Heterogeneous Catalysis*. Germany : Wiley-VCH Verlag GmbH, Weinheim, 1997.

KARÁSKOVÁ, K. et al. Effect of promoters in Co-Mn-Al mixed oxide catalyst on N_2O decomposition. *Chemical Engineering Journal*. 2010, 160, 480–487.

KAWI, S., LIU, S.Y., SHEN S.-C. Catalytic decomposition and reduction of N_2O on Ru/MCM-41 catalyst. *Catalysis Today*. 2001, 68, 237–244.

KENVIN, J.C., WHITE, M.G. Prepration and characterization of supported mononuclear metal complexes as model catalysts. *Langmuir*. 1991, 7, 1198–1205.

KLYUSHINA, A., et al. Advantages of stainless steel sieves as support for catalytic N_2O decomposition over K-doped Co_3O_4. *Catalysis today*. 2015, In Press, Corrected Proof.

KOVANDA, F. et al. Mixed oxides obtained from Co and Mn containing layered double hydroxides: Preparation, characterization, and catalytic properties. *Journal of Solid State Chemistry*. 2006, 179, 812–823.

KOZLOVA, S.A., KIRIK, S.D. Post-synthetic activation of silanol covering in the mesostructure silicate materials MCM-41 and SBA-15. *Microporous and Mesoporous Materials*. 2010, 133, 124–133.

LEE, H.S. et al. High thermoelectric power in a Na_xCoO_2 thin film prepared by sputtering with rapid thermal annealing. *Current Applied Physics*. 2015, 15, 412-416.

LIMNELL, T. et al. Physicochemical stability of high indomethacin payload ordered mesoporous silica MCM-41 and SBA-15 microparticles. *International Journal of Pharmaceutics*. 2011, 416, 242–251.

LIN, H.-K. et al. Synthesis, characterization and catalytic oxidation of carbon monoxide over cobalt oxide. *Catalysis Letters*. 2003, 88 (3–4), 169–174.

LIU, S. et al. The influence of the alcohol concentration on the structural ordering of mesoporous silica: cosurfactant versus cosolvent. *Journal of Physical Chemistry B*. 2003, 107, 10405–10411.

LOPES, I., DAVIDSON, A., THOMAS, C. Calibrated Co_3O_4 nanoparticles patterned in SBA-15 silicas: Accessibility and activity for CO oxidation. *Catalysis Communications*. 2007, 8, 2105–2109.

MAKHLOUF, M.T., ABU-ZIED, B.M., MANSOURE, T.H. Direct Fabrication of Cobalt Oxide Nano-particles Employing Glycine as a Combustion Fuel. *Physical Chemistry*. 2012, 2 (6), 86–93.

MARTIN, D., DUPREZ, D. The effects of support and of particle size on the redox properties of rhodium. *Applied Catalysis A-General*. 1995, 131, 297–307.

MARTINEZ-HERNÁNDEZ, A., FUENTES, G.A. Redistribution of cobalt species in Co-ZSM5 during operation under wet conditions in the reduction of NOx by propane. *Applied Catalysis B: Environmental*. 2005, 57 (3), 167–174.

MATSUMURA, Y., HASHIMOTO, K., MOFFAT, J.B. Mechanism for the formation of carbon dioxide in the catalytic oxidation of carbon monoxide and methane on silica. *Catalysis Letters*. 1992, 13, 283–288.

MEYNEN, V., COOL, P. and VANSANT, E.F. Verified syntheses of mesoporous materials. *Microporous and Mesopororous Materials.* 2009, 125, 170–223.

MWENESONGOLE, Ellen. *A Raman- and XRD study of the crystal chemistry of cobalt blue*. South Africa, 2008. Diploma thesis. Dept. of Chemistry, University of Pretoria, Pretoria. Promoter P. van Rooyen.

NA, C. W. et al. Controlled transformation of ZnO nanobelts into CoO/Co_3O_4. *CrystEngComm*. 2012, 14, 3737–3741.

NAKAI, K., NAKAMURA, K. Pulse chemisorption measurement <metal dispersion measurement>. *BEL CAT Application note, CA-APP-002.* 2003, 1–6.

OBALOVÁ, Lucie. *Materiály na bázi hydrotalcitu pro katalytický rozklad N_2O*. Ostrava, Czech Republic, 2003. Disertační práce. VŠB – Technická univerzita Ostrava. Promoter L'. Dobrovský.

OBALOVÁ, Lucie. *Materiály na bázi hydrotalcitu pro katalytický rozklad N_2O*. Ed. 1. Ostrava : VŠB-TU Ostrava, Fakulta metalurgie a materiálového inženýrství, 2008. 99 p. ISBN 978-80-248-1884-9.

OBALOVÁ, L. et al. Effect of potassium in calcinated Co-Mn-Al layered double hydroxide on the catalytic decomposition of N_2O. *Applied Catalysis B: Environmental.* 2009, 90, 132–140.

OBALOVÁ, L. et al. Structure-activity relationship in the N_2O decomposition over Ni-(Mg)-Al and Ni-(Mg)-Mn mixed oxides prepared from hydrotalcite-like precursors. *Journal of Molecular Catalysis A: Chemical*. 2006, 248, 210–219.

OBALOVÁ, L. et al. Structure-activity relationship in the N_2O decomposition over Ni-(Mg)-Al and Ni-(Mg)-Mn mixed oxides prepared from hydrotalcite-like precursors. *Journal of Molecular Catalysis A: Chemical*. 2006, 248, 210–219.

PARK, K.-C., YIM, D.-J., IHM, S.-K. Characteristics of Al-MCM-41 supported Pt catalysts: effect of Al distribution in Al-MCM-41 on its catalytic activity in naphthalene hydrogenation. *Catalysis Today*. 2002, 74, 281–290.

PARKER, S.F. The role of hydroxyl groups in low temperature carbon monoxide oxidation. *Chemical communications*. 2011, 47, 1988–1990.

PÉREZ-RAMIREZ, J. et al. Formation and control of N_2O in nitric acid production. Where do we stand today? *Applied Catalysis B: Environmental*. 2003, 44, 117.

PIETERSE, J.A.Z., VAN DEN BRICK, R.W. Method for the decomposition of N_2O, catalyst therefor and preparation of this catalyst. United States Patent, 7,901,648 B2. Date of patent March 8, 2011.

PITKAAHO, S. et al. Oxidation of perchloroethylene-Activity and selectivity of Pt, Pd, Rh, and V_2O_5 catalysts supported on Al_2O_3, Al_2O_3–TiO_2 and Al_2O_3–CeO_2. Part 2. *Applied Catalysis B: Environmental*. 2012, 126, 215–224.

PIUMETTI, M. et al. Mesoporous silica supported Rh catalysts for high concentrationN_2O decomposition. *Applied Catalysis B: Environmental*. 2015, 165, 158–168.

POLADI, R.H.P.R. and LANDRY, C.C. Synthesis, characterization and catalytic properties of microporous/mesoporous material, MMM-1. *Journal of Solid State Chemistry*. 2002, 167, 363–369.

PRIETO, G. et al. Cobalt supported on morphologically tailored SBA-15 mesostructures: The impact of pore length on metal dispersion and catalytic activity in the Fischer–Tropsch synthesis. *Applied Catalysis A-General.* 2009, 367, 146–156.

REBENSTORF, B., LARSSON, L., LARSSON, R. Catalysis by coordinatively unsaturated surface compounds of chromium(II), iron(II), cobalt(II) and nickel(II) on silica gel. II. Decomposition of N_2O, reduction of N_2O by CO and oxidation of CO by O_2. *Acta Chemica Scandinavica A*. 1978, 32, 461–465.

RIVALLAN, M. et al. Adsorption and reactivity of nitrogen oxides (NO_2, NO, N_2O) on Fe-zeolites. *Journal of Catalysis*. 2009, 264, 104–116.

ROYER, S., DUPREZ, D. Catalytic oxidation of carbon monoxide over transition metal oxides. *Chem.Cat.Chem*. 2001, 3, 24–65.

SALEK, G.P. et al. Low-temperature carbon monoxide and propane total oxidation by nanocrystalline cobalt oxides. *Applied Catalysis B: Environmental*. 2014, 147, 1–7.

SCHUMACHER, V. et al. Method for the catalytic decomposition of N_2O. United States Patent, 6,743,404 B1. Date of patent June 1, 2004.

SCHWEFER, M. Catalyst for decomposing N_2O, its use and method for the production thereof. United States Patent, 6,890,499 B2. Date of patent May 10, 2005.

SEGURA, Y. et al. Characterisation and reactivity of vanadia-titania supported SBA-15 in the SCR of NO with ammonia. *Applied Catalysis B: Environmental*. 2005, 61, 69–78.

SEGURA, U.Y. *Synthesis, characterisation and catalytic activity of vanadia-titania catalysts*. Belgium, 2006. PhD Dissertation. Universitaire Instelling Antwerpen. Promoter E. F. Vansant.

SIMIONATO, M., ASSAF, E.M. Preparation and Characterization of Alumina-Supported Co and Ag/Co Catalysts. *Materials Research*. 2003, 6 (4), 535–539.

SWAMY, C.S. et al. Method for decomposing N_2O utilizing catalysts comprising calcined anionic clay minerals. United States Patent, 5,407,652 A. Date of patent April 18, 1995.

SZEGEDI, Á., POPOVA, M., MINCHEV, C. Catalytic activity of Co/MCM-41 and Co/SBA-15 materials in toluene oxidation. *Journal of Material Science*. 2009, 44, 6710–6716.

ŠPONER, J. et al. Coordination and properties of cobalt in the molecular sieves CoAPO-5 and -11. *Microporous and Mesoporous Materials*. 2000, 37, 117–127.

TANG, C. et al. An efficient strategy for highly loaded, well dispersed and thermally stable metal oxide catalysts. *Catalysis Communications*. 2011, 12, 1075–1078.

TANG, C.W., WANG, C.B. CHIEN, S.H. Characterization of cobalt oxides studied by FT-IR, Raman, TPR and TG-MS. *Thermochimica Acta*. 2008, 473, 68–73.

THORMÄHLEN, P., SKOGLUNDH, M., FRIDELL, E., ANDERSSON, B. Low-temperature CO oxidation over platinum and cobalt oxide catalysts. *Journal of Catalysis*. 1999, 188, 300–310.

VALIEV, M. et al. NWChem: a comprehensive and scalable open-source solution for large scale molecular simulations. *Computer Physics Communications*. 2010, 181, 1477–1489.

VANSANT, E.F., VOORT VAN DER, P., VRANCKEN, K.C. Characterization and modification of the silica surface. New York: Elsevier, 1995, xv, 556 p. Studies in surfance science and catalysis, 93. ISBN 04-448-1928-2.

VAN VEEN, J.A.R., JONKERS, G., HESSELNIK, W.H. Interaction of transition-metal acetylacetonates with γ-Al_2O_3 surfaces. *Journal of the Chemical Society, Faraday Transactions*. 1. 1989, 85 (2), 389–413.

VOORT VAN DER, P. et al. Synthesis and characterization of supported vanadium oxides by adsorption of the acetylacetonate complex. *Journal of the Chemical Society, Farraday Transactions*. 1996, 92 (19), 3635–3642.

VOORT VAN DER, P. et al. The uses of polynuclear metal complexes to develop designed dispersions of supported metal oxides: Part I. Synthesis and characterization. *Interface science*. 1997, 5, 169–197.

WANG, C. *Synthesis, characterization and catalytic performance of novel cobalt mesoporous/microporous catalysts*. United States of America, 2009. PhD Dissertation. Yale University. Promoter G. L. Haller.

WANG, C. et al. Synthesis, characterization and catalytic performance of highly dispersed Co-SBA-15. *Journal of Physical Chemistry C*. 2009, 113 (33), 14863–14871.

WANG, C.-B. et al. Characterization and catalytic oxidation of carbon monoxide over supported cobalt catalysts. *Catalysis Letters*. 2006, 107 (3–4), 223–230.

WANG, H. et al. Sulfur doped Co/SiO2 catalysts for chirally selective synthesis of single walled carbon nanotubes. *Chemical communications*. 2013, 49, 2031.

WANG, Y. et al. Characterization of Rh-based catalysts with EPR, TPR, IR and XPS. *Journal of Molecular Catalysis A: Chemical*. 1999, 149, 51–61.

WATZENBERGER, O. AGAR, D. Thermal decomposition of N_2O. United States Patent 6,328,941 B1. Date of patent December 11, 2001.

WEBB, P.A. Introduction to Chemical Adsorption Analytical Techniques and their Applications to Catalysis, MIC Technical Publications Micromeritics Instrument Corp., Georgia, January 2003.

WECKHUYSEN, B.M. Synthesis, spectroscopy and catalysis of [$Cr(acac)_3$] complexes grafted onto MCM-41 materials: Formation of polyethylene nanofibres within mesoporous crystalline aluminosilicates. *Chemistry – A European Journal*. 2000, 6 (16), 2960–2970.

XIA, Y., MOKAYA, R. Aluminosilicate MCM-48 materials with enhanced stability via simple post-synthesis treatment in water. *Microporous and Mesoporous Materials*. 2004, 68, 1–10.

XIA, Y., MOKAYA, R. On the hydrothermal stability of mesoporous aluminosilicate MCM-48 materials. *Journal of Physical Chemistry B*. 2003, 107, 6954–6960.

XIE, X. et al. Low-temperature oxidation of CO catalysed by Co_3O_4 nanorods. *Nature*. 2009, 458, 746–749.

XIE, Y. et al. Oxidation reaction on neutral cobalt oxide clusters. experimental and theoretical studies. *Physical Chemistry Chemical Physics*. 2010, 12, 947–959.

XU, X. et al. SBA-15 based catalysts in catalytic N2O decomposition in a model tail-gas from nitric acid plants. *Applied Catalysis B: Environmental*. 2004, 53, 265–274.

XU, X. et al. Characterization and catalytic performance of Co/SBA-15 supported gold catalysts for CO oxidation. *Materials Research Bulletin*. 2006, 41, 406–413.

YAO, Y.Y. The oxidation of hydrocarbons and CO over metal oxides: III. Co_3O_4. *Journal of Catalysis.* 1974, 33, 108–122.

YAKOVLEV, A.L., ZHIDOMIROV, G.M. Quantum chemical study of nitrous oxide adsorption and decomposition on Lewis acid sites. *Catalysis Letters*. 1999, 63, 91–95.

WECKHUYSEN, B.M., et al. Synthesis, spectroscopy and catalysis of [Cr(acac)(3)] complexes grafted onto MCM-41 materials: Formation of polyethylene nanofibres within mesoporous crystalline aluminosilicates. *Chemistry-A European Journal*. 2000, 6, 2960–2970.

ZAMANI, C. et al. Mesoporous silica: A suitable adsorbent for amines. *Nanoscale Research Letters.* 2009, 4, 1303–1308.

ZHANG, F. et al. NO SCR with propane and propene on Co-based alumina catalysts prepared by co-precipitation. *Applied Catalysis B: Environmental*. 2007, 73, 209–219.

ZHANG, F., et al. Clay-based SiO_2 as active support of gold nanoparticles for CO oxidation catalyst: Pivotal role of residual Al. *Catalysis Communications*. 2013, 35, 72–75.

Climate Change Indicators in the United States. United States Environmental Protection Agency. [Published on 02/07/2014]. Available at:
http://www.epa.gov/climatechange/science/indicators/ghg/ghg-concentrations.html.

River Sources of Green House Gases. Environmental News Network. [Published on 21/12/2010]. Available at: http://www.enn.com/ecosystems/article/42147.

Sorbent Synthesis and Application. University of Strathclyde. [Published on 08/10/2010]. Available at:
http://info.chem.strath.ac.uk/people/academic/lorraine_gibson/research/sorbents.

Look for Chemicals. Aluminum acetylacetonate. [Published on 20/07/2014]. Available at:
http://www.lookchem.com/Aluminum-acetylacetonate/.

Look for Chemicals. Bis(acetylacetonato)cobalt. [Published on 20/07/2014]. Available at:
http://www.lookchem.com/cas-140/14024-48-7.html.

Look for Chemicals. Rhodium(III) acetylacetonate. [Published on 20/07/2014]. Available at:
http://www.lookchem.com/cas-142/14284-92-5.html.

Fundamental coordination chemistry. Department of chemistry and biochemistry, University of Alaska Fairbanks. [Published on 30/05/2014]. Available at:
http://chem.uaf.edu/howard/Rhodium.htm.

8 LIST OF FIGURES

9 LIST OF TABLES

10 LIST OF ABBREVIATIONS AND SYMBOLS

Acac	Acetylacetonate
ATR-FTIR	Attentuated total reflectance Fourier transform infrared
DRIFT	Diffuse reflectance infrared Fourier transform
DR UV-Vis	Diffuse reflectance ultraviolet visible
EPMA	Electron probe mico-analysis
FTIR-PAS	Fourier transform infrared photoacoustic spectroscopy
GHSV	Gas hourly space velocity
IET	Institute of Environmental Technology
KM	Kubelka-Munk
MCM-41	Mobil composition of matter no. 41
MDD	Molecular designed dispersion
SBA-15	Santa barbara amorphous no. 15
SEM-EDX	Scanning electron microscopy with energy dispersive X-ray
TGA	Thermogravimetric analysis
TOF	Turnover frequency
TPD-NH_3	Temperature programmed desorption of ammonia
TPR-H_2	Temperature programmed reduction by hydrogen
WHSV	Weight hourly space velocity
XPS	X-ray photoelectron spectroscopy
XRD	X-ray diffraction

A_m	cross-sectional area (nm^2)
c_{A0}	inlet N_2O concentration ($mol.m^{-3}$)
c_p	specific heat capacity of N_2 ($J.kg^{-1}.K^{-1}$)
d_p	particle diameter (mm)
D_t	internal diameter of reactor (mm)
G	superficial mass velocity ($kg.s^{-1}.m^{-2}$)
ΔH_r	reaction heat ($J.mol^{-1}$)
k	kinetic constant, 1st order rate law ($m^3.s^{-1}.g^{-1}$)
L_b	bed length (mm)
M_{Co}	molecular weight of cobalt ($g.mol^{-1}$)
$m_{Co(acac)2}$	weight of cobalt acetylacetonate (g)
$M_{Co(acac)2}$	molecular weight of cobalt acetylacetonate ($g.mol^{-1}$)
$m_{catalyst}$	weight of catalyst (g)

$m_{support}$	weight of silica support (g)
N_A	Avogadro´s number, $6.022.10^{23}$ mol^{-1}
$n_{N2O,\ reacted}$	number of N_2O molecules converted per time (mmol. $g^{-1}.h^{-1}$)
n_{Rh}	concentration of rhodium (mmol.g^{-1})
Δp	pressure drop (Pa)
p_0	atmospheric pressure (Pa)
Pe_p	Peclet number (-)
R_∞	sample reflectance spectrum at infinite sample depth (-)
S_{BET}	BET surface area ($m^2.g^{-1}$)
ΔT_{ad}	adiabatic increase of temperature (K)
$\dot{V}$	volume flow of gas reaction mixture ($m^3.s^{-1}$)
V_m	monolayer capacity (mol.g^{-1})
X	conversion of reactive gas (-)
x	gas mole fraction at the reactor outlet (-)
x^o	gas mole fraction at the reactor inlet (-)
w_{Co}	weight percent of cobalt (%)
α_{OH}	silanol number ($OH.nm^{-2}$)
β_0	parameter ($kg.s^{-2}.m^{-2}$)
δ_{OH}	concentration of hydroxyl groups (mmol.g^{-1})
ε	porosity (-)
μ	dynamic viscosity of nitrogen (Poise)
η	internal effectiveness factor (-)
ρ	density of nitrogen ($kg.m^{-3}$)

11 LIST OF PUBLICATIONS

11.1 The topic of doctoral dissertation

- **Articles**

KUBOŇOVÁ, L., JIRÁTOVÁ, K., MAMULOVÁ KUTLÁKOVÁ, K., PEIKERTOVÁ, P., OBALOVÁ, L., COOL, P. Catalytic activity of cobalt grafted on ordered mesoporous silica materials modified with aluminum in N_2O decomposition and CO oxidation. *Microporous and Mesoporous Materials*. Under review.

KUBOŇOVÁ, L., FRIDRICHOVÁ, D., WACH, A., KUŚTROWSKI, A., OBALOVÁ, L., COOL, P. Catalytic activity of rhodium grafted on ordered mesoporous silica materials modified with aluminum in N_2O decomposition. *Catalysis today*. 2015. In Press, Corrected Proof. DOI: 10.1016/J.CATTOD.2015.03.019.

KUBOŇOVÁ, L., OBALOVÁ, L., FRIDRICHOVÁ, D., COOL, P. Surface activation of mesoporous ordered silica materials by aluminum and rhodium, their characterization and catalytic activity for N_2O decomposition. *Chemické listy*. 2014, 8, 768. ISSN: 1213-7103.

- **Oral and poster presentations at conferences**

KUBOŇOVÁ, L., OBALOVÁ, L., ČAPEK, L., COOL, P. Surface activation of mesoporous ordered silica materials by aluminum and cobalt, their characterization and catalytic activity for N_2O decomposition. In: *12th Pannonian Symposium on Catalysis: September 16–20, 2014, Castle Trest, Czech Republic*.

KUBOŇOVÁ, L., OBALOVÁ, L., FRIDRICHOVÁ, D., COOL, P. Surface activation of mesoporous ordered silica materials by aluminum and rhodium, their characterization and catalytic activity for N_2O decomposition. In: *International Symposium on Air&Water Pollution Abatement Catalysis: September 1–5, 2014, Krakow, Poland*.

KUBOŇOVÁ, L., OBALOVÁ, L., COOL, P. Surface activation of mesoporous ordered silica materials, their characterization and catalytic activity of N_2O reduction. In: *5th International Symposium of Advanced Micro- and Mesoporous Materials: September 6–9 2013, Golden Sands, Bulgaria*.

11.2 Other topics during Ph.D. study

- **Articles**

KUBOŇOVÁ, L., LANGOVÁ, Š., NOWAK, B., WINTER, F. Thermal and hydrometallurgical recovery methods of heavy metals from municipal solid waste fly ash. *Waste Management*. 2013, 33, 2322–2327. DOI: 10.1016/j.wasman.2013.05.022.

KUBOŇOVÁ, L., OBALOVÁ, L., SKOVRANEK, L., TROPPOVÁ, I. The balancing of VOC concentration fluctuations by adsorption/desorption process on activated carbon. *Adsorption*. 2013, 19, 1–7. DOI: 10.1007/s10450-013-9490-y.

KUBOŇOVÁ, L., OBALOVÁ, L., VLACH, O., TROPPOVÁ, I., KALOUSEK, J. Modelling of NO adsorption in fixed bed on activated carbon. *Chemical and Process Engineering*. 2011, 32 (4), 367–377. ISSN 0208-6425.

POTYKOVÁ, I., OBALOVÁ, L., KUBOŇOVÁ, L., OBROUČKA, K. The balancing of NO concentration fluctuations by adsorption/desorption process on activated carbon. *Separation and Purification Technology*. 2011, 78, 245–248. DOI: 10.1016/j.seppur.2011.01.035.

- **Poster presentations at conferences**

KUBOŇOVÁ, L., LANGOVÁ, Š., NOWAK, B., WINTER, F. Thermal and hydrometallurgical recovery methods of heavy metals from municipal solid waste fly ash. In: *40th International Conference of Slovak Society of Chemical Engineering (SSCHE): May 27–31, 2013, Tatranské Matliare, Slovakia*.

KUBOŇOVÁ, L., OBALOVÁ, L., SKOVRANEK, L., TROPPOVÁ, I. The balancing of VOC concentration fluctuations by adsorption/desorption process on activated carbon. In: *ISEH 2012: November 22–23, 2012, Ostrava, Czech Republic*.

TROPPOVÁ, I., OBALOVÁ, L., SKOVRANEK, L., KUBOŇOVÁ, L. The balancing of VOC concentration fluctuations by adsorption / desorption process on activated carbon. In: *ISSHAC-8: Effects of Surface Heterogeneity in Adsorption and Catalysis on Solids: August 27–31, 2012, Krakow, Poland*.

KUBOŇOVÁ, L., OBALOVÁ, L., VLACH, O., TROPPOVÁ, I., KALOUSEK, J. Modelling of NO adsorption in fixed bed on activated carbon. In: *38th International Conference of SSCHE: May 23–27, 2011, Tatranské Matliare, Slovakia.*